Dissertation

submitted to the

Combined Faculties for the Natural Sciences and for Mathematics

of the Ruperto-Carola University of Heidelberg, Germany

for the degree of

Doctor of Natural Sciences

Presented by

Diplome de Master - Naga Venkata Gayathri Vegesna

Born in: Bhimavaram, India

Oral examination: 15th of December 2016

Molecular regulation of *de novo* Golgi biogenesis

Referees:

Dr. Peter Lenart

Prof. Dr. Walter Nickel

Summary

The Golgi complex (GC) is a central organelle of the secretory pathway. It receives and distributes material from and to other cellular organelles and is thus involved in basic cellular processes such as differentiation, cell motility or signal transduction. In mammalian cells the GC acquires a highly dynamic and unique morphology that quickly disassembles before mitosis and reassembles thereafter. The molecular regulators involved in these processes however remain largely elusive.

To understand the molecular mechanisms of Golgi biogenesis and its regulation in detail, I used a combinatory approach of RNAi and diffraction limited laser nanosurgery to deplete cells of their GC and monitor its *de novo* biogenesis in the karyoplasts by time-lapse and correlative light and electron microscopy.

To first identify proteins that could play a role in Golgi biogenesis, I screened the Human Protein Atlas database and chose 31 proteins localized exclusively to the GC and classified them based on their behaviour upon Brefeldin A (BFA) treatment of cells. This showed that 13 proteins behaved like Golgi enzymes and relocated to the endoplasmic reticulum after BFA treatment. Another 8 proteins showed Golgi matrix-like behaviour and remained distributed throughout the cytoplasm as distinct Golgi remnants. The remaining 10 proteins showed a TGN/centrosome-like localisation after BFA treatment. Among the 18 Golgi matrix-like and TGN/centrosome-like proteins, I could validate the siRNA knockdown in 7 candidate proteins. Functional analysis of these 7 protein candidates by using laser nanosurgery to deplete the GC together with the target proteins and subsequent blocking their protein synthesis through RNAi showed an acceleration of the early phase of Golgi biogenesis upon depletion of GMAP210. Individual depletions of the 6 other Golgi proteins tested showed only a slight delay or no effect on Golgi biogenesis. However, double depletions of GRASP65 & 55 or GRASP65 & Giantin resulted in delays in the kinetics of the early phase of Golgi biogenesis for several hours. Ultra-structural analyses by correlative light and electron microscopy showed that the double depletion of GRASP65 & 55 affected the flattening of Golgi cisternae, an event that occurs in the later phases of Golgi biogenesis, and

resulted in the accumulation of swollen cisternae even at the end of the experiments. In addition, the formation of complex and convoluted Golgi intermediates that usually occur in early phases during Golgi biogenesis was delayed or impaired in GRASP65 & 55 double depleted cells.

The delay in the ability to form Golgi precursors in GRASP65 & 55 double depleted cells shows the important role of these two Golgi matrix proteins acting in concert in the initial stages of the process. In contrast to the existing literature data, I could not identify any evidence of the involvement of GRASP65/55 in Golgi stacking during *de novo* Golgi biogenesis from my experiments. The results of this PhD work further suggest that, most likely there is no single master regulator for the Golgi biogenesis and there is a significant degree of functional redundancy among Golgi matrix proteins involved in the process.

Zusammenfassung

Der Golgi Apparat (GA) ist ein zentrales Organell des Sekretorischen Weges. Er nimmt Material von anderen Organellen auf und verteilt sie an ihren Zielort. Deshalb ist der GA an grundlegenden zellulären Prozessen wie die Zelldifferenzierung, Zellmotilität oder Signalübertragung beteiligt. In Gewebekulturzellen nimmt der GA eine einzigartige und dynamische Morphologie an, die unmittelbar vor der Zellteilung zerfällt und danach wieder aufgebaut wird. Die Regulierung beider Prozesse auf molekularer Ebene ist weitgehend unverstanden.

Um die molekularen Mechanismen der Golgi Biogenese besser zu verstehen wurde in der vorliegenden Arbeit eine Kombination von RNA Interferenz (RNAi) und Beugungs-limitiertem Laserskalpell benutzt um zunächst den Golgi von Zellen zu entfernen und danach seine Biogenese mittels Fluoreszenzmikroskopie-basierten Zeitrafferaufnahmen und korrelierter Licht und Elektronenmikroskopie zu studieren.

Um Proteine zu identifizieren die möglicherweise eine Rolle bei der Golgi Biogenese spielen wurde zunächst die Datenbank des „Human Protein Atlas" Projekts durchsucht und 31 Proteine ausgesucht, die ausschließlich auf dem GA lokalisieren. Diese wurden dann anhand ihres Verhaltens nach der Behandlung von Zellen mit Brefeldin A (BFA) klassifiziert. Dies identifizierte 13 Proteine, die sich wie Golgi Enzyme verhalten, da sie sich nach BFA Behandlung zum endoplasmatischen Retikulum umverteilten. Weitere 8 Protein verhielten sich wie Proteine der Golgi Matrix die sich nach BFA Behandlung auf diskrete Golgi Überreste im Zytoplasma umverteilen. Die restlichen 10 Proteine zeigten nach BFA Behandlung eine Verteilung wie Proteine des *trans*-Golgi Netzwerkes (TGN) oder Zentrosomen. Von den 18 Golgi Matrix- und TGN-ähnlichen Proteinen konnten für 7 siRNAs gefunden werden, die die Expression der entsprechenden Proteine unterdrücken. Funktionelle Analysen dieser 7 Proteine bei denen der GA zunächst mittels Laserskalpell von Zellen entfern wurde und anschließend die Neusynthese der entsprechenden Proteine mittels RNA Interferenz unterdrückt wurde, zeigten dass die Unterdrückung des Proteins GMAP210 die frühe Phase der Golgi Biogenese beschleunigt. Experimente mit den verbleibenden 6 Proteinen zeigten nur einen

geringen oder keinen Effekt auf die Golgi Biogenese. Die gleichzeitige Unterdrückung der Protein Synthese von GRASP65 und GRASP55 oder GRASP65 und Giantin verzögerte dagegen die Kinetik der Golgi Biogenese um mehrere Stunden. Ultrastrukturanalysen mittels korrelativer Licht- und Elektronenmikroskopie zeigten, dass die gleichzeitige Unterdrückung der Synthese von GRASP65 und GRASP55 einen Effekt auf die Abflachung der Golgi Zisternen, ein Vorgang der späten Golgi Biogenese, hat. Dies hatte eine Anhäufung angeschwollener Zisternen am Ende der Experimente zur Folge. Weiterhin war die Biogenese komplexer Golgi Vorläufer Strukturen wie sie in der frühen Phase der Golgi Biogenese vorkommen, durch die gleichzeitige Unterdrückung der Proteinsynthese von GRASP65 und GRASP55 verzögert und gestört. Dies zeigt die Bedeutung der Zusammenwirkung dieser beiden Proteine in der frühen Phase der Golgi Biogenese. Im Gegensatz zu Literaturdaten konnte anhand der hier vorliegenden experimentellen Daten keine Evidenz für die Funktion von GRASP65&55 beim Golgi „Stacking“ gefunden werden.

Die Ergebnisse dieser Arbeit deuten darauf hin, dass es sehr wahrscheinlich kein „Master Regulator“ der Golgi Biogenese gibt und signifikante funktionelle Überlappungen zwischen Golgi Matrix Proteinen bei der Golgi Biogenese existieren.

Table of Contents

Summary iii

Zusammenfassung v

Table of Contents vii

List of Figures xi

Acknowledgements xiii

Abbreviations xv

1 Introduction 17

1.1 Anterograde and retrograde trafficking 18

1.1.1 Anterograde trafficking 18

1.1.2 Retrograde trafficking 20

1.2 Role of Golgi apparatus in the secretory pathway 21

1.3 Structural organisation of the Golgi complex 21

1.4 Golgi Proteins 23

1.4.1 Golgi matrix proteins 24

1.4.1.1 GM130 25

1.4.1.2 GRASP55 and 65 25

1.4.1.3 GMAP210 27

1.4.1.4 Giantin/GOLGB1 28

1.4.1.5 TMF/ARA160 29

1.4.1.6 TMEM165 29

1.5 Golgi Biogenesis in Mammalian cells 30

1.5.1 Golgi disassembly 30

1.5.2 Golgi biogenesis/re-assembly 32

1.5.3 Experimental approaches to study Golgi biogenesis 34

1.5.3.1 Chemical approaches 34

1.5.3.2 Laser nanosurgery approach to study Golgi biogenesis 35

2 Aims 39

3 Results 40

3.1 Experimental approach to identify the regulators of Golgi biogenesis 40

3.1.1 Classification of Golgi localised proteins using Brefeldin A treatment 40

3.1.2 A combinatory approach: RNAi and laser nanosurgery 43
3.2 Validating the depletion of candidate proteins upon RNAi and laser nanosurgery 44
3.3 Ultrastructure of the Golgi after Golgi biogenesis 45
3.4 Time-lapse analysis of Golgi biogenesis 46
3.4.1 Kinetics of Golgi biogenesis 46
3.5 Ultra structure of Golgi precursors in GRASP55/65 depleted cells 48
3.6 VSVG assay to check the efficiency of the cargo transport from ER to Golgi .. 49
3.7 Duration of phase 1 in mitotic cells upon double knockdown of GRASPs..... 50
4 Discussion 70
4.1 Combinatory approach to identify the molecular regulators of Golgi biogenesis 72
4.2 Selection and Classification of candidate proteins 73
4.3 Effect of protein depletions on Golgi ultrastructure 74
4.4 Initial stages of Golgi biogenesis – the rate limiting step 75
4.5 Ultrastructure of Golgi precursors during Golgi biogenesis 77
4.6 Golgi biogenesis in mitotic cells 77
4.7 Redundancy of Golgi proteins in Golgi biogenesis 78
4.8 Proposed role of GRASPs 79
5 Outlook 81
6 Materials 83
6.1 Cell culture 83
6.1.1 Eukaryotic cell lines 83
6.1.2 Reagents for Cell culture 83
6.1.3 Cell culture and imaging media 83
6.1.4 Chemicals and drugs 84
6.1.5 Buffers and solutions 84
6.1.6 Special equipment and material/Others 85
6.2 Microcontact printing 86
6.2.1 Reagents 86
6.2.2 Other equipment and material 86
6.3 Oligonucleotides 86
6.4 Immunofluorescence 87
6.4.1 Primary Antibodies 87
6.4.2 Secondary Antibodies 88

6.5 Electron Microscopy 89
6.5.1 Chemicals 89
6.5.2 Fixative and solutions 89
6.5.3 Other materials 90
6.6 Microscopic setups 91
6.6.1 Wide field and electron microscopes 91
6.6.2 Confocal Microscopes 91
6.7 Software tools for data analysis and web tools 91
6.7.1 Software tools 91
6.7.2 Web tools 91
7 Methods 93
7.1 Soft Lithography/Microcontact printing 93
7.1.1 Production of PDMS stamps 93
7.1.2 Printing of fibronectin lines on coverslips and seeding cells 93
7.2 Cell biology 94
7.2.1 Cell culture 94
7.2.2 Plating cells 95
7.2.3 Freezing and thawing cells 95
7.2.4 Transfection of eukaryotic cells 96
7.2.5 Brefeldin A (BFA) Treatment 97
7.2.6 Immunofluorescence 97
7.3 Laser nanosurgery and Microscopy 98
7.3.1 Calibration of laser nanosurgery system 98
7.3.2 Laser nanosurgery to deplete the Golgi apparatus from the cell 98
7.3.3 Laser inscription for tracing back the cells 99
7.3.4 Time lapse imaging of the karyoplast 99
7.3.5 Wide field imaging of fixed cells 100
7.3.6 Confocal imaging of fixed cells 100
7.3.7 Automated imaging of Mitotic cells 100
7.3.8 Correlative light and electron microscopy (CLEM) 101
7.3.8.1 Cell preparation 101
7.3.8.2 EM fixation protocol 102
7.3.8.3 EM Fixation protocol with Malachite green 103
7.3.8.4 Etching of the glass coverslip 104
7.3.8.5 Trimming and Sectioning of the resin block 105
7.3.9 Quantification of the time-lapse/Golgi biogenesis 105
7.4 VSVG assay 106

7.4.1 Protocol for VSVG assay 106
7.5 Computational Biology 107
7.5.1 Image Analysis 107
7.5.2 Image J 107
7.5.2.1 Analysis of Golgi biogenesis 107
7.5.2.2 Analysis upon Brefeldin A treatment 108
7.5.2.3 Quantification of luminal width of Golgi cisternae 108
7.5.3 Cell Profiler 108
7.5.3.1 Analysis of Golgi biogenesis 108
7.5.3.2 Analysis of ER to Golgi transport by VSVG assay 110
7.5.4 MatLab 112
7.5.5 R Studio 118
7.5.5.1 Plotting the Golgi biogenesis results 118
7.5.5.2 Plotting Golgi biogenesis data from mitotic cells 119
7.5.5.3 Plotting the data from VSVG assay 120
8 References 123

List of Figures

Figure 1 Secretory Pathway 17
Figure 2 COPII coat assembly 19
Figure 3 COPI coat assembly 20
Figure 4 Structural organisation of Golgi 22
Figure 5 Polarised Golgi stack 23
Figure 6 Golgi disassembly and biogenesis during mitosis 32
Figure 7 Models of Golgi biogenesis 33
Figure 8 Laser nanosurgery approach 36
Figure 9 Time-lapse characterisation of *de novo* Golgi biogenesis 37
Figure 10 Project outline and experimental setup 52
Figure 11 Classification of Golgi proteins upon BFA treatment - Class I 53
Figure 12 Classification of Golgi proteins upon BFA treatment - Class II 54
Figure 13 Classification of Golgi proteins upon BFA treatment - Class III 55
Figure 14 Validation of candidate protein depletions upon RNAi and laser nanosurgery 56
Figure 15 CLEM images of *de novo* Golgi upon depletion of candidate proteins 57
Figure 16 Lipid droplets in TMEM165 depleted cells 58
Figure 17 Phases in Golgi biogenesis 59
Figure 18 Time-lapse curve of Golgi biogenesis 60
Figure 19 Time-lapse curves of GRASP double depletion and control 61
Figure 20 CLEM of Golgi precursors upon double depletion of GRASP65 & 55 compared to control 62
Figure 21 Duration of phase 1 in Golgi biogenesis upon depletion of Golgi proteins 63
Figure 22 Duration of phase 2 in Golgi biogenesis upon depletion of Golgi proteins 64
Figure 23 Time course of temperature sensitive VSVG (VSV-G ts045) upon its release from the ER 65
Figure 24 Comparison of ER to Golgi transport by VSVG assay in control and GRASP double knockdown 66

Figure 25 Golgi biogenesis during mitosis in GRASP 65 & 55 depleted cells 67
Figure 26 Time-lapse curve showing duration of phase 1 in mitotic cells.....68
Figure 27 Duration of phase 1 in mitotic cells upon depletion of GRASPs 69
Figure 28 Events occurring at ultra structural level during Golgi biogenesis in control and GRASP double depletion.....79

Acknowledgements

Firstly I would like to thank Rainer Pepperkok for giving me the opportunity to do my PhD in his lab. I would like to thank him for his continuous support and fruitful discussions throughout the project. He was very supportive and always gave a positive feedback during discussions. The training I received during this period helped me improve a lot in terms of scientific thinking and writing. I would also like to thank my TAC members Peter Lenart, Walter Nickel and John Briggs for their suggestions and guidance throughout my PhD. I would like to also thank Peter Lenart and Walter Nickel for agreeing to be referees for my thesis. I would like to thank Alba Diz-Munoz and Sebastain Schuck to accept my request to be part of my thesis committee.

I would like to thank Paolo Ronchi for being very helpful and teaching me all the techniques needed for my project. I would like to thank him for guiding me throughout the project, for all the suggestions, discussions and for helping me at all times. I would like to thank Fatima Verissimo for helping me evaluate and improve my scientific presentations and for her continuous support and discussions. I would like to thank Aliaksandr Halavatyi for being such a kind and nice person and for sharing his mathematical knowledge at all times. I would also like to thank him for his help with scripting and coding to analyse my data. I would like to thank Miriam Reiss for being such a nice and friendly person and helping me with all my questions and also helping me translate and deal with German administrative matters. I would also like to thank Juan Jung for his help with data analysis of my last experiments. I would also like to thank rest of the Pepperkok group members Anthi, Magda, Emiliana, Sanjana and Floriana for being very nice, helpful and supportive throughout my PhD.

I would like to thank Stefan Terjung for his quick help with the cutting microscope whenever there was a problem. I would also like to thank Christian Tischer for his help with Cell profiler. I would like to thank Volker Hilsenstein for his support and help with the automated microscopic setup. I would also like to thank all the other ALMF staff for their constant help with microscopy.

I would like to thank all my friends in Heidelberg and at EMBL with whom I had great times throughout my stay. I would like to thank my parents for their continuous support and love at all times. Sadly my dad didn't make it through the end of my PhD but he is always in my thoughts. I would like to specially thank my mom for being strong and supportive even during our hard times. I would also like to thank my closest family members and cousins for their love and support. I would like to thank my dearest husband, whom I came to know during my PhD for being such a lovely and fun person. It hasn't been easy to stay far away from him and I would like to thank him for his constant love, support. This thesis is dedicated to my parents.

Abbreviations

ER	Endoplasmic Reticulum
GC, Golgi	Golgi Complex
BFA	Brefeldin A
COPI	Coat Protein Complex I
COPII	Coat Protein Complex II
VTC	Vesicular Tubular Carrier
ERGIC	ER-to-Golgi Intermediate Compartment
VSVG	Vesicular Stomatitis Virus Glycoprotein
Arf-GEF	Arf-Guanosine nucleotide Exchange Factor
GTP	Guanine Tri Phosphate
TGN	Trans Golgi Network
GRASP	Golgi ReAssembly and Stacking Protein
GRASP65	Golgi ReAssembly and Stacking Protein of 65 KD
GRASP55	Golgi ReAssembly and Stacking Protein of 55 KD
GRASPs	GRASP55 and GRASP65
RNAi	RNA interference
FRAP	Fluorescence Recovery After Photobleaching
FI	Fluorescence Intensity
CLEM	Correlative Light and Electron Microscopy
ERES	ER exit sites
HPA	Human Protein Atlas database
IF	Immuno-Fluorescence
EM	Electron Microscopy

FI	Fluorescence Intensity
GM130	Golgi Matrix protein of 130 KD
GMAP210	Golgi Microtubule Associated Protein of 210 KD
TMEM165	Trans MEMbrane protein of 165 KD
TMF	TATA element Modulating Factor
TIFI	Total Integrated Fluorescence Intensity

1 Introduction

Proteins, which are commonly described as the building blocks of life are constantly synthesised by cells and need to be transported to different cellular destinations to perform their functions. Various steps involved in the synthesis, modification and transportation of these proteins through membrane bound organelles are described as the secretory pathway. It involves a series of steps in which the proteins are transported from the Endoplasmic Reticulum (ER) towards the plasma membrane or other cellular compartments (Figure 1).

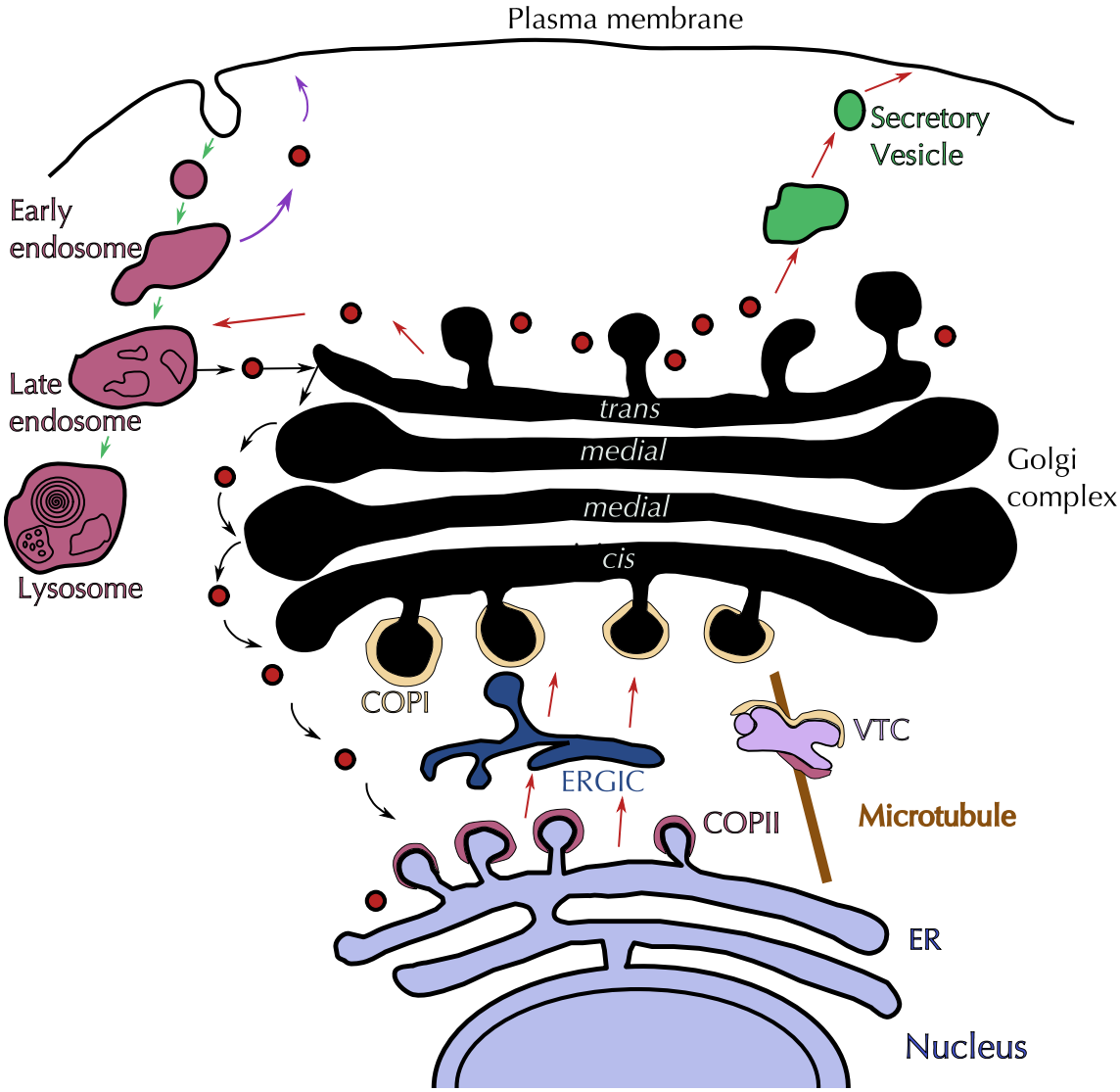

Figure 1 Secretory Pathway

Schematic representation of the secretory pathway with its membrane bound compartments. It shows the journey of proteins from ER to the plasma membrane via anterograde trafficking (red arrows) through

the Golgi complex. The proteins are recycled back to the ER via retrograde traffic retrograde traffic (black arrows).

Most of the proteins are transported as vesicular structures coated with different coat complexes through anterograde trafficking. ER resident proteins involved in this process are recycled back to the ER through retrograde trafficking. The secretory proteins undergo various modifications during this process, making them functional and are transported to their respective cellular destinations. This process is highly conserved in eukaryotic cells and involves membrane bound organelles such as the Endoplasmic Reticulum (ER) and Golgi complex. To introduce the topic of my thesis, this chapter will be focused on the secretory pathway and the Golgi complex.

1.1 Anterograde and retrograde trafficking

1.1.1 Anterograde trafficking

Transport of proteins from the ER towards the Golgi or plasma membrane is defined as anterograde trafficking. In Figure 1, red arrows represent the anterograde trafficking and black arrows represent the retrograde trafficking. Proteins exit the ER only after critical quality control mechanisms that prevent the release of improperly folded proteins (Mancias and Goldberg 2005). Chaperones within the ER transiently associate with proteins and ensure their proper folding. The improperly folded proteins are retained by the chaperones in the ER or degraded.

Newly synthesised proteins are concentrated by the vesicular coat complex COPII at the specialized ribosome free areas on the ER, called as ER exit sites (Malkus, Jiang, and Schekman 2002; Palade 1975). The proteins are then packaged into COPII coated vesicles. The formation of COPII coat is initiated by the activation of small GTPase Sar1 by a GEF protein Sec12 (Saito et al. 1998). The activated Sar1 (Sar1-GTP) recruits cytoplasmic Sec23-Sec24 heterodimer through the interaction with Sec23 (Yoshihisa, Barlowe, and Schekman 1993). Sec23-Sec24 heterodimers bind to Sar1 and polymerise forming pre-budding complex, which forms the inner coat of the COPII vesicle (Figure 2). The pre-budding complex recruits cargo proteins and then Sec13-Sec31 heterotetramer is recruited forming the outer COPII coat (Figure 2). The formation of

COPII coated vesicles involving different coat components is depicted in the Figure 2. Once the COPII coated vesicles bud from the ER, the COPII coat disassembles by GTP hydrolysis on Sar1. This occurs with the help of GAP activity of Sec23-Sec24 and is accelerated by Sec13-31 (Antonny et al. 2001; Yoshihisa et al. 1993).

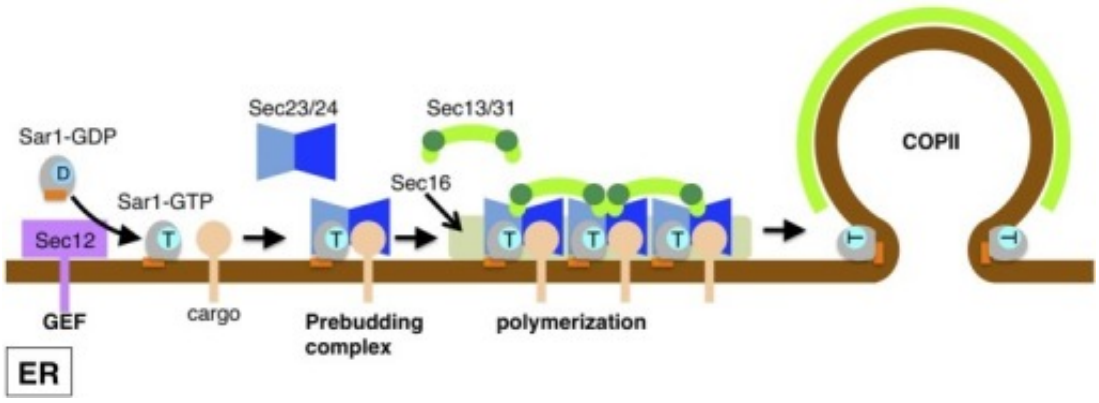

Figure 2 COPII coat assembly

Schematic representation of proposed model for COPII coat assembly process. Figure adapted from (Yorimitsu, Sato, and Takeuchi 2014).

The COPII coated vesicles in mammalian cells are suggested to fuse by homotypic fusion to form large carriers called Vesicular Tubular Carriers (VTCs) (Stephens and Pepperkok 2001). The mechanisms of fusion of these vesicles for releasing COPII to form VTCs are not clearly understood. VTCs are transient intermediates between the ER and Golgi and traffic along microtubules towards the Golgi (Presley et al. 1997; Scales, Pepperkok, and Kreis 1997). During ER to Golgi transport VTCs are coated with the vesicular coat complex COPI (Scales et al. 1997; Shima et al. 1999), which is involved in the recycling of proteins from post ER membranes back to the ER**.** It is not clear whether VTCs later fuse with the Golgi or mature into a *cis* Golgi cisterna (Martínez-Menárguez et al. 1999). In addition to VTCs a so-called ER-to-Golgi Intermediate Compartment (ERGIC), which is defined by localisation of ERGIC-53 to it, has been proposed to exist between the ER and Golgi complex. But unlike VTCs, ERGIC has been suggested to be a stable compartment to which the COPII coated vesicles can fuse (Ben-Tekaya et al. 2005; Hauri et al. 2000; Schweizer et al. 1990; Stephens and Pepperkok 2001).

1.1.2 Retrograde trafficking

Proteins involved in fusion events, export factors and ER resident proteins travelling from ER to Golgi are recycled back to ER via COPI coated vesicles (Ballensiefen et al. 1998; Malkus et al. 2004). This process begins with the recruitment of Arf-GEF (Arf-Guanosine nucleotide Exchange Factor), which activates the small GTPase Arf1. Upon activation, Arf1 is recruited to the Golgi and initiates binding of the COPI coat complex. This COPI coat complex consists of seven subunits (α, β, β′, γ, δ, ε and ζ) that are recruited from the cytoplasm by Arf1. The two sub-complexes of α/β′/ε-COP and β/γ/δ/ζ-COP form outer and inner coats of the COPI complex respectively (Figure 3). Despite of these two sub-complexes, COPI coat is recruited *en bloc* to the Golgi membrane through direct interaction with membrane bound Arf1 (Hara-Kuge et al. 1994). Similar to COPII, the inner coat recruits cargo proteins and once the COPI complex is properly assembled, vesicles pinch off from the Golgi membrane (Yu, Breitman, and Goldberg 2012). COPI coated vesicles containing cargo either diffuse or actively travel along the microtubules towards the ER (Chen et al. 2005). Similar to COPII, the COPI coat is usually disassembled or destabilised before fusing to the target compartment by the hydrolysis of Afr1 GTP. The schematic representation of COPI coat assembly involving various components is shown in Figure 3.

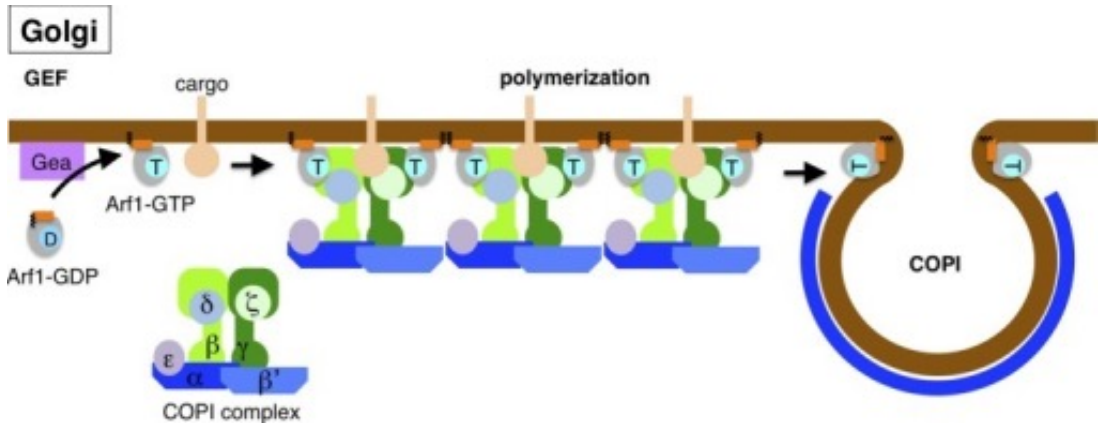

Figure 3 COPI coat assembly

Schematic representation of proposed model for COPI coat assembly process. Figure adapted from (Yorimitsu et al. 2014).

1.2 Role of Golgi apparatus in the secretory pathway

The Golgi complex or Golgi apparatus plays a key role in the secretory pathway. It is also a carbohydrate factory, involved in the biosynthesis of glycolipids (Mellman and Simons 1992). Golgi is considered as the main contributor for post-translational modification of lipids and proteins (Potelle, Klein, and Foulquier 2015). The proteins are subjected to post-translational modifications such as glycosylation, phosphorylation, sulphation, proteolytic cleavage and sorted into different cellular destinations at the Golgi (Mellman and Simons 1992). These modifications are required for proper folding of the proteins and to make them functional.

1.3 Structural organisation of the Golgi complex

The Golgi complex is made up of flattened, membrane bound disc like structures called Golgi cisternae (Farquhar and Palade 1981). In most plants, fungi, flies and invertebrates Golgi stacks are distributed in the cytoplasm. In most lower eukaryotes, the Golgi complex consists of one or more discrete Golgi stacks per cell (Lowe 2011). However, some eukaryotic species such as *Saccharomyces cerevisiae* don't have stacked Golgi, instead the individual cisternae are scattered throughout the cytoplasm (Preuss et al. 1992). In higher eukaryotes, these cisternae are arranged on top of each other to form a Golgi stack and in vertebrates the stacks are typically linked to form the Golgi ribbon located in the juxta-nuclear position (Figure 4).

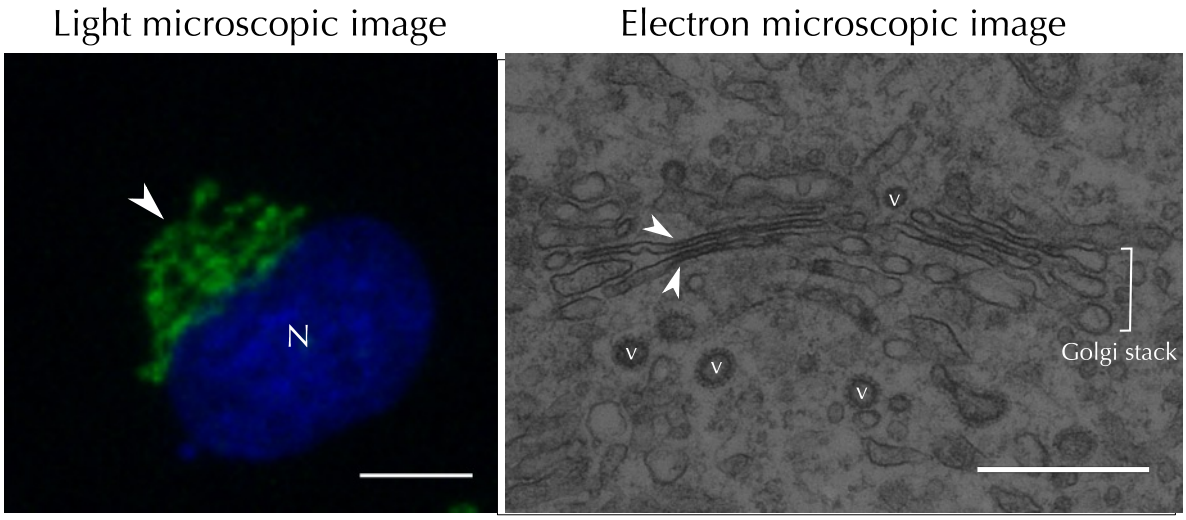

Figure 4 Structural organisation of Golgi

Left panel shows juxta-nuclear Golgi complex (Green) in mammalian cells indicated by an arrow head; N: nucleus. The right panel shows electron microscopic ultra structure of Golgi apparatus with stacks of cisternae linked to form a Golgi ribbon. Arrowheads show individual cisternae and vesicles are indicated with letter v. Scale bars: 10 μm (left) and 500 nm (right) respectively.

The Golgi stack maintains a *cis* to *trans* polarity (Figure 5). The secretory proteins enter the Golgi through its *cis* side and exit through its *trans* side (Dunphy and Rothman 1985). The movement of cargo proteins through the Golgi stack is not clearly understood and has been highly debated. There are different models proposed to explain this process (Glick and Luini 2011). Among them, the cisternal maturation model and the vesicular transport model are two main models. The first model proposes that the Golgi cisternae act as transient compartments for cargo to carry them forward. They are formed by the homotypic fusion of COPII or other ER carriers, gradually mature into a TGN cisterna and finally disintegrate into secretory vesicles or carriers (Bannykh and Balch 1997; Bonfanti et al. 1998; Mironov et al. 2003). The second model proposes that the cisternae are rather stable compartments through which the cargo moves via vesicles (Pfeffer 2010).

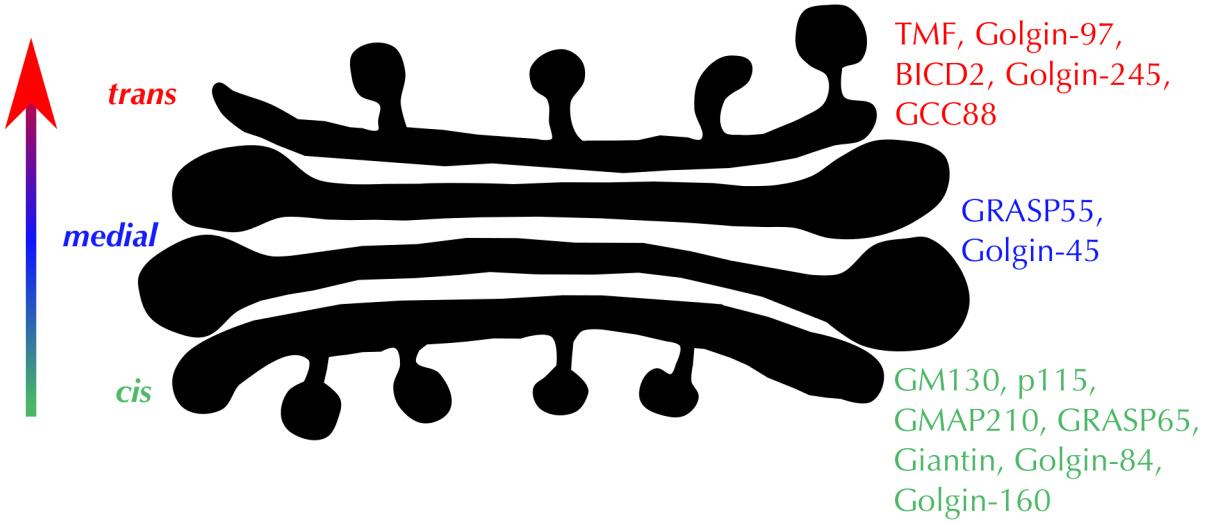

Figure 5 Polarised Golgi stack

Golgi stack shows a *cis* to *trans* polarity. The names on the right hand side are examples of different Golgi proteins and their localisation in the Golgi stack.

1.4 Golgi Proteins

Golgi complex is a highly dynamic organelle and is able to rapidly disassemble and reassemble under physiological conditions, e.g., at the onset and end of mitosis respectively. This suggests the existence of molecular mechanisms to maintain its structure and identity (Ramirez and Lowe 2009). In agreement with this idea, early biochemical and morphological studies detected proteinaceous cross bridges linking adjacent cisternae (Cluett and Brown 1992; Franke et al. 1972; Turner and Whaley 1965). Fractionation experiments revealed detergent-insoluble proteinaceous structure to which Golgi enzymes could attach (Slusarewicz et al. 1994). These insoluble proteinaceous structures were suggested to form a structural scaffold or the Golgi matrix. Some examples of proteins associated with this structural scaffold are GM130, GRASP55 and GRASP65.

Interestingly, the same proteins were found to be accumulated in cytoplasmic punctate structures upon treatment with Brefeldin A (BFA) (Xiang and Wang 2011). BFA is a fungal metabolite that inactivates the small GTPase ADP-ribosylation factor-1 (Arf1), prevents the membrane recruitment of COPI-coat and blocks the protein transport from the ER to the Golgi (Klausner, Donaldson, and Lippincott-Schwartz 1992). BFA treatment results in the disassembly of the Golgi and relocation of the Golgi enzymes

into the ER. The Golgi matrix proteins remain in the cytoplasm as punctate structures (Lippincott-Schwartz et al. 1991) and the Trans Golgi network is redistributed as a tubular network (Klausner et al. 1992; Wei and Seemann 2010). The effects of Brefeldin A treatment are reversible, hence the Golgi complex reforms upon removal of the drug.

1.4.1 Golgi matrix proteins

Several components of this Golgi matrix have been identified. They localise to *cis, medial* or *trans* cisternae of the Golgi. These Golgi matrix proteins include Golgins and GRASPs that play an important role in membrane traffic and structural organization of the Golgi. These proteins are suggested to be important in post-mitotic reassembly and stacking of the Golgi cisternae (Marra et al. 2001).

Golgins are coiled coil proteins, typically anchored to Golgi membranes and mostly present in the *cis, trans* faces and on the rims the Golgi stack. Apart from their Golgi localisation and coiled coil domains, these proteins interact with small GTPases (Sinka et al. 2008). These interactions may promote their recruitment to specific Golgi compartment or regulate their functions. Golgins were first identified in patients suffering from a variety of auto-immune diseases. These proteins form homodimers and attach to the Golgi membranes via their Carboxy terminus (Munro 2011). The rod like structures formed on the surface of Golgi due to the coiled coil domains of Golgins are proposed to be involved in various tethering events. These tethering events include linking of the Golgi cisternae, Golgi stacks, capture of transport intermediates and Golgi elements even over relatively large distances (Waters and Pfeffer 1999). They were also shown to be important in maintaining Golgi integrity. The members of the Golgin family have diverse structure and functions. The following section includes literature results on the proteins studied in this project. Some of them were classified as mammalian Golgins (Barr and Short 2003) (GM130, GRASP55, GRASP65, Giantin and GMAP210) and others were identified as Golgi localized proteins (TMF1 and TMEM165).

1.4.1.1 GM130

GM130 is a coiled coil protein localised to the Golgi complex. It was first detected through antisera raised to detergent and salt resistant matrix fraction from Golgi stacks of rat liver. It was shown to be localised to *cis* Golgi and was proposed to play a role in maintaining *cis* Golgi structure (Nakamura et al. 1995). It was also shown that GM130 together with GRASP65 is necessary for the formation of Golgi ribbon in mammalian cells (Puthenveedu et al. 2006). There is an enormous amount of literature data on diverse roles of GM130 in different cellular processes till date. Some of which propose role of GM130 in tethering COPI coated vesicles to the Golgi via its complex with p115 and Giantin (Alvarez et al. 2001; Linstedt et al. 2000). Other experimental evidence has shown that GM130 is phosphorylated during mitosis and this inhibits its binding to p115 and this process is reversed upon dephosphorylation (Lowe, Gonatas, and Warren 2000). GM130 is also shown to contribute to pericentriolar localization of the Golgi through its interaction with the centrosome, in mammalian cells (Kodani et al. 2009).
Depletion of GM130 has been shown to slow down the ER to Golgi traffic by transport studies using Vesicular Stomatitis Virus G protein (VSVG) *in vivo* (Diao et al. 2008). But this effect was not observed in BSC1 cells with the same transport assay (Tängemo et al. 2011), which implies that this might be cell type specific. GM130 has been proposed to play a role in various other processes such as membrane tethering and fusion (Diao et al. 2008), cell polarization (Baschieri et al. 2015), migration (Nakamura 2010), spindle formation (Wei et al. 2015), autophagy (Chang et al. 2012), centrosome morphology regulation (Kodani and Sütterlin 2008) and also in developmental stages of humans (Shamseldin et al. 2016). Hence there is no coherent view on its role and it is questionable to which extent these are direct functions of GM130. So, despite of various proposed roles of GM130 from literature the precise function of this protein in the Golgi complex is not so clear.

1.4.1.2 GRASP55 and 65

The Golgi Re-Assembly Stacking Protein family (GRASP) includes GRASP65 and GRASP55, the numbers referring to their molecular mass (in KDa) on SDS PAGE. They

were first identified in cell free systems mimicking the mitotic disassembly and re-assembly of Golgi complex (Barr et al. 1997). Based on experiments on cell free systems, they have been proposed to play a crucial role in stacking of Golgi cisternae and regulation of Golgi disassembly and re-assembly during mitosis (Barr et al. 1997; Shorter et al. 1999). Despite of being known for several years, literature results addressing the role of GRASPs are still very contradictory.

GRASP65 was first identified as a target of N-ethylmaleimide (NEM), which prevents the mitotic reassembly of Golgi cisternae into stacked structures (Barr et al. 1997). Later on GRASP55 was also identified as a NEM sensitive membrane protein and is also shown to be required for the stacking of the cisterna (Shorter et al. 1999). It has also been shown that GRASP65 and 55 play an essential complementary role in cisternal stacking.

Experiments performed by microinjection of GRASP65 antibodies into mitotic cells showed a failure to form proper Golgi stacks after cell division. Hence, GRASP65 was proposed to be directly involved in stacking of the Golgi cisternae (Wang et al. 2003a). In support to this finding, it was later shown by another group that the simultaneous double depletion of GRASPs resulted in a complete disassembly of the Golgi. Hence the GRASP55 and 65 were proposed to be involved in Golgi stacking in mammalian cells via a common mechanism (Y. Xiang and Wang 2010). On the contrary, RNAi experiments to deplete GRASP65 or GRASP55 resulted in only a reduction in number of cisternae per stack but the overall organization of Golgi membranes was not affected (Sütterlin et al. 2005). As the microinjection experiments involved IgG antibodies, there is a possibility that they cross-link the Golgi proteins and hence inhibit the disassembly of the Golgi preventing their entry into mitosis. Studies performed later also observed that simultaneous double depletion of GRASP65/55 resulted in disrupted cisternal flatness, not affecting cisternal stacking (Lee et al. 2014). They also observed that simultaneous depletion of GRASP65, GRASP 55 and Golgin 45 led to complete disassembly of Golgi stack and they suggested that the total amount of adhesive energy gluing the cisternae dictates Golgi cisternal stacking irrespective of the molecules involved in the process (Lee et al. 2014).

To better understand the structural role of these proteins, experiments were performed to obtain their crystal structures. The crystal structure showed that both of these proteins contain an N-terminal GRASP domain and two tandem PDZ domains with high sequence homology (Wang, Satoh, and Warren 2005). Further analysis of their crystal structures revealed homotypic interactions where GRASP domain forms a dimer in which peptide binding pockets of the two neighboring PDZ2 domains face each other. These domains are further connected by C-terminal tail of one GRASP domain that inserts into binding pocket of the PDZ1 domain in another dimer (Feng et al. 2013). Biochemical analysis showed that both these contacts are rather weak and are needed in combination for formation of GRASP mediated Golgi stack (Feng et al. 2013). Another study on the crystal structure revealed interaction of GM130 with GRASP65 via the PDZ domains (PDZ1 and PDZ2) of GRASP65. Based on the experimental evidence in this investigation, it was shown that GM130 and GRASP65 are necessary to mediate membrane fusion events occurring during Golgi assembly to form a Golgi ribbon (Hu et al. 2015).

Along with all these conflicting structural roles of GRASPs, there are literature studies suggesting many diverse functions of these proteins. This include their role in regulating spindle dynamics (Sütterlin et al. 2005), controlling cell growth (Sütterlin et al. 2005), establishing cell polarity (Bisel et al. 2008), transport of receptors (D'Angelo et al. 2009) and sorting of cargo (Xiang et al. 2013). Recently, a GRASP65 knockout mice has been generated and there was no evident growth or morphological defects observed (Veenendaal et al. 2014). With this huge amount of contradicting and inconsistent data the precise role of GRASPs is still not clearly understood.

1.4.1.3 GMAP210

GMAP210 (Golgi Microtubule Associated Protein 210) is a peripheral Golgi protein that interacts with microtubules and localises at the *cis* Golgi. It has extensive coiled coil regions and hence belongs to the Golgin family of proteins. Biochemical studies involving lipid membranes have shown that GMAP210 is involved in connecting highly curved liposomes to flatter ones and this asymmetric tethering was relied on motifs that

sense membrane curvature. Hence it is suggested to be highly important to maintain Golgi structure due to rapidly changing membrane curvature during vesicular trafficking (Drin et al. 2008).

It was shown that GMAP210 recruits γ-tubulin containing complexes to the Golgi membranes independent of Golgi localisation within the cell. Over expression of GMAP210 was shown to disrupt the microtubule network and induce fragmentation of the Golgi complex. Hence, it is proposed to participate in the maintenance and structural integrity of Golgi (Infante et al. 1999). However, similar effect of Golgi fragmentation can also observed in cells treated with Nocodazole due to the disruption of microtubules. Hence it is uncertain to what extent this is a direct effect in case of GMAP210.

The role of GMAP210 in anterograde and retrograde trafficking has also been highly debated. One study showed that depletion of GMAP210 disrupts the Golgi ribbon leaving the Golgi stack and trafficking unperturbed (Ríos et al. 2004; Yadav, Puri, and Linstedt 2009), while the other studies reported that its overexpression results in blockage of trafficking (Friggi-Grelin, Rabouille, and Therond 2006; Pernet-Gallay et al. 2002). Another recent study showed that depletion of GMAP210 resulted in loss of Golgi cisternae and accumulation of vesicles (Sato et al. 2014). This protein has also been implicated to play a role in linking the Golgi to the centrosome (Ríos et al. 2004) and ciliogenesis (Follit et al. 2008). Taken together, all the uncertain and conflicting experimental evidence makes the role of this protein still unclear.

1.4.1.4 Giantin/GOLGB1

Giantin was identified as a Golgi localised and well conserved macro Golgin (Seelig et al. 1994) appeared to be an integral component of the Golgi membrane. Based on its localisation and physical properties it is proposed to be involved in forming inter-cisternal cross-bridges of the Golgi (Linstedt and Hauri 1993). Another study showed that Giantin is involved in spatial organisation of the Golgi ribbon instead of stacking. In this study, Giantin was exogenously expressed in Drosophila S2 cells resulting in clustered Golgi stacks similar to mammalian Golgi ribbon (Koreishi et al. 2013).

Apart from the above-mentioned structural roles of Giantin, the following are few other diverse functions proposed in the literature. As mentioned earlier, Giantin was shown to bind p115 and it was found on COPI vesicles which are docked to Golgi via GM130 (on Golgi membranes) and p115 acting as a connecting bridge (Sönnichsen et al. 1998). Golgi is identified as a target organelle for certain clinical conditions such as myopathy (Sahashi et al. 2004), systemic lupus erythematosus and Sjögren's syndrome (Nozawa et al. 2004) due to the presence of auto-antibodies for Giantin in the serum of affected patients. Experimental evidence also shows an important role of Giantin in ciliogenesis (Asante et al. 2013). Due to the lack of proper evidence for the specific role this protein in the Golgi complex, further investigation is necessary to clearly understand its function.

1.4.1.5 TMF/ARA160

TMF/ARA160 (TATA element Modulating Factor) was first identified and characterized as a co-activator for androgen receptor (AR). It was identified in many screens as a putative transcription factor or chromatin-remodelling factor. It was shown to be localised to nucleus and the Golgi complex (Mori and Kato 2002). Later on it was identified as an evolutionarily conserved Golgin. Depletion of TMF through RNAi resulted in dispersal of Golgi membranes around the cell suggesting its role in Golgi organization (Fridmann-Sirkis, Siniossoglou, and Pelham 2004). TMF was also shown to be involved in retrograde trafficking through its interaction with Rab6 (Yamane et al. 2007). *In silico* analysis has shown the association of this protein with microtubules and thus involved in spatial orientation of Golgi (Elkis et al. 2015). This protein is also implicated as an essential regulator for differentiation and maturation of mammalian sperm (Lerer-Goldshtein et al. 2010). Due to lack of enough experimental evidence the role of TMF in the Golgi complex is not fully understood.

1.4.1.6 TMEM165

TMEM165 is a trans-membrane protein that belongs to uncharacterized protein family that are well conserved throughout evolution. Deficiency of this protein causes

Congenital Disorder of Glycosylation (CDG) (Foulquier et al. 2012). The specific role of this protein in the Golgi complex has not been investigated so far.

This protein family share common characteristics with cation/Ca^{2+} exchanger superfamily. Defects in TMEM165 showed an affect on Ca^{2+} and pH homeostasis. Hence, TMEM165 was proposed to be Ca^{2+}/H^{+} antiporter and defects in this protein resulting in Ca^{2+} and pH homeostasis could explain the glycosylation defects (Demaegd et al. 2013). A deep intronic splice mutation of this gene results in a novel type of CDG (TMEM165-CDG) with bone dysplasia as a key feature (Zeevaert et al. 2013). Based on its expression and localisation in lactating mammary gland it was also proposed to act as mammary Golgi calcium transporter (Reinhardt, Lippolis, and Sacco 2014).

1.5 Golgi Biogenesis in Mammalian cells

Golgi is a highly dynamic organelle and it changes its architecture and shape with continuous trafficking events occurring across its compartments. In mammalian cells, during mitosis, the peripheral membrane proteins are released into the cytoplasm, the Golgi ribbon is disassembled and stacks of cisternae are broken down into smaller vesicles. In later stages of mitosis the Golgi is re-assembled and forms a functional Golgi complex in daughter cells. The Golgi disassembly has been proposed to act as a check-point for the cell to enter mitosis and blockage of this process leads to cell cycle arrest in G2 (Colanzi and Corda 2007). The simplest explanation for the necessity of Golgi disassembly during mitosis is to equally distribute the Golgi ribbon among the daughter cells.

1.5.1 Golgi disassembly

The Golgi disassembly process involves unlinking the Golgi ribbon, vesiculation, unstacking of Golgi cisternae (Figure 6b-d), and partitioning of the Golgi into daughter cells (Wang and Seemann 2011). The upper panel of the Figure 6 shows the Golgi disassembly process with images showing the Golgi during interphase, prophase and pro-metaphase (Figure 6a-c). The Golgi fragmentation or ribbon unlinking during mitosis is achieved through Arf1 budding, independent of COPI (Misteli and Warren 1994; Xiang et al. 2007). As mentioned earlier from literature studies, phosphorylation

of GRASP65 and GM130 are necessary for unstacking of Golgi during mitosis. Studies also showed that during mitosis the tethering complex of Giantin-p115-GM130 is disrupted due to phosphorylation of GM130 by Cdk1 and hence vesicles cannot fuse to the target membranes resulting in disruption of Golgi complex (Levine et al. 1996; Lowe et al. 1998). Phosphorylation of GRASP65 is regulated by plk1 and Cdk1 (Lin et al. 2000; Wang et al. 2003b) while GRASP55 is phosphorylated by ERK2 and Cdk1 (Jesch, Lewis, et al. 2001; Yi Xiang and Wang 2010a). Thus the experimental evidence shows that mitotic fragmentation of Golgi is achieved by the phosphorylation action of mitotic kinases, and vesiculation by Arf1 and COPI coat complex (Tang et al. 2008). The vesicles generated during this process are enriched in Golgi enzymes and SNARE proteins.

Upon disassembly into vesicular structures, they are evenly distributed throughout the cytoplasm (Axelsson and Warren 2004; Jesch, Mehta, et al. 2001). At this stage it was also observed that a significant amount of mitotic Golgi membranes localise to spindle poles and associate with astral microtubules (Jokitalo et al. 2001; Seemann et al. 2002; Shima et al. 1998). These mitotic clusters are polarised and *cis*-Golgi proteins are spatially separated from *trans* similar to Golgi organisation in interphase cells (Shima et al. 1997). Experimental evidence also suggests that the spindle plays an important role in partitioning an intact Golgi between daughter cells (Wei and Seemann 2009).

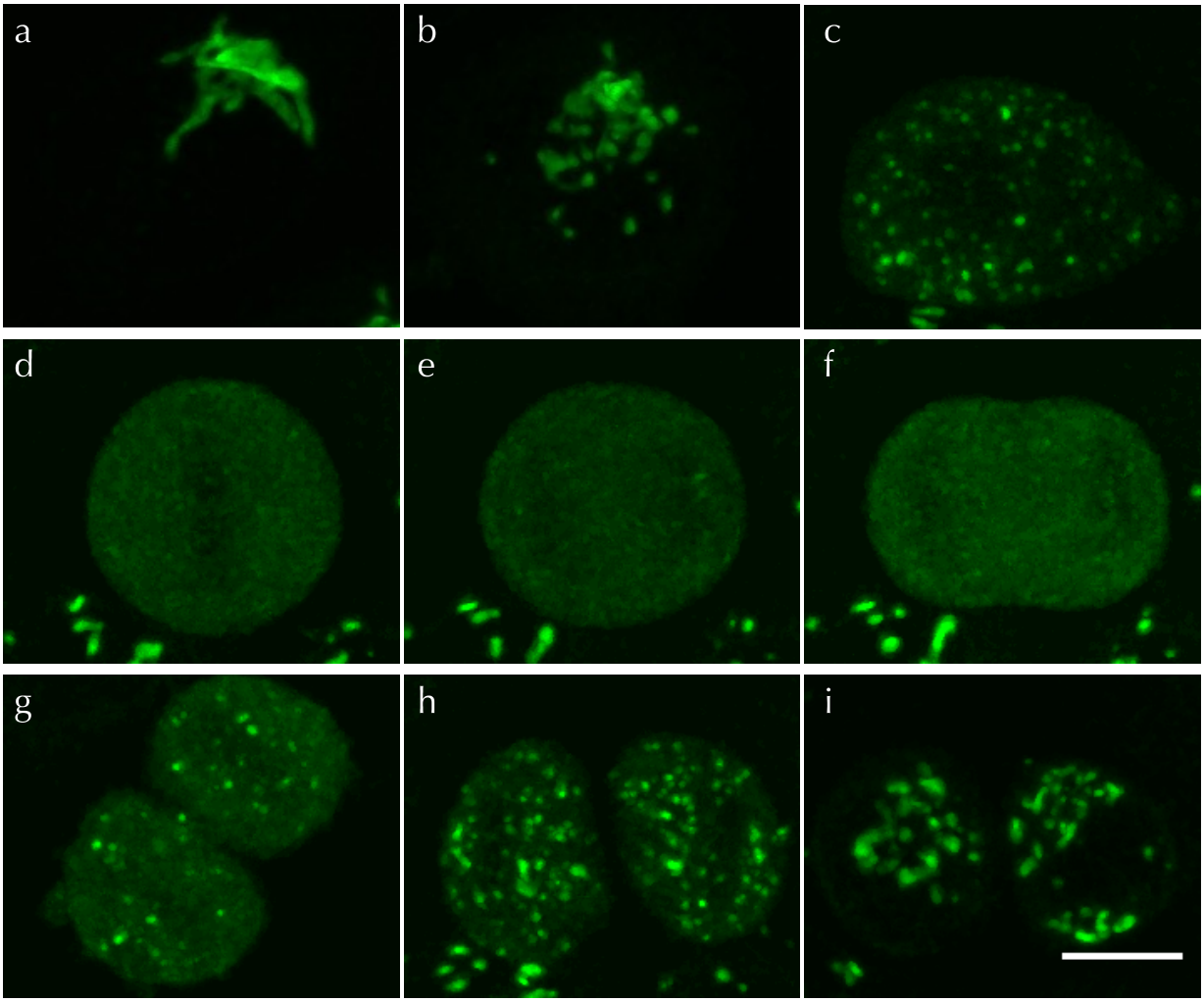

Figure 6 Golgi disassembly and biogenesis during mitosis

Organization of Golgi complex in different stages of mitosis showing Golgi disassembly and re-assembly. The upper panel shows the Golgi ribbon during interphase (a), unlinking of Golgi ribbon during early prophase (b), and prometaphase (c) respectively. The middle panel shows the mitotic haze during metaphase till anaphase (d-f). The lower panel shows Golgi re-assembly during telophase (g) and cytokenisis (h) proceeding towards the interphase (i). Scale bar: 10μm

1.5.2 Golgi biogenesis/re-assembly

Upon segregation into daughter cells, the mitotic Golgi membranes re-assemble during telophase and cytokinesis as shown in the lower panel of Figure 6g-i. Membrane fusion and cisternal stacking mediate the biogenesis/re-assembly process. The membrane fusion was shown to be achieved by SNARE proteins. They assemble on opposite membranes into a SNAREpin complex resulting in membrane fusion (Rothman and Warren 1994; Weber et al. 1998) and formation of Golgi cisternae. Disassembly of SNAREpin complex occurs upon membrane fusion (Müller et al. 1999). The single

cisternae were proposed to form Golgi stacks by de-phosphorylation of Golgi stacking proteins (GRASPs and GM130) mediated by protein phosphatase PP2A (Protein serine/threonine phosphatase type 2A). Despite of all the studies so far and various proteins suggested to be involved in this process, their precise role and detailed molecular mechanism during Golgi biogenesis is still not clearly understood.

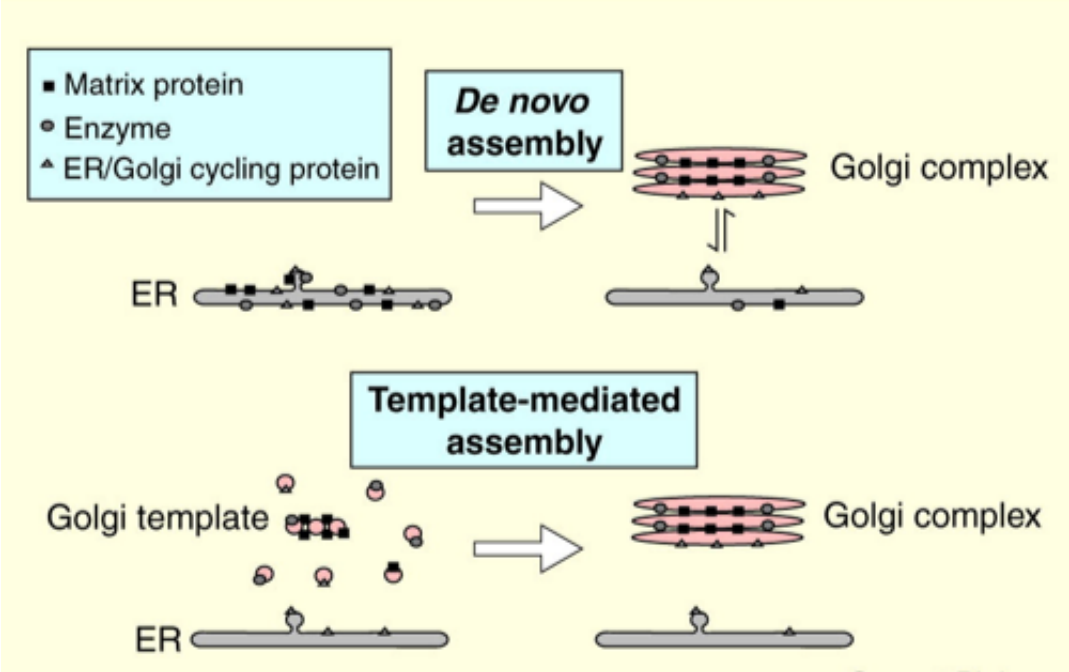

Figure 7 Models of Golgi biogenesis

Schematic representation of two main proposed mechanisms of Golgi re-assembly/biogenesis during mitosis. 1.*De novo* assembly in which Golgi proteins produced from ER can self-organise to form a new Golgi that is in dynamic equilibrium with ER and 2.Template mediated assembly where a new Golgi is produced around a pre-existing template which is independent from the ER (Figure adapted from (Lowe 2002)).

It has been long under debate if the Golgi vesicles remain as independent structures and are stochastically distributed or if they are reabsorbed into the ER and partitioned together with ER during metaphase. Based on the evidence for these two ideas, there are two main proposed mechanisms for Golgi biogenesis, the *de novo* assembly and template-mediated assembly (Barr 2004) (Figure 7).

The template-mediated assembly is based on the hypothesis that these vesicles remain as independent entities and serve as a template for Golgi biogenesis during mitosis (Axelsson and Warren 2004; Jesch, Mehta, et al. 2001; Jesch and Linstedt 1998; Jokitalo et al. 2001; Lucocq and Warren 1987; Terasaki 2000). The *de novo* assembly mechanism suggests that the Golgi biogenesis occurs through ER derived material that is

incorporated to form a new Golgi in the daughter cells (Thyberg and Moskalewski 1992; Zaal et al. 1999).

1.5.3 Experimental approaches to study Golgi biogenesis

The dynamic nature of Golgi complex allows it to rapidly change its morphology upon treatment with certain chemicals or molecular tools. And mostly these processes are reversible and can restore a functional Golgi with its original morphology. Hence these approaches have been used as a complement to mitosis, to study Golgi disassembly and re-assembly.

1.5.3.1 Chemical approaches

To address the question of possible template-mediated or *de novo* Golgi biogenesis, several approaches using chemical treatments have been used. One of them is treatment with Brefeldin A (BFA), which results in the disassembly of the Golgi and re-absorption of Golgi enzymes in the ER. The Golgi matrix proteins remain however in the cytoplasm as punctate structures. Upon washing out the drug, the Golgi is re-assembled again forming a fully functional and intact Golgi (Kasap et al. 2004; Lippincott-Schwartz et al. 1989; Puri and Linstedt 2003). These findings have been proposed to be consistent with the *de novo* Golgi biogenesis. But as the Golgi matrix remnants remain scattered all over the cytoplasm (Seemann et al. 2000), it can also be possible that these Golgi remnants act as a template for Golgi biogenesis.

Later on, experiments were performed with H89 in combination with BFA to inhibit COPII recruitment resulting in redistribution of Golgi matrix proteins into the ER (Puri and Linstedt 2003) in addition to the Golgi enzymes. The matrix proteins showed a faster exit from the ER upon washing out the drugs. As the Golgi matrix proteins (BFA remnants) were sensitive to ER blockage by H89 and re-emerge at faster rates, it was suggested that they cycle via the ER to the Golgi complex (Puri and Linstedt 2003), hence favouring the *de novo* biogenesis.

Another chemical approach to address the question of Golgi biogenesis was using Nocodazole treatment. Nocodazole treatment of mammalian cells results in depolymerisation of microtubules and Golgi proteins are re-distributed into peripheral

mini-stacks. This has been proposed to occur via the ER and would thus provide evidence for Golgi *de novo* biogenesis (Cole et al. 1996). Another experimental approach used chemical inactivation of the Golgi in intact cells (Jollivet et al. 2007). Experimental results in this case showed the formation of a new Golgi-like structure but it could not acquire a normal Golgi architecture and function. Therefore template mediated Golgi biogenesis was favoured by this study.

1.5.3.2 Laser nanosurgery approach to study Golgi biogenesis

In mammalian cells, the Golgi is present in a very close proximity to the nucleus making it almost impossible to deplete it from cells without damaging the cell and nucleus. Hence, different chemical approaches (BFA, Nocodazole etc.,) mentioned earlier were used to address the question of Golgi biogenesis. The common drawback of these approaches is the inability to completely deplete the Golgi and its remnants from living cells. These methods can alter the distribution of the proteins or morphology of Golgi but are not well suited to address the question of *de novo* Golgi biogenesis. Hence, to address this question of Golgi biogenesis, our lab has developed a laser nanosurgery method to deplete the Golgi from intact cells and follow the karyoplasts using time-lapse microscopy to see if it can synthesise a new Golgi (Tängemo et al. 2011).

The Golgi is depleted by severing actin stress fibres leading to retraction of the plasma membrane and finally dissection of the cell into a karyoplast and Golgiplast (Figure 8). The karyoplasts didn't show any Golgi like structures or stacked cisternae both in light and electron microscopy analysis (Tängemo et al. 2011). Except centrioles all other membrane organelles of the early secretory pathway including ER exit sites were detected in the karyoplasts (Tängemo et al. 2011).

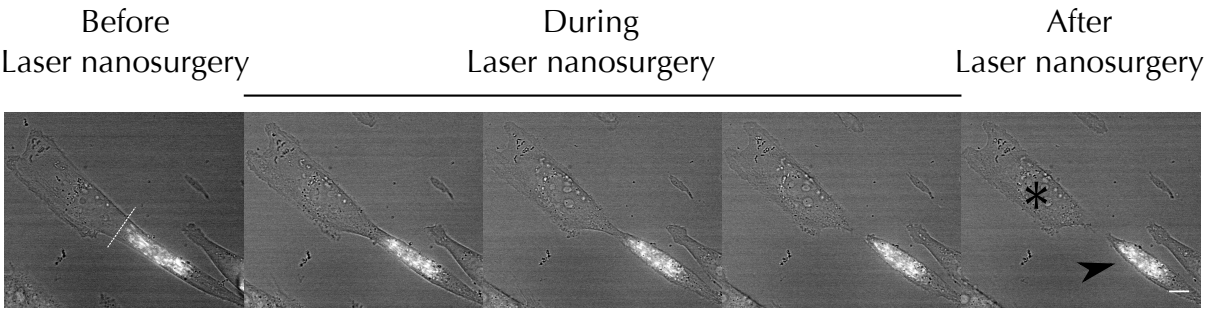

Figure 8 Laser nanosurgery approach

The panel of images show the cell subjected to laser nanosurgery. The dotted line indicates site of the laser nanosurgery. The Golgi complex is shown in white (GalT-GFP). Asterisk indicates the resulting karyoplast and arrowhead indicates Golgiplast upon laser nanosurgery.

Discrete structures with GFP tagged Golgi protein appeared at 6 hr and later after the nano-surgery acting as transport carriers (Tängemo et al. 2011). At later time points, these structures started to cluster at the juxta nuclear region and colocalised with Golgi markers such as GM130, TGN46 and Giantin. Electron microscopic analysis of the karyoplasts at 12 hr or later after laser nanosurgery showed either dispersed ministacks or normal sized Golgi stacks. The newly synthesised Golgi was fully functional and transport competent. This provides strong evidence that *de novo* Golgi biogenesis can occur in mammalian cells (Tängemo et al. 2011).

1.5.3.2.1 Detailed time-lapse analysis of Golgi biogenesis

To understand the integration of dynamic processes such as ER export, Golgi formation and organization of microtubule network, a detailed time-lapse analysis of the *de novo* Golgi biogenesis after laser nanosurgery was performed.

The quantitative analysis of Golgi biogenesis with high temporal resolution in several cells revealed three distinct phases of this process (Ronchi et al. 2014). In phase 1 the there was a steady increase in the fluorescence intensity (FI) of YFP-tagged Golgi enzyme marker in the ER (of karyoplast) along with small post-ER carriers being produced occasionally. At the ultra structural level, there was no evidence of any stacked Golgi like structures at this stage. The carriers produced in phase 1 were not very stable and they disappeared within few minutes of their formation (Figure 9). During the transition from phase 1 to phase 2, these small post-ER carriers collided and

fused with each other occasionally, resulting in the formation of more stable and larger structures (Ronchi et al. 2014).

In phase 2, these structures further grew in size with exponential kinetics and started to attract and fuse with other smaller structures (Figure 9). Correlative Light and Electron Microscopic (CLEM) analysis showed larger structures formed during this phase did not show a typical Golgi like ultrastructure. Instead, they were clusters of juxtaposed membrane bound structures, which appeared to be convoluted and compact. Some structures in the cluster were starting to flatten acquiring cisternae like shapes indicative of the beginning of a stacking process.

In phase 3, the larger structures that had formed during phase 2 clustered into a single structure at the juxta-nuclear location (Figure 9). CLEM analysis showed clusters of ministacks in phase 3 in contrast to Golgi ribbons in control cells. Based on the electron microscopic analysis, the formation of a stacked Golgi occurs by remodelling interconnected membrane precursor structures from phase 2.

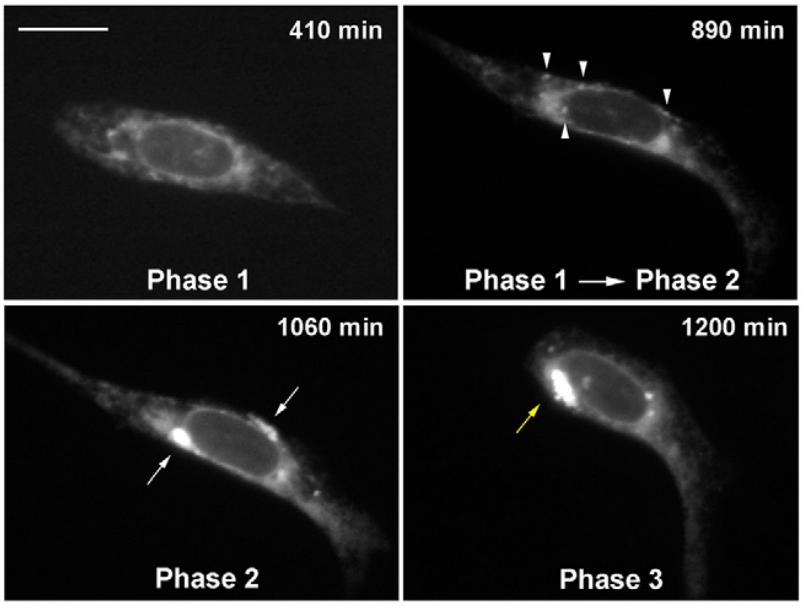

Figure 9 Time-lapse characterisation of *de novo* Golgi biogenesis

YT2 cells were subjected to laser nanosurgery to remove the Golgi. Golgi biogenesis was then followed in the karyoplast by time-lapse microscopy. The images show an example of Golgi biogenesis followed at 2 min time intervals. The four characteristic time points from the time-lapse are shown. Phase 1 shows a steady state accumulation of Golgi marker in the ER. During the transition between phase 1 and phase 2, post ER structures were clearly visible over the ER background (marked with arrowheads). In phase 2, Golgi precursors become larger and brighter (white arrows). In phase 3, all the post-ER material cluster at a single perinuclear position (yellow arrow). Scale bar: 20μm. Figure taken from (Ronchi et al. 2014).

1.5.3.2.2 Dynamics and molecular composition during Golgi biogenesis

The molecular composition of the Golgi precursors was assessed, by labelling different Golgi proteins at different phases of the Golgi biogenesis. The data suggests that different proteins associate with Golgi precursors at different time points and hence might contribute to different steps in the process (Ronchi et al. 2014). It was also observed that the Golgi matrix proteins appear much earlier than the endogenous Golgi enzymes during Golgi biogenesis (Tängemo et al. 2011). Also the levels of Golgi matrix proteins tested were dependent on the stage of the Golgi biogenesis. For example, in phase 2, levels of GM130, GRASP65, GRASP55 and CLASP2 were present in higher amounts compared to Giantin and AKAP9, which still remained low (Ronchi et al. 2014).

2 Aims

The question of key molecular regulators in the Golgi biogenesis process and their roles is still unclear. Despite of a number of Golgi proteins being known, their role and importance in Golgi biogenesis is far from being clearly understood.

Here, I took advantage of our laser nanosurgery approach to achieve an acute and apparently complete depletion of the Golgi and its associated proteins. To prevent their subsequent re-synthesis during Golgi biogenesis and to understand their involvement in the biogenesis process, I used siRNA treatments in combination. With this experimental approach the main goal of my PhD project was to identify key molecular regulators and their roles in the Golgi biogenesis process.

The following are specific questions I addressed in this thesis:

1. Identify new promising candidates playing an important role in Golgi biogenesis, in addition to established Golgi matrix proteins.
2. Test whether the acute depletion of selected candidates by nanosurgery and siRNA mediated inhibition of their re-synthesis affects the Golgi biogenesis process.
3. If so, what could be the possible mechanisms by which these proteins regulate Golgi biogenesis?

3 Results

3.1 Experimental approach to identify the regulators of Golgi biogenesis

The outline of the project and experimental approach is shown in Figure 10.

3.1.1 Classification of Golgi localised proteins using Brefeldin A treatment

In order to identify the potential regulators of Golgi biogenesis process, I took advantage of the Human Protein Atlas (HPA) database (Berglund et al. 2008) that comprises information on spatial distribution of most of the proteins in the human genome. It also contains Immuno-Fluorescence (IF) images showing their localisation in three different cell lines. A list of 500 Golgi localised proteins was obtained from the HPA database. This list also includes proteins with additional localisations like cytoplasm, nucleus or other organelles apart from their Golgi localisation.

These proteins with additional localisations can possibly be cargo proteins, travelling through the secretory pathway. Hence these proteins might not play a critical role in the Golgi biogenesis process. Also, the experimental approach we use to identify the role of the candidate proteins is laser nanosurgery in combination with RNAi to achieve an acute depletion of the protein. This approach can be used to acutely deplete proteins only that are exclusively localised to Golgi. So our main selection criterion to shortlist the candidate proteins (from the list of 500 proteins) was to choose proteins exclusively localised to the Golgi. This was done to filter out any cargo proteins that might be travelling through the Golgi (hence localised to the Golgi and elsewhere) and to ensure the acute depletion of the selected protein by our experimental approach. Among the 500 proteins in the list, only 76 proteins were annotated to be exclusively Golgi localised in all the three cell lines. This list was further validated and assessed by looking at the IF images of each of them as they are available at the HPA data base and excluding proteins with additional localisations. Some of the proteins that had conflicting results from different experiments regarding their localisation were also excluded from the list.

Only a final list of 31 Golgi proteins was made, as there was limited availability of antibodies for other candidates. The list includes well known to unknown Golgi proteins. Our list also includes less well-characterized proteins containing structural domains that might be important for the Golgi biogenesis process. The list includes peripheral Golgi proteins containing trans-membrane and integral membrane domains (GMAP210, TMEM165, TMCO3, GOLIM4, GOLM1, GOLGB1, SYNGR2, TMED10), coiled coil domains (GM130, CCDC146, AKAP9, SNAPIN), Golgins and Golgi structural proteins (GM130, GRASP65, GRASP55, TMF1, GOLGA5, BICD2, USO1, GCC1, COG8). I also included uncharacterized proteins in the context of Golgi (TMEM165, CCDC146, TMCO3, DENN4DB, PLEKHA3), few known and unknown enzymes localised to the Golgi (B4GalT, GalNT2, MANEA, GAK, DYRK4). I performed an Immuno-staining with the antibodies for all these proteins and confirmed their exclusive Golgi localisation.

Golgi proteins have been classified into different categories based on their structure and function. In particular, previous studies have shown that a number of proteins are detergent insoluble and remain associated to the Golgi upon detergent treatment. Hence, these proteins were suggested to form a scaffold or Golgi matrix (Cluett and Brown 1992; Franke et al. 1972; Slusarewicz et al. 1994; Turner and Whaley 1965). Several studies over the years have attributed to the structural role of many of these proteins. Interestingly, the same proteins were found to be accumulated in cytoplasmic punctate structures upon treatment with Brefeldin A (BFA) (Xiang and Wang 2011). Along with Golgi matrix proteins, the Trans-Golgi Network (TGN) associated proteins were also remnants of the Golgi upon BFA treatment. The Golgi matrix proteins were localised as punctate structures in the cytoplasm and TGN associated proteins were localised at the TGN while Golgi enzymes were completely redistributed in the ER (Klausner et al. 1992; Wei and Seemann 2010).

The Golgi remnants are definitely part of the Golgi (unlike cargo proteins), and might play an important role in Golgi biogenesis. So our working hypothesis is that the remnants of Golgi upon BFA treatment might be important for the formation of a functional Golgi. Hence, to identify the proteins showing similar localisations to Golgi

matrix and TGN, I performed BFA treatment and classified the proteins into three different groups. To achieve this, I treated the cells with BFA for 30 min to disassemble the Golgi and looked at the localisations of the selected proteins. The Table 3.1 below shows the classification of Golgi proteins based on their localisation upon BFA treatment.

Class I	**Class II**	**Class III**
GMAP210	TMCO3	TMF1
GRASP65	GOLGA5	Giantin
GRASP55	GOLIM4	GOLM1
TMEM165	B4GalT1	MANEA
GM130	GalNT2	CCDC146
USO1	BICD2	AKAP9
COG8	GCC1	SYNGR2
RASGEF1A	BET1L	ACBD3
	DENND4B	GAK
	SNAPIN	PDE4DIP
	PLEKHA3	
	DYRK4	
	TMED10	

Table 3.1 Classification of Golgi proteins upon BFA treatment

The selected Golgi proteins were classified into different groups based on their behaviour upon BFA treatment.

The proteins behaving like Golgi matrix that were re-distributed in cytoplasm as clear punctate structures upon BFA treatment were grouped as Class I (Figure 11). The proteins that were exclusively or mostly localised in the ER like structures were grouped into Class II (Figure 12). Interestingly, I also identified few proteins showing a centrosome-like localisation upon BFA treatment (Figure 13). The proteins that were localised at the TGN or at centrosome like structures were grouped into Class III (Figure 13). Proteins CCDC146, GOLM1, GAK and MANEA showed a centrosome-like

localisation upon BFA treatment. The remaining proteins in this group showed either TGN or centrosome-like localisations using different fixation methods.

According to our hypothesis, the roles of Class I and Class III proteins were further investigated using laser nanosurgery and RNAi.

3.1.2 A combinatory approach: RNAi and laser nanosurgery

I used a combinatory approach of RNAi with laser nanosurgery to achieve an acute depletion of Golgi proteins of interest. Laser nanosurgery is used to deplete the Golgi and all its associated proteins from the cell and RNAi is performed to inhibit the re-synthesis of the protein of interest. It has been shown by our lab that the Golgi can be synthesized *de novo* upon its depletion by laser nanosurgery (Tängemo et al. 2011). Hence the combination of these two approaches allows us to achieve an acute depletion of the protein of interest and follow the Golgi biogenesis process in its absence. We hypothesize that the acute depletion of key regulators of Golgi biogenesis may result in changes in kinetics of the process or in ultra structure of the Golgi. Hence, to identify the effect of specific protein depletion, the Golgi biogenesis process was followed by time-lapse imaging and the final Golgi structure was observed using Correlative Light and Electron Microscopy (CLEM).

To achieve this, the first step is to treat cells with siRNA for specific protein and deplete the Golgi from the cell using laser nanosurgery. In order to deplete Golgi from cells, they need to be seeded on coverslips coated with fibronectin lines. This allows the cells to stretch and move along lines, resulting in displacement of Golgi from the nucleus (Tängemo et al. 2011). The cells were then treated with siRNA targeting the specific genes of interest and subjected to laser nanosurgery to deplete Golgi.

To be able to find back the same cells for time-lapse imaging, we inscribe a pattern inside glass coverslip around the cell of interest using a 355 nm UV laser (see Methods section). The inscription is performed several microns below the sample (inside the glass) to ensure that it doesn't affect the cells.

At the end of time-lapse imaging the cells need to be processed for EM. This involves a series a steps using various chemicals and finally embedding the cells into a resin. The

orientation of the coverslip and the approximate position of the cells can be very easily lost during this process. Also the inscribed pattern will not be visible after flat embedding of the sample for EM, as it was inscribed inside the glass coverslip and not on the surface. And at the end of this process it will be very tedious and almost impossible to find back the same cell unless we have markings on the surface of the coverslip to do so. Hence, to find back the cell at electron microscopic level, a protocol was developed and optimised by our lab for Correlative Light and Electron Microscopy (CLEM) (see 7.3.8). To describe the method briefly, after fixation of cells for EM, their position was traced back using inscribed pattern inside the coverslip and the time-lapse imaging data. High-energy UV laser pulses were used to remove or etch the surface of the coverslip on both sides of the cell of interest. These etched marks were then used for locating the cells in the resin or epon and were further processed to obtain serial sections of the entire cell. Thus CLEM was used to observe the ultra structure of Golgi upon depletion of protein candidates, during or after Golgi biogenesis.

3.2 Validating the depletion of candidate proteins upon RNAi and laser nanosurgery

To validate the acute depletion of the candidate proteins, the amount of protein in the Golgi depleted cells was compared to the neighbouring control cells after the Golgi biogenesis. It should be noted that the neighbouring control cells in this case were also treated with siRNA simultaneously as the Golgi depleted cells. Hence the amount of protein in the control cells will also be reduced, by the end of the experiments (typically 20-22 hr after nanosurgery).

As mentioned in 3.1.1 I chose the proteins from Class I and Class III to perform laser nanosurgery experiments in combination with RNAi. The BSC1-GalT GFP cell lines were optimized in the lab for laser nanosurgery experiments. As their genome was not fully sequenced, I designed 2 siRNAs per protein for all the proteins under view, based on human gene sequences. Among the 17 proteins tested 7 (GM130, GRASP55, GRASP65, GMAP210, TMEM165, TMF1 and GOLGB1) of them showed a clear knockdown by IF (data not shown). So I started the laser nanosurgery experiments with

these 7 candidate proteins. Proteins from the Class I (GRASP55, GRASP65, GMAP210 and TMEM165) and Class III (TMF1 and GOLGB1) were depleted individually. Cells were treated with the siRNA to inhibit the synthesis of new protein and the Golgi was depleted.

The cells were fixed and labelled for the depleted proteins 20-22 hr after the Golgi biogenesis to validate their depletion. The IF images showed an acute depletion of the candidate proteins in Golgi depleted cells compared to the neighbouring control cells in which the Golgi was not depleted (Figure 14). It must be noted that the amount of protein in the neighbouring control cells will also be reduced at this stage due to siRNA treatment.

All the knockdowns showed an acute depletion of the protein when compared with their neighbouring control cells after Golgi biogenesis. The double knockdown of GRASP55 and 65 also showed an acute depletion of the two proteins (Figure 14). Despite of the depletion, the Golgi or a Golgi like structure was reformed in the karyoplast after the Golgi biogenesis in all the cases (Figure 14).

3.3 Ultrastructure of the Golgi after Golgi biogenesis

Despite of the successful reformation of the Golgi or a Golgi like structure, as judged by light microscopy, there might be perturbations in the Golgi structure after Golgi biogenesis upon depletion of the candidate proteins. To check whether the ultra structure of the Golgi is not perturbed and the Golgi is properly stacked, I looked at the ultra structure using Correlative Light and Electron Microscopy (CLEM).

I used CLEM as mentioned earlier to find back the cells by etching the glass coverslip around the cells of interest, post fixation. The cells were fixed upon 20-22 hr after laser nanosurgery and subjected to chemical fixation for EM.

The Golgi ultra structure of all the control cells treated with Neg9 siRNA upon laser nanosurgery and Golgi biogenesis showed a clearly stacked Golgi structure (Figure 15). However, most of them represented Golgi mini-stacks and not a clear Golgi ribbon as observed in case of untreated cells. The depletion of different individual proteins also showed a similar Golgi morphology either with stacked cisternae or Golgi ribbon

(Figure 15). Interestingly, the depletion of TMEM165 showed an accumulation of lipid droplet like structures after the Golgi biogenesis in 3 out of 5 cells imaged (Figure 16). The reasons for this accumulation were not further investigated, as it didn't affect the Golgi biogenesis and stacking. The depletion of individual proteins did not show any evident changes in the Golgi morphology. Hence, I performed double depletions of candidate proteins to see if this has an effect on the Golgi ultrastructure.

A stacked Golgi was formed in all the cases including the double depletion of GRASP55 and 65 (Figure 15). But the double depletion of GRASP55 and 65 showed swollen cisternae (Figure 15). To quantify this effect the maximum luminal width of the Golgi cisternae was quantified in 6 control cells and 5 cells depleted for GRASP55 and 65 using ImageJ. There was a 3.5 fold increase in the luminal width of the cisternae in GRASP double depletion compared to the control cells (Table 3.2).

3.4 Time-lapse analysis of Golgi biogenesis

3.4.1 Kinetics of Golgi biogenesis

To quantify and compare the kinetics of the Golgi biogenesis upon depletion of protein candidates systematically, we used Cell Profiler and MatLab (see Methods section). Cell Profiler was used to segment and measure the fluorescence intensities (FIs) of the post-ER structures or Golgi precursors throughout the time-lapse movie for each cell. Firstly, to segment the post-ER structures produced during Golgi biogenesis, the Golgi depleted cell of interest must be identified throughout the time-lapse movie. This was done manually by drawing a mask around the cell of interest (cell mask) through the entire time-lapse movie (Figure 17). As the background intensity varied between different time-lapse movies, a background subtraction was performed for individual time-lapse movies. This was done by drawing a background mask (in the area without any cells), through the entire time-lapse movie.

Dynamic background subtraction per object was used as a thresholding method to segment the post-ER structures for the individual frames in the time-lapse movie (Figure 17). The total integrated FI (TIFI) of the segmented post-ER structures was measured. The segmentation results were compared to the time-lapse movies as a

quality control to ensure proper analysis. To compare the data between different cells and conditions, the TIFI of the Golgi precursors was normalised to its maximum value in each time-lapse movie. Then, the normalised TIFIs of the Golgi precursors were plotted with respect to time (time-lapse curve) (Figure 18). The quantitative analysis of time-lapse curves from several cells showed three distinct phases in the Golgi biogenesis (Figure 18) as also seen before (Ronchi et al. 2014).

Upon comparing the time-lapse movies with their corresponding time-lapse curves, I observed that different phases of Golgi biogenesis correspond to different slopes of the plot over time. Changes in the TIFI slopes correspond to the changes of its time derivative values. Hence, to approximate the numerical derivative of these noisy time-lapse curves I used total-variation regularisation algorithm (Chartrand 2011) implemented in MatLab, that eliminates the impact of stochastic noise on calculated derivatives. Processing quantified time-lapse TIFIs of Golgi precursors from individual cells with this algorithm resulted in derivative functions that exhibit sharp jumps at time points where original time-lapse curves change their growth rates (Figure 18b). First switching point (T1) typically corresponded to the switch from low (lag phase 1) to high (phase 2) derivative values (Figure 18a). At the second switching point (T2) derivatives became smaller, that corresponded to the switch from fast growing phase 2 to saturation at phase 3 (Figure 18a). To identify these special switching time points (T1 and T2) from the time-lapse curves we used edge detection analysis for estimated derivative functions (Canny 1986). The duration of phase 1 is calculated from T1 and the duration of phase 2 is calculated as the difference between T2 and T1. To check how well selected numerical differentiation procedure approximates growth of quantified intensity curves, I performed integration of calculated derivative functions and plotted integrated curves over original data (thick blue line in Figure 18a). In a very few cases the GFP signal was very weak and data was very noisy and hence the switching points T1 and T2 could not be properly identified, hence this data was not considered. A few examples of time-lapse curves obtained from control cells and GRASP65 & 55 double depleted cells are shown in Figure 19.

The duration of phase 1 and phase 2 was acquired from 10 cells per condition with different protein depletions. The results of the analysis did not show any significant delay in phase 1 of Golgi biogenesis upon depletion of individual Golgi proteins, compared to the control cells (Figure 21). However, there was an acceleration of 2.6 hr (mean value) in the duration of phase 1, upon single depletion of GMAP210 (p value = 0.036). The double depletions of GRASP65 & 55 (p value = 0.0046) and GRASP65 & Giantin (p value = 0.005) resulted in 5.45 hr and 4.38 hr (mean values) delay in phase 1 of Golgi biogenesis, respectively (Figure 21). There was no significant delay or acceleration in phase 2 upon depletion of the candidate proteins (Figure 22).

3.5 Ultra structure of Golgi precursors in GRASP55/65 depleted cells

Next, I wanted to look whether there is any difference in the intermediate structures during Golgi biogenesis upon double depletion of GRASP65 & 55 compared to control cells. So I performed CLEM during the initial stages of Golgi biogenesis, where I observed a delay in the kinetics upon GRASP double depletion. To do this I fixed the cells when I started to see the appearance of many individual Golgi precursors, which marks the transition between phase 1 and phase 2. I obtained data from a total of 4 cells, 2 from double depletion (GRASP65 & 55) and 2 from control in their transition from phase 1 to 2. I observed that the control cells showed clear Golgi intermediates which were membrane bound compact and convoluted structures as reported earlier (Ronchi et al. 2014). I could not observe these structures in the GRASP55/65 double depleted cells both in transition from phase 1 to 2 (Figure 20) and 2 to 3. In GRASP55/65 double depleted cells, I only observed an accumulation of post ER material and some membrane bound cisternae like structures instead of clear intermediates (Figure 20). This suggests the delay in their formation or inability to form these intermediate structures that are necessary for maturation of Golgi precursors into a proper Golgi stack. These results also support the role of GRASP65 and 55 in earlier phases of Golgi biogenesis, which can be the reason for unflat cisternae in the Golgi ultrastructure at the end of Golgi biogenesis (Figure 15).

3.6 VSVG assay to check the efficiency of the cargo transport from ER to Golgi

To test if the delay in the Golgi biogenesis upon knockdown of GRASP55 and GRASP65 could be due to delay in the ER export, I performed a quantitative ER to Golgi VSVG transport assay. This assay is a well-established method in our lab that uses the temperature sensitive viral membrane protein tsO45G to study the efficiency of cargo transport from the ER. At non-permissive temperature 39.5 °C tsO45G accumulates in the ER and at 31.5 °C, it is transported along the Golgi to the plasma membrane.

The BSC1-GalT cells were transfected with either control siRNA or GRASP65 and GRASP55 siRNA for 48 hrs. The cells are then infected with an adenovirus expressing YFP-tagged ts045G for 1 hr at 37 °C and then upon washing and removal of the virus they are transferred to 39.5 °C and incubated for 16-18 hr.

To study the efficiency of VSVG cargo export from ER to Golgi, it is necessary to identify a time-point where a moderate amount of protein reaches the Golgi, not completely saturating it nor allowing it to reach plasma membrane. To identify this time point, we performed a time-course and looked at the localisation of the protein after its release from the ER in BSC1-GalT cells (Figure 23). Based on these results, I chose 20 min time point for the experiments, as most of the protein localised to the Golgi with a small fraction in the ER and none at the plasma membrane. I performed the VSVG assay in control cells (Neg9) and in cells treated with GRASP65 and 55 siRNA. In order to segment and measure the amount of protein in the Golgi channel, the cells labelled for Golgi marker protein (GM130) after fixation. The integrated FI of the VSVG in the total cell and the Golgi was measured (using the Golgi mask) were measured. The ratio of integrated FI of the Golgi to integrated FI of the total cell were normalised to the zero time point (t0) of the respective depletions. The results are plotted as a box plot and each point represents the ratio of an individual cell and dot in the centre of the boxplot represents the mean value (Figure 24). The results of the experiment show that there is no significant delay in the transport of the cargo from ER

to Golgi in GRASP55/65 double knockdown cells compared to control cells (Figure 24). These results suggest that the ER to Golgi traffic is not affected by double depletion of GRASP65 and 55. So the delay in the Golgi biogenesis, as described above (3.4.1), might be due to the improper tethering and stabilization of the Golgi precursors that occur during the phase 1.

3.7 Duration of phase 1 in mitotic cells upon double knockdown of GRASPs

To check the effect of double depletion of GRASPs under physiological conditions, we followed the Golgi biogenesis in cells undergoing mitosis. To do this, I performed time-lapse imaging of mitotic cells treated for 72 hr with either control siRNA or siRNAs for GRASP55/65 (Figure 25). To identify the mitotic cells for imaging HeLa cells stably expressing H2B-mCherry (DNA) and GalNacT2-GFP (Golgi) were used and adaptive feedback microscopy was used to automatically pick mitotic cells in pro-metaphase (see 7.3.7).

The microscope was set up to acquire low-resolution pre-scan images (1X zoom), which are analysed online using the Cell cognition software package. The software uses a classifier to identify mitotic cells that has previously been trained by a training image set. Once a pro-metaphase cell is identified the software acquires high-resolution images (4X zoom) of H2B-mCherry and GalNacT2-GFP for an hour by taking z-stacks covering the entire cell, every 2.5 min.

In cells identified during pro-metaphase, the Golgi starts to disassemble and the Golgi fragments disappear into the mitotic haze during metaphase. At later time-points during mitosis (anaphase to telophase transition), the Golgi precursors reappear to form an intact Golgi in the daughter cells (Figure 25). To analyse the kinetics of Golgi re-appearance, Golgi structures were segmented throughout the time-lapse series by cell profiler and their integrated intensities plotted versus time. The time-lapse data showed similar behaviour to *de novo* Golgi biogenesis upon laser nanosurgery as shown earlier (Figure 26). The duration of phase 1 is calculated as the time between the disappearance of the Golgi fragments during metaphase and their re-appearance during the transition

between anaphase and telophase. As the Golgi biogenesis in mitotic cells occurs in less than an hour, even at 2.5 min resolution time-lapse movies had much less number of frames compared to nanosurgery experiments and the data was less noisy (Figure 26). So I only used edge detection analysis directly on the estimated normalised TIFIs of individual cells to identify the switching points T1 and T2, in this case identifying the disappearance (as a sudden drop in normalised TIFI) and re-appearance (as a sharp increase in normalised TIFI of Golgi precursors) of the Golgi complex (Figure 26). The duration of phase 1 was calculated as the difference between T2 and T1.

The phase 2 in mitotic cells is very short (only a few minutes), as all the Golgi precursors start to appear almost at once, fuse and give rise to a complete Golgi in daughter cells and this can be seen as a steep increase in normalised TIFI in Figure 26. The time scale of the whole process is very short (~ 1 hr) as expected. Data was obtained from 15 cells per condition and the normalised FITI of the Golgi precursors was plotted with respect to time and duration of phase 1 was extracted (Figure 26).

The average time taken for the mitosis (from pro-metaphase till the end of telophase) in the control cells was 49.5±2.1 min and in GRASP 65 & 55 knockdown was 46.6±2.6 min. This suggests that knockdown of GRASPs doesn't effect the duration of mitosis significantly. In the high resolution imaged fields containing 5-10 cells per field, there were 1-2 cells undergoing mitosis every hour. So the average percentage of mitotic cells found every hour in the high resolution imaged field in control cells was 20.39±3.12% and in GRASP double knockdown was 23.6±4.4%.

This shows that the GRASP double depletion also didn't affect the frequency of mitosis or number of cells going into mitosis. These results suggest that GRASP65 & 55 are not crucial for the cells to enter mitosis. The average duration of phase 1 in control condition was 37.3±1.7 min and for GRASP double knockdown was 37.5±2.85 min. So there was also no significant difference of time taken for phase 1 between the control and the GRASP65 & 55 double knockdown (Figure 27).

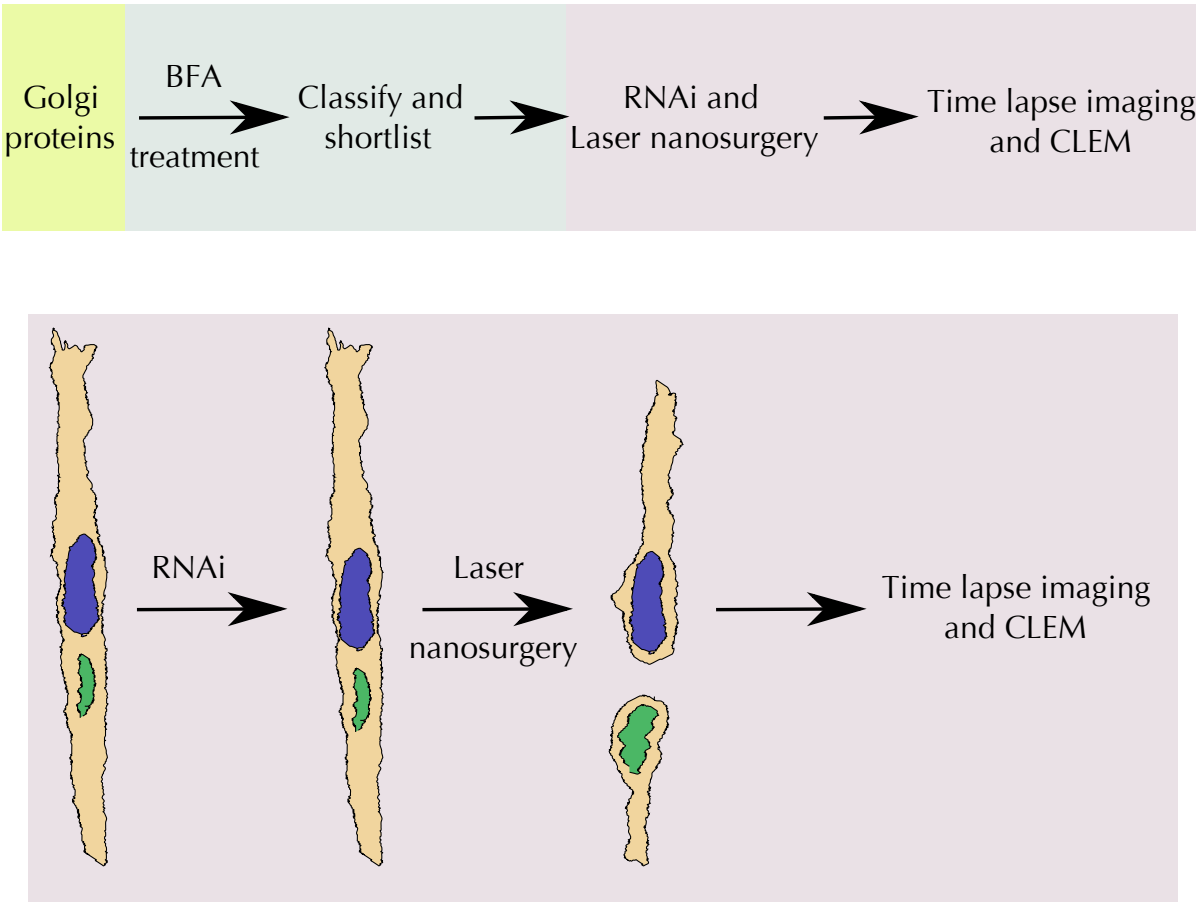

Figure 10 Project outline and experimental setup

The upper panel of the schematic shows outline of the project. This involves selection of Golgi proteins from Human Protein atlas project, shortlisting the candidate proteins, RNAi and laser nanosurgery experiments to deplete candidate proteins followed by time-lapse imaging and CLEM to identify their role in Golgi biogenesis. The lower panel of the schematic shows the experimental setup in detail. The cells seeded on fibronectin lines (allow them to stretch and move giving rise to displacement of the Golgi) are treated with siRNA for specific proteins for 4 hr. Then they are subjected to laser nanosurgery to deplete the Golgi from the cell. The karyoplast is followed by time-lapse imaging for 20-22 hr and the final Golgi structure is obtained using CLEM.

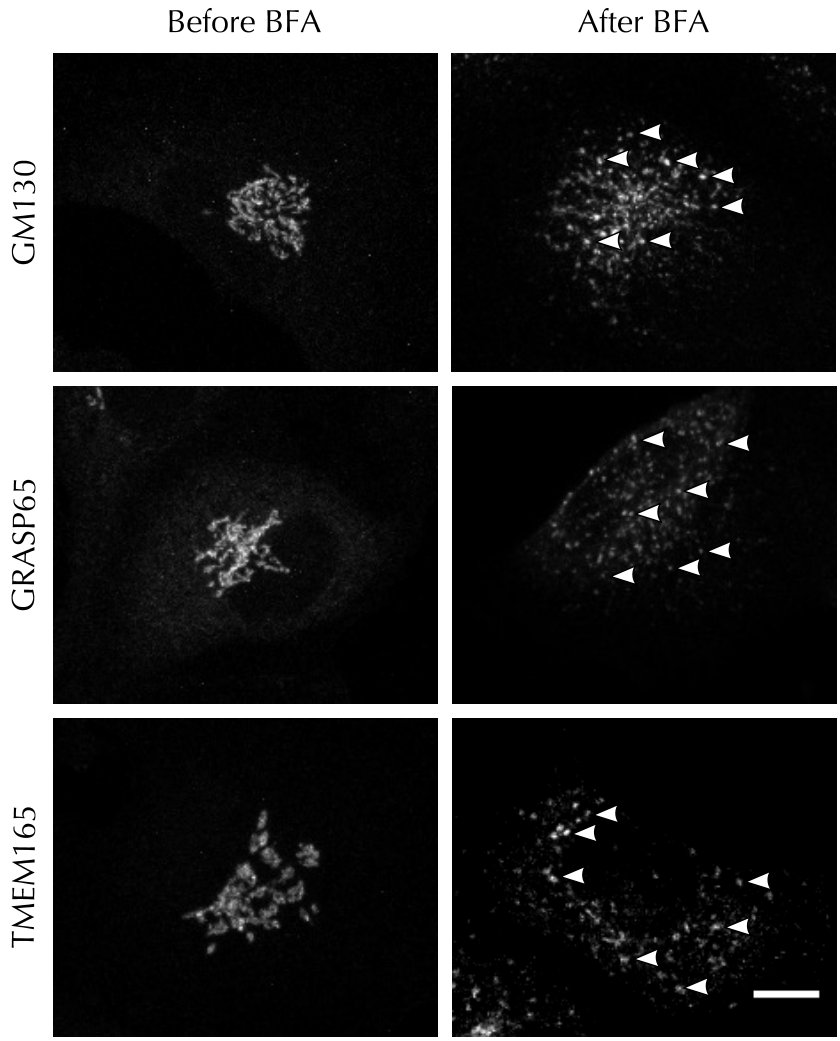

Figure 11 Classification of Golgi proteins upon BFA treatment - Class I

Immuno-staining of the candidate proteins (GM130, GRASP65 and TMEM165) without BFA treatment (left) and with 30 min of BFA treatment (right). Upon BFA treatment the proteins are localised to punctate structures, some of which are indicated by arrowheads. All the proteins with similar localisation were grouped into Class I. Scale bars: 10 μm

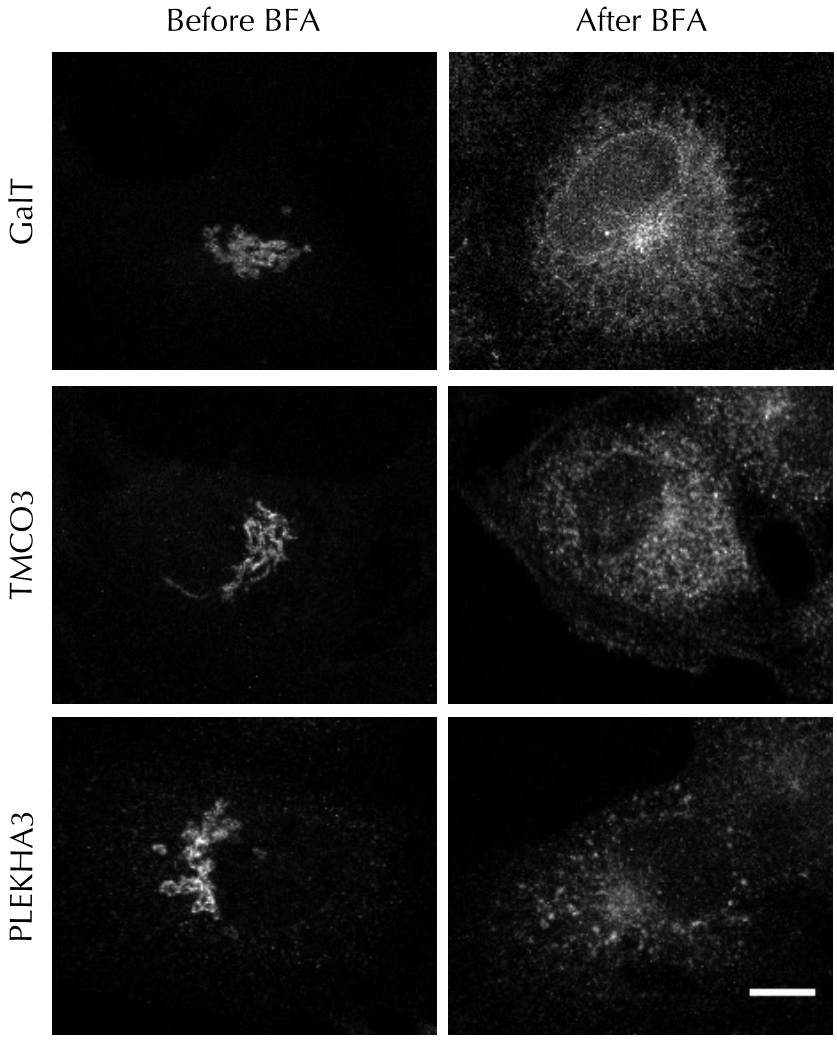

Figure 12 Classification of Golgi proteins upon BFA treatment - Class II

Immuno-staining of the candidate proteins with their respective antibodies (GalT, TMCO3 and PLEKHA3) without BFA treatment (left) and with 30 min of BFA treatment (right). Upon BFA treatment the proteins GalT and TMCO3 are localised to ER like structures. PLEKHA3 is localised mostly to the ER like structures with additional punctate structures. The proteins with similar localisations were grouped into Class II. Scale bars: 10 μm

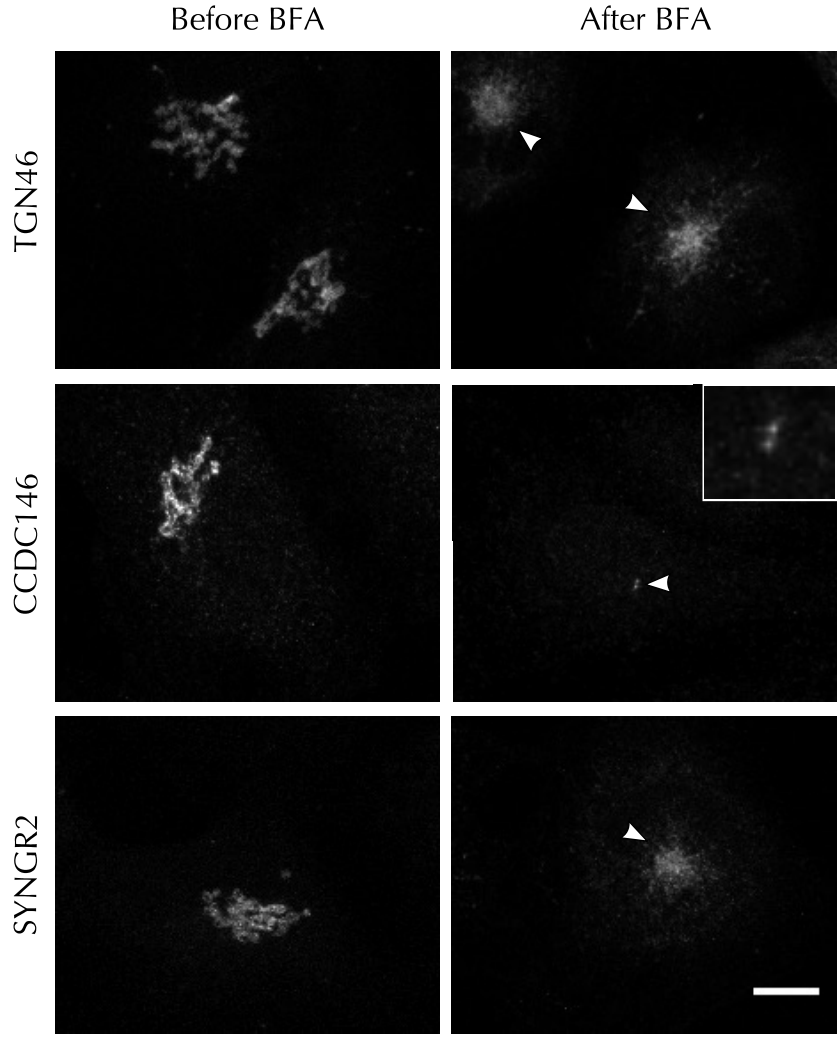

Figure 13 Classification of Golgi proteins upon BFA treatment - Class III

Immuno-staining of the candidate proteins (TGN46, CCDC146 and SYNGR2) with (30 min) (right) and without (left) BFA treatment. Upon BFA treatment the proteins TGN46 and SYNGR2 are localised to trans-Golgi like structures represented by arrowheads. CCDC146 is localised to centrosome like structures indicated by arrowheads. The proteins with either localised to trans-Golgi network or centrosome like structures were grouped into Class III. Scale bars: 10 μm.

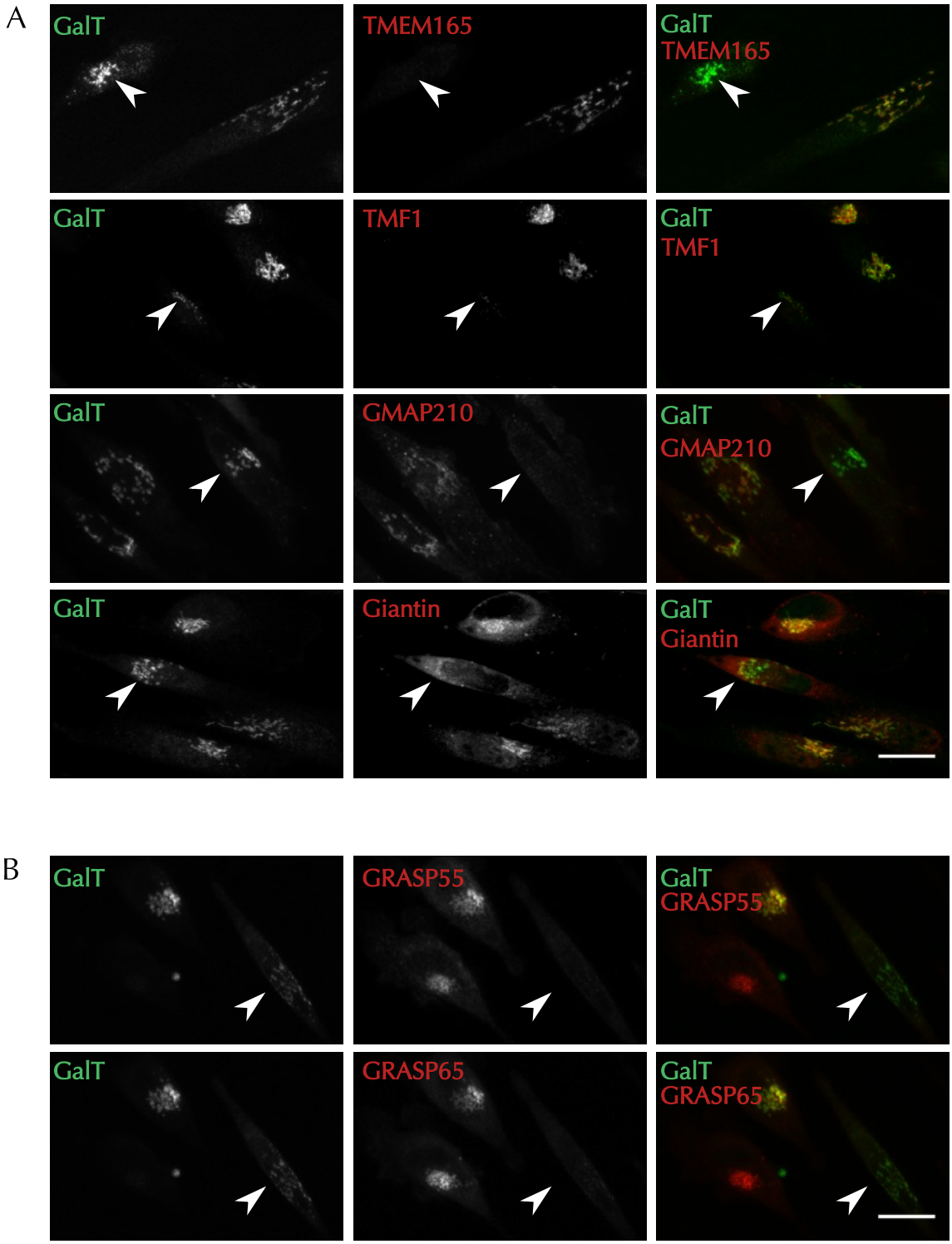

Figure 14 Validation of candidate protein depletions upon RNAi and laser nanosurgery

BSC1 GalT-GFP cells expressing GalT-GFP were treated with single siRNA (A) and two siRNAs (B) for specific protein candidates (labelled in red) for 4 hr and subjected to laser nanosurgery to deplete the Golgi. The karyoplasts were followed using time-lapse imaging and fixed with PFA upon 20-22 hr after laser nanosurgery. The cells are then immuno-labelled for specific proteins of the respective knockdown. Cells marked with arrowheads are the Golgi depleted cells. Scale bars: 10 μm.

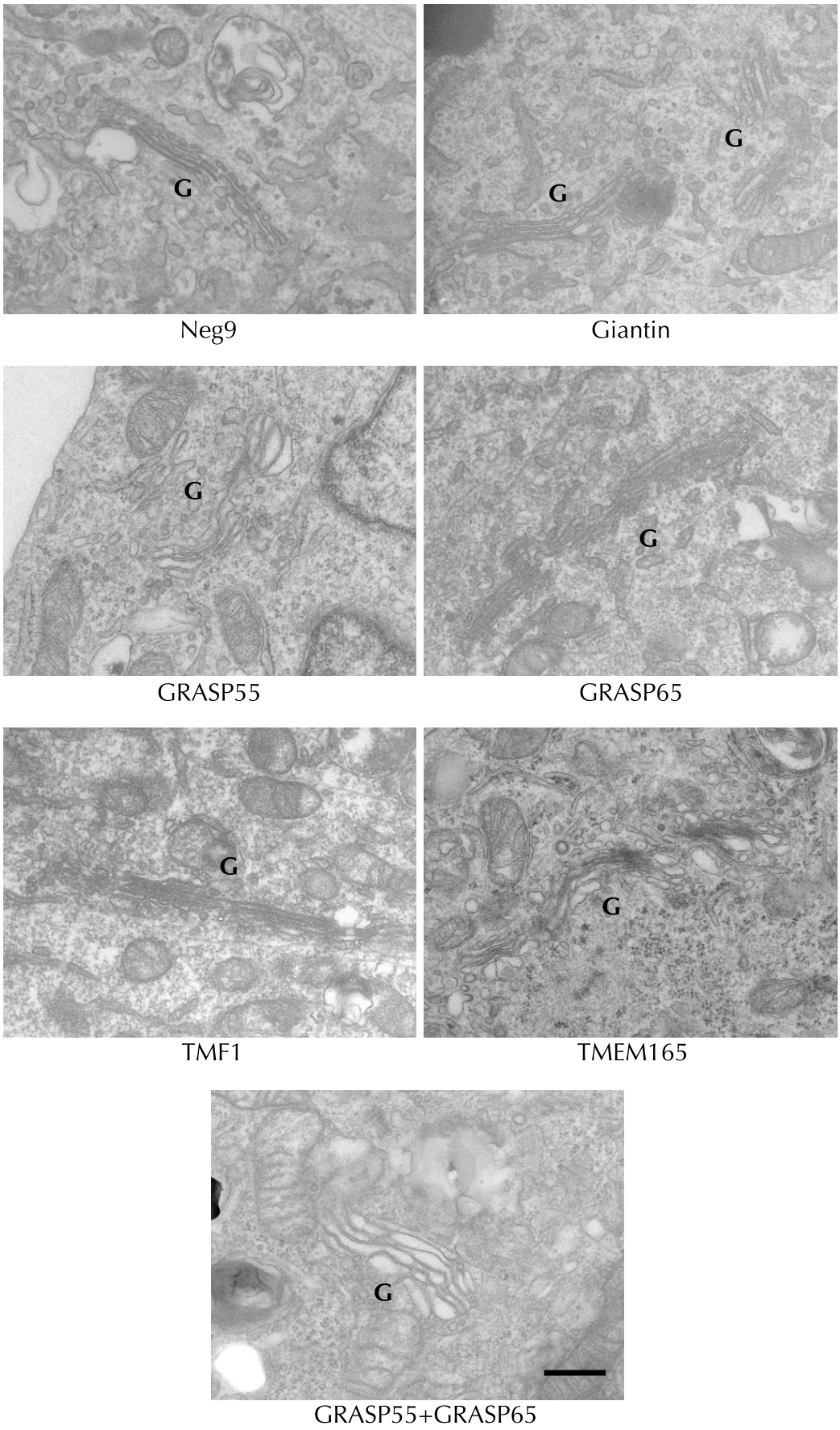

Figure 15 CLEM images of *de novo* Golgi upon depletion of candidate proteins

The BSC1 GalT-GFP cells were treated with control siRNA, Neg9 or GOLGB1 or GRASP65 or GRASP55 or TMF1 or TMEM165 or GRASP65 and GRASP55 siRNA and were subjected to laser nanosurgery to

deplete Golgi. The Golgi biogenesis was followed by a time-lapse microscopy and the cells were fixed after 20-22 hr and processed for CLEM. The EM images show a *de novo* Golgi, upon single depletion of candidate proteins (GOLGB1, GRASP55 and GRASP65, TMF1, TMEM165) and double depletion of GRASP55 and GRASP65. The images show Golgi with stacked cisternae. Scale bar: 500nm, G: Golgi.

siRNA	Average maximum luminal width per cisterna (nm)	Average number of stacks per cell
Neg9 (control)	26.48 (75)	3.66
GRASP65+55	83.53 (98)	5.2

Table 3.2 Quantification of maximum luminal width of Golgi cisternae and number of stacks upon double depletion of GRASPs

The BSC1 GalT-GFP cells were treated with control Neg9 siRNA or GRASP65 and GRASP55 siRNA and were subjected to laser nanosurgery to deplete Golgi. The Golgi biogenesis was followed by a time-lapse microscopy for 20-22 hr and the cells were fixed and processed for CLEM. The quantification of EM images from control cells (n=6) and GRASP double depletion (n=5) showing the average maximum luminal width per cisterna and average number of stacks per cell. The numbers in brackets indicate the number of cisterna quantified.

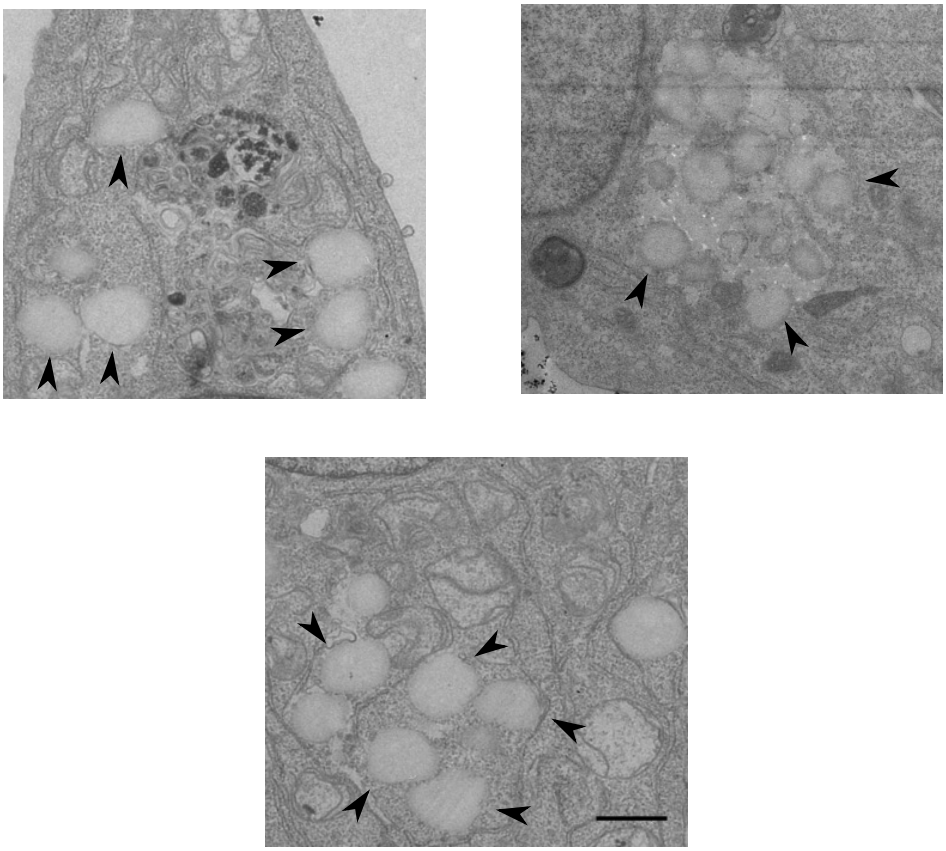

Figure 16 Lipid droplets in TMEM165 depleted cells

BSC1 GalT-GFP cells were treated with control Neg9 siRNA or TMEM165 siRNA and were subjected to laser nanosurgery to deplete Golgi. The Golgi biogenesis was followed by a time-lapse microscopy for and the cells were fixed and processed for CLEM. The EM images from three cells show an accumulation of lipid droplets after 20-22 hr of Golgi biogenesis. Arrowheads indicate a few lipid droplets. Scale bar: 1 μm.

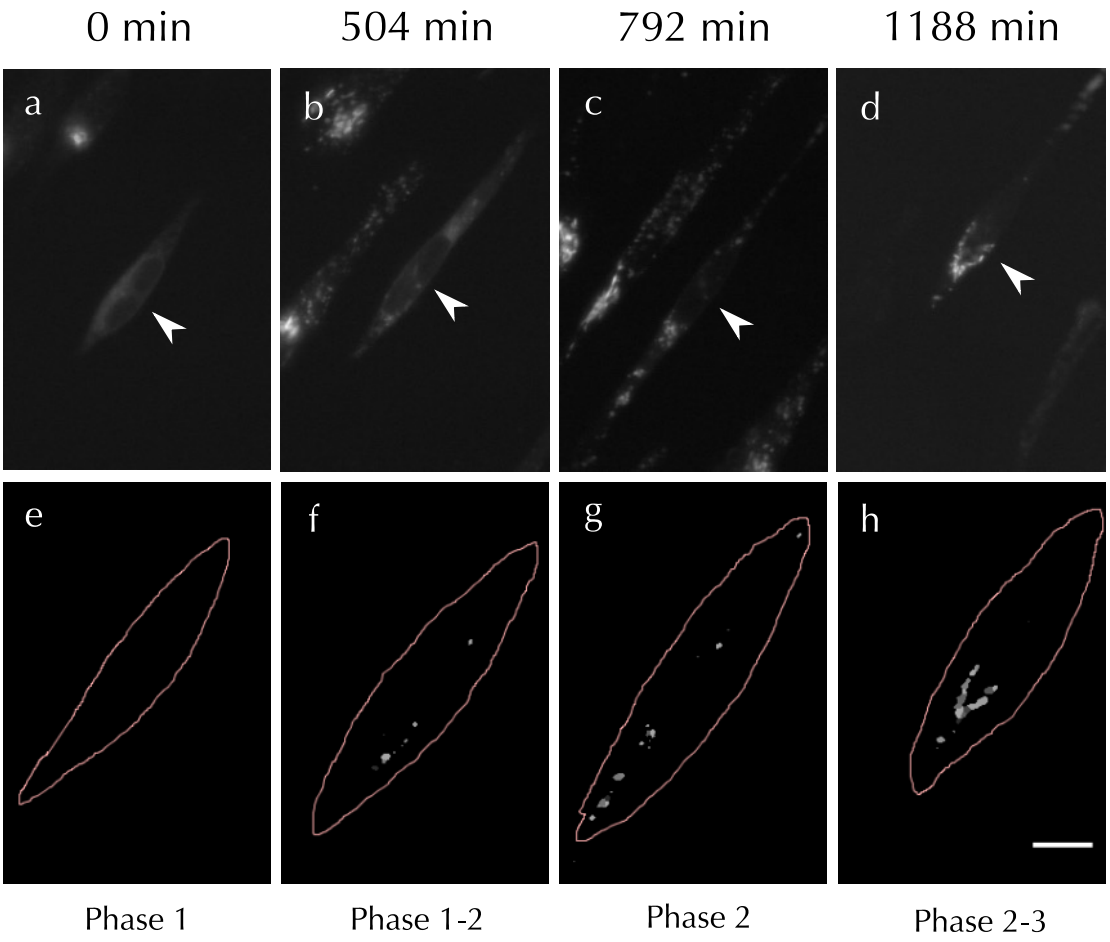

Figure 17 Phases in Golgi biogenesis

Upper panel shows the karyoplast of a control cell at different time points that was followed by time-lapse imaging. The arrowheads in the upper panel indicate the Golgi depleted cell after laser nanosurgery. The lower panel shows the corresponding cell mask to segment the cell and post-ER structures segmented by using Cell profiler pipeline. The images represent cells at different phases of the Golgi biogenesis. The images show segmented post-ER structures (f) during the transition from phase 1 to phase 2, their clustering during phase 2 (g) and merging of these clusters together (h) during the transition from phase 2 to phase 3.

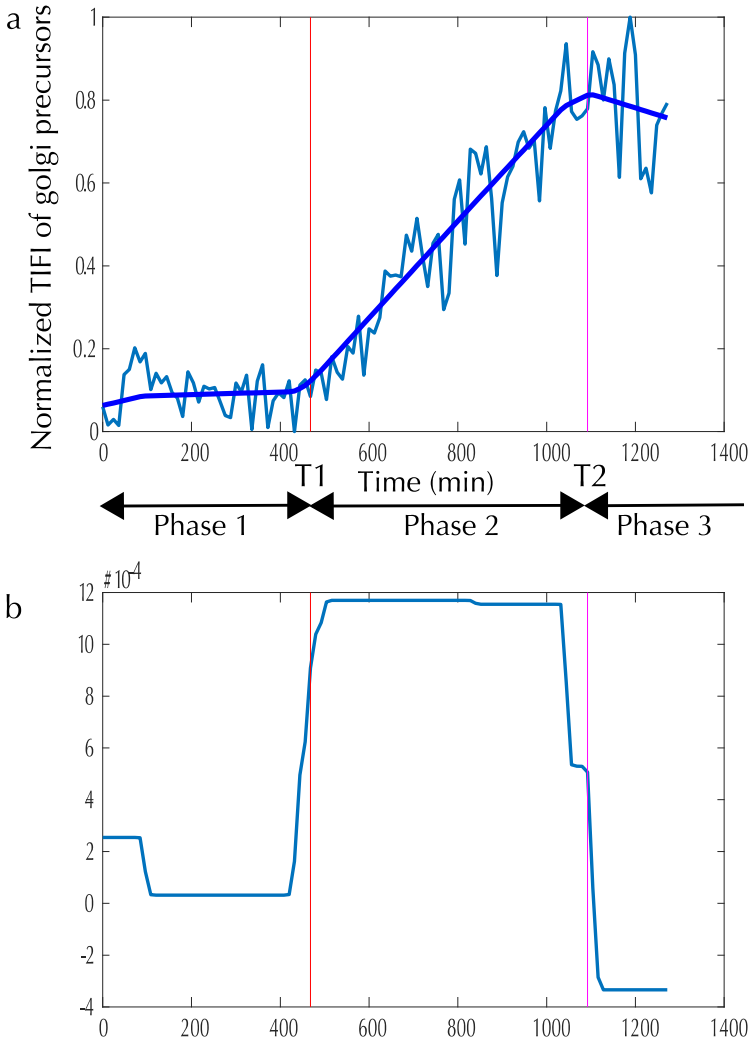

Figure 18 Time-lapse curve of Golgi biogenesis

The upper panel (a) shows normalized TIFI of Golgi precursors plotted against time in a control cell. The lower panel (b) shows the numerical derivative calculated using total-variation regularisation algorithm. T1 and T2 are the switching points identified from the derivative by using edge detection analysis. T1 represents the duration of phase 1 and T2-T1 represents the duration of phase 2 respectively. The thick blue line in the time-lapse curve represents the integration of the calculated derivative functions.

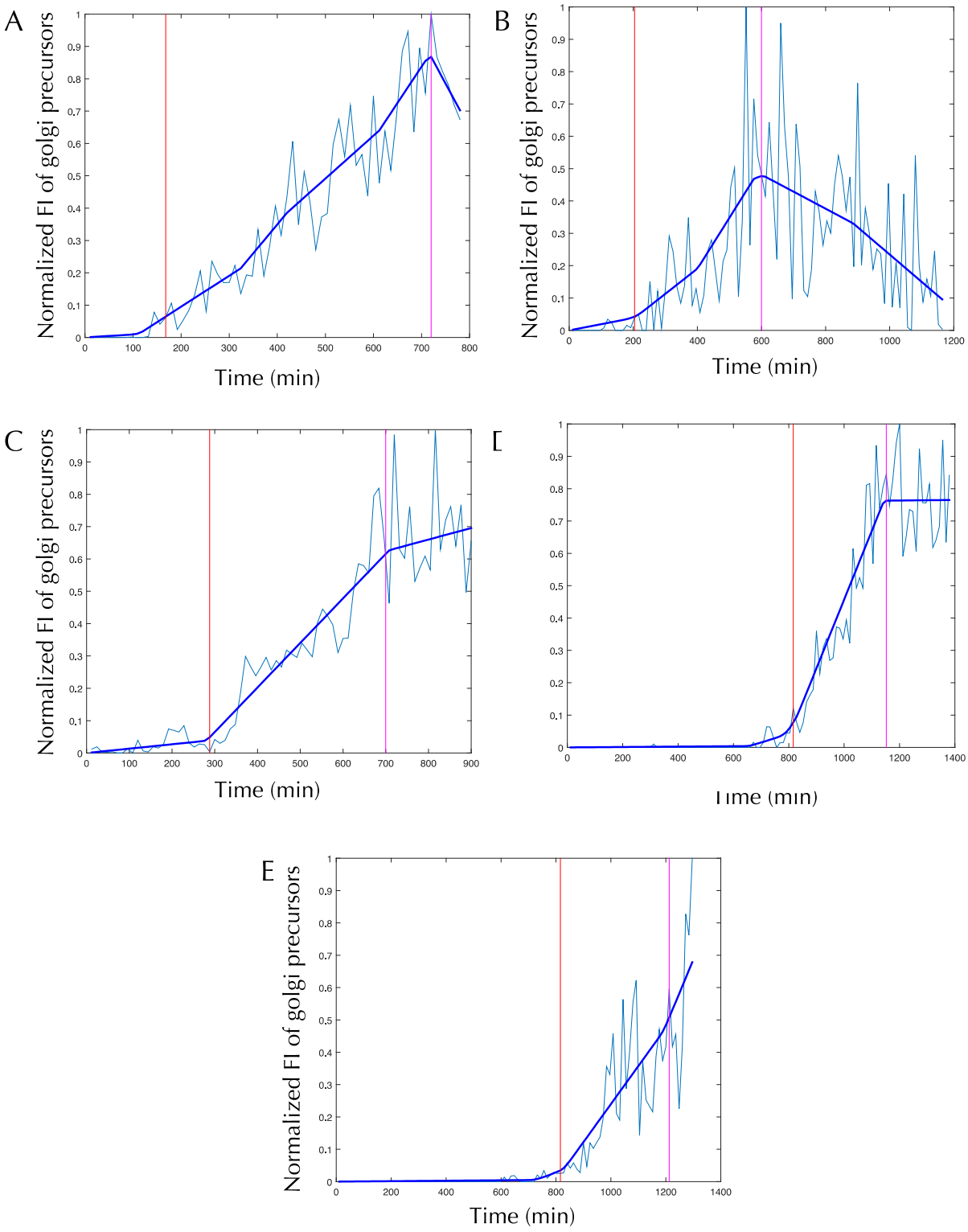

Figure 19 Time-lapse curves of GRASP double depletion and control

BSC1 GalT-GFP cells were treated with control Neg9 siRNA or GRASP65 and GRASP55 siRNA and were subjected to laser nanosurgery to deplete Golgi. The Golgi biogenesis was followed by a time-lapse microscopy and Golgi precursors were segmented using Cell profiler and the TIFI of the structures was extracted. The plots show normalized TIFI of Golgi precursors plotted against time for individual cells (A, B, C and D). Edge detection analysis was used to identify the switching points from calculated numerical derivative. Plots A, B and C are obtained from time-lapse movies of control cells and Plots D and E from GRASP65 and 55 double depleted cells. The thick blue lines in the time-lapse curve represent the integration of the calculated derivative functions.

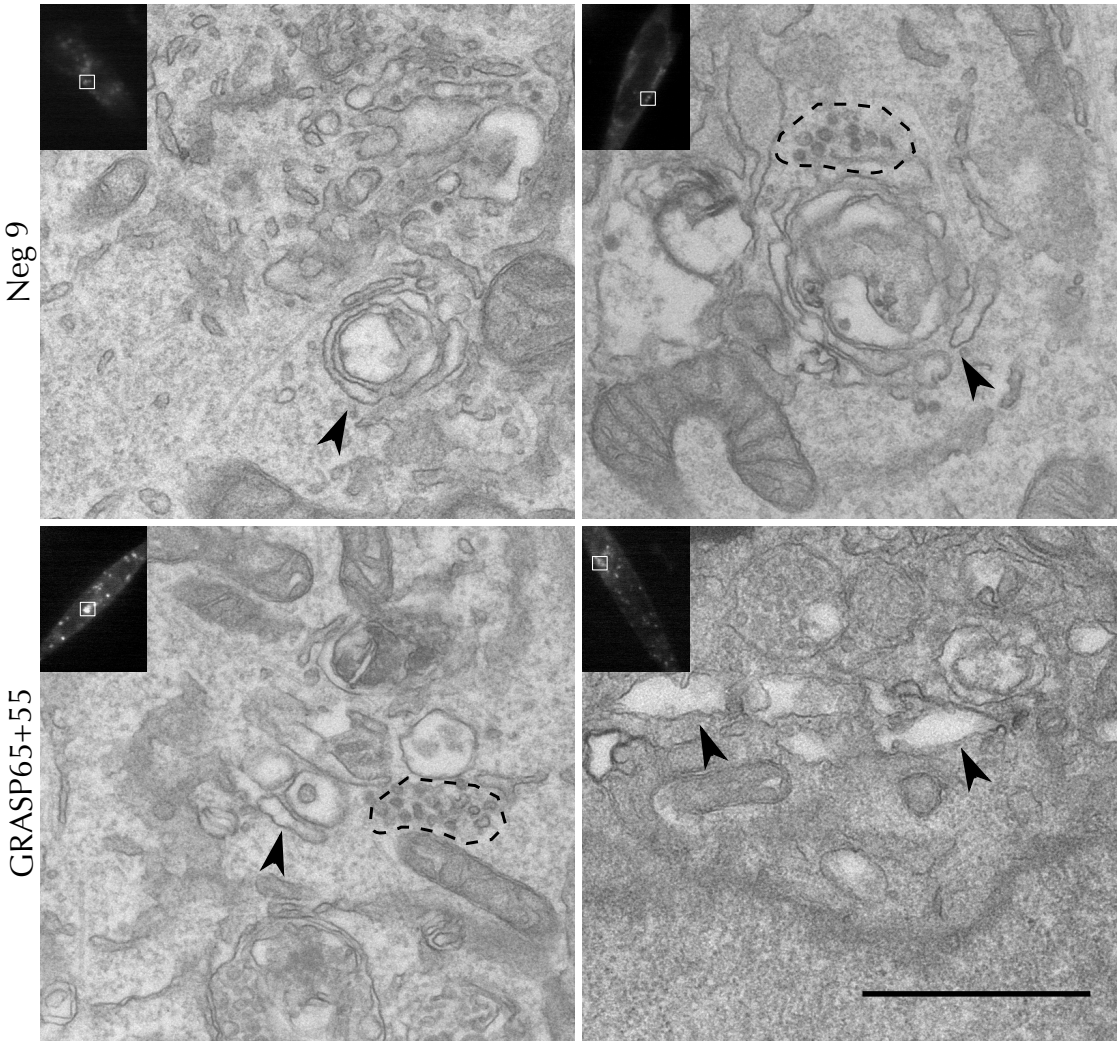

Figure 20 CLEM of Golgi precursors upon double depletion of GRASP65 & 55 compared to control

The BSC1 GalT-GFP cells were treated with control siRNA (Neg9) or GRASP65 & 55 siRNA and were subjected to laser nanosurgery to deplete Golgi. The Golgi biogenesis was followed by a time-lapse microscopy and the cells were fixed immediately when Golgi precursors (phase 1->2) were observed and processed for CLEM. The EM images show Golgi precursors produced during Golgi biogenesis in both conditions. The images show membrane bound compact and convoluted structures (arrowheads) in control condition together with accumulation of small vesicles and post-ER material (region enclosed with dotted lines). The cells depleted for GRASPs show membrane bound structures (different from control) (arrowheads) and accumulation of post-ER material (region enclosed with dotted lines). Scale bar: 1μm.

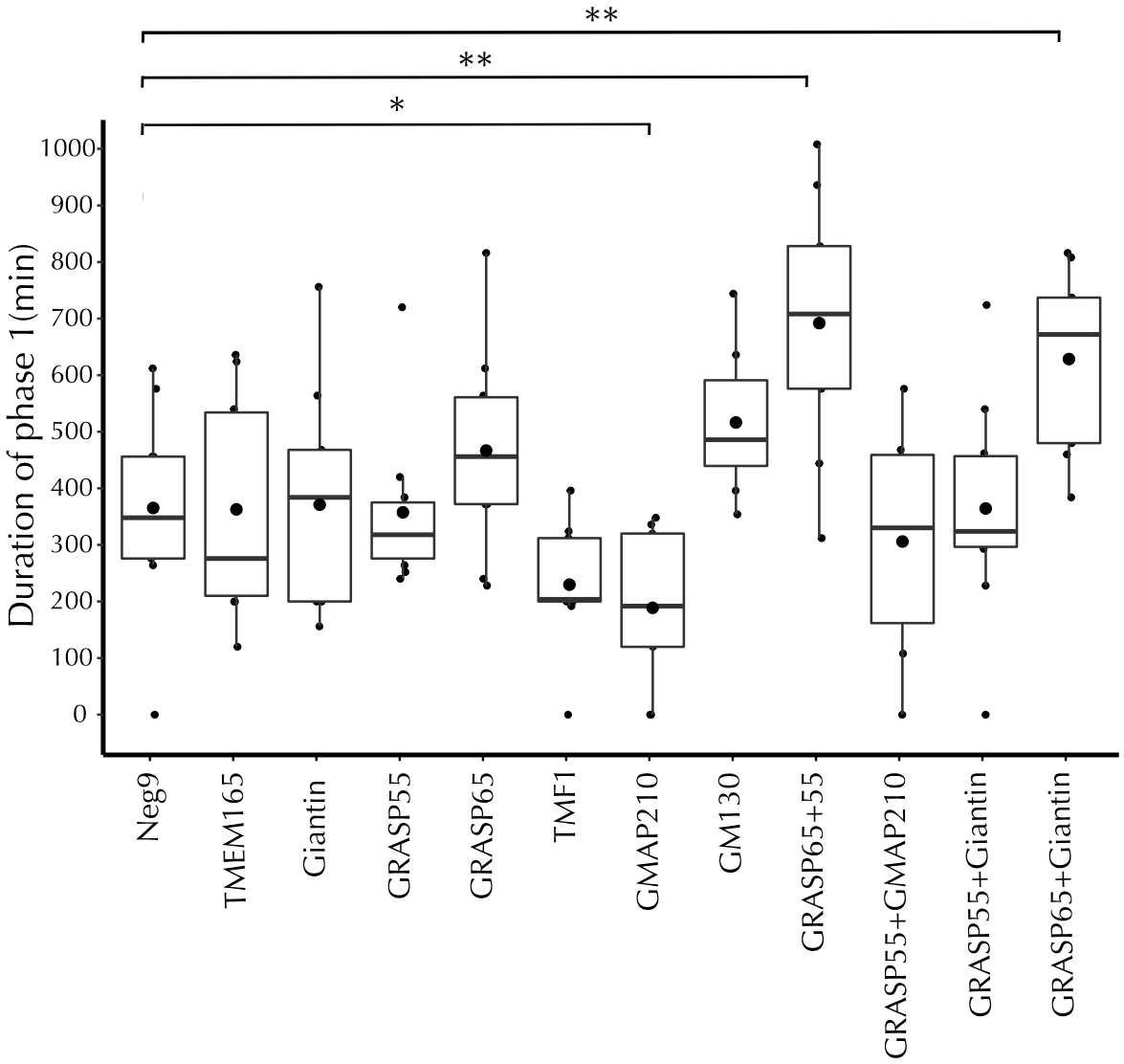

Figure 21 Duration of phase 1 in Golgi biogenesis upon depletion of Golgi proteins

The duration of phase 1 extracted from the time lapse data upon depletion of different proteins is plotted as a box plot. Each point in the plot represents a cell (n=10). The mean value of each condition is represented as a black dot and line represents the median. The p value for depletion of GMAP210 compared to Neg9 is 0.036. The p values for the double depletions of GRASP65 and 55, GRASP65 and Giantin are 0.0046 and 0.005, respectively.

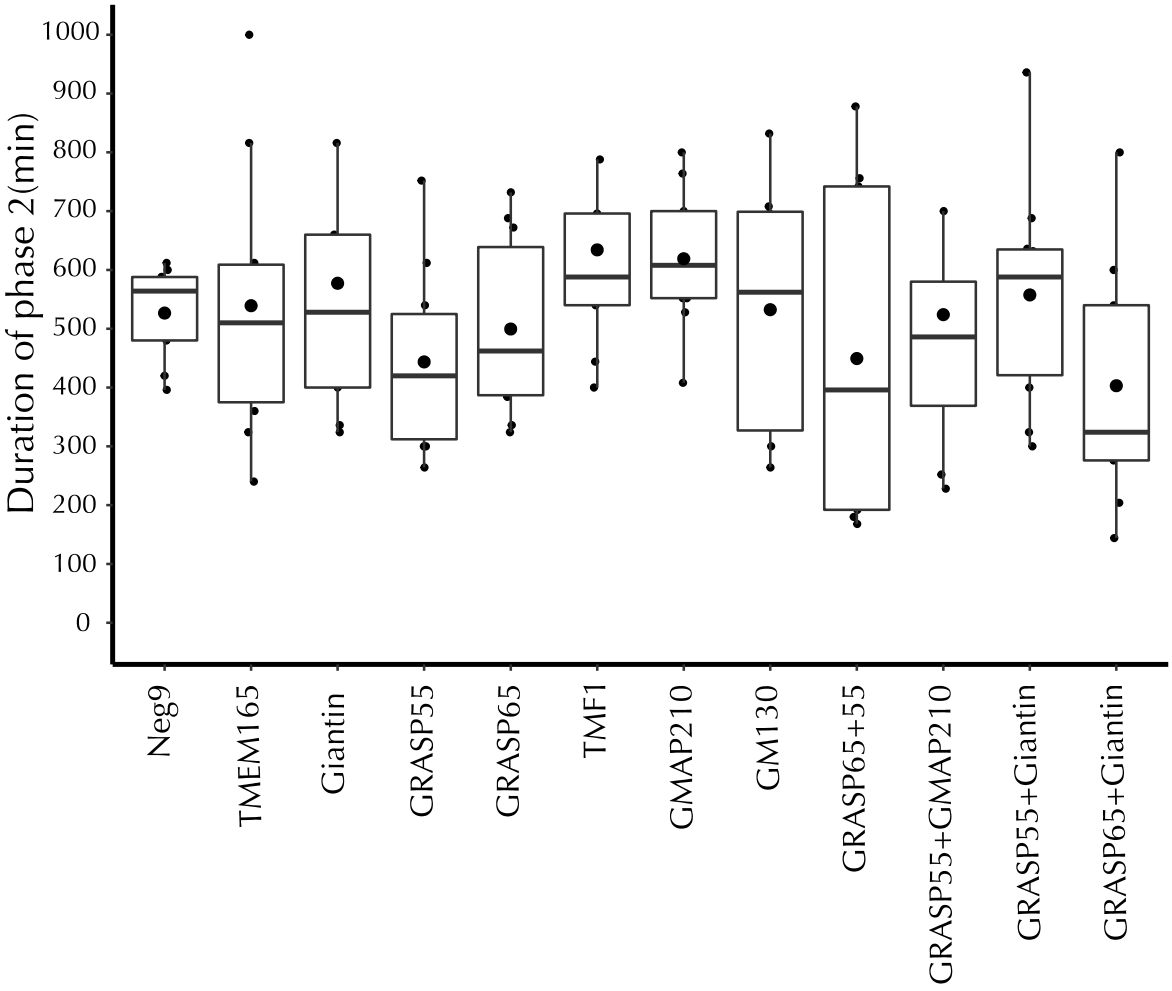

Figure 22 Duration of phase 2 in Golgi biogenesis upon depletion of Golgi proteins

The duration of phase 2 extracted from the time lapse data upon depletion of different proteins is plotted as a box plot. Each point in the plot represents a cell (n=10). The median is represented as a line and the mean value is represented as a black dot for each condition.

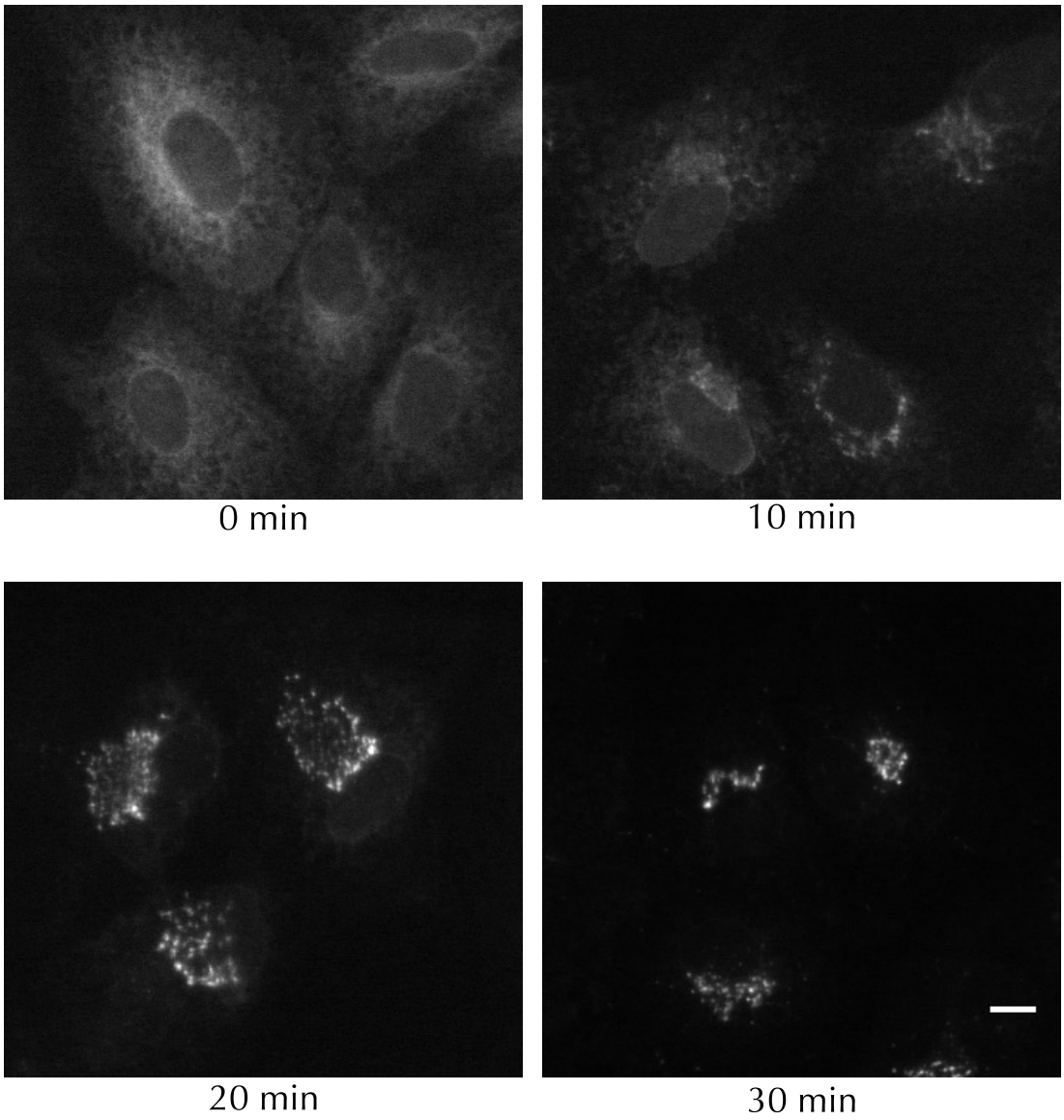

Figure 23 Time course of temperature sensitive VSVG (VSV-G ts045) upon its release from the ER

BSC1 cells infected with adenovirus to express a YFP-tagged temperature-sensitive vesicular stomatitis virus G protein (VSV ts045-G) for 1 hr at 37 °C and then upon washing and removal of the virus they are transferred to 39.5 °C and incubated for 16-18 hr. The cells were then shifted to 31.5 °C to release the protein and fixed at different time-points. Images show the change of localisation of the protein from the ER to the Golgi. Scale bar: 10 μm.

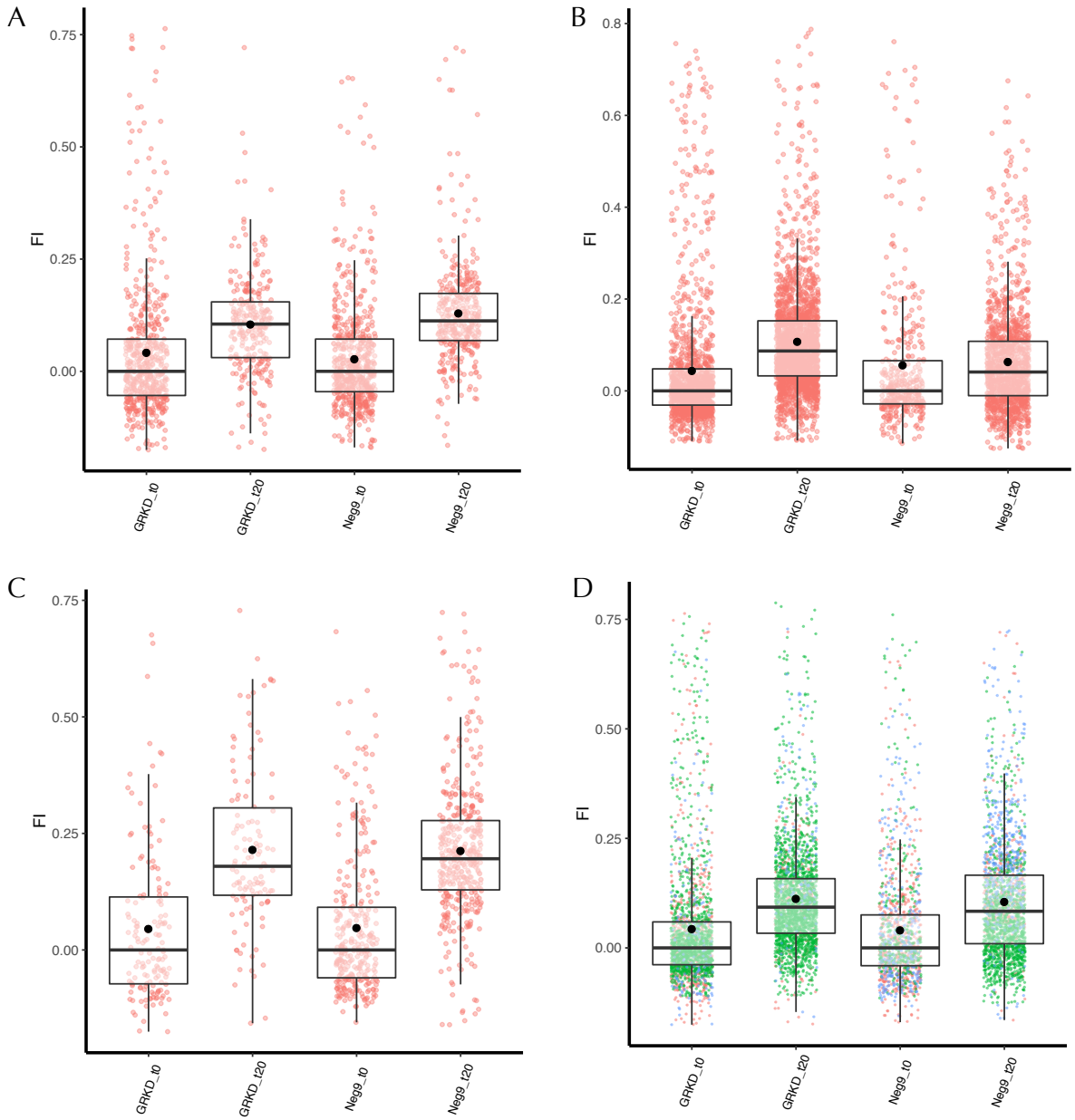

Figure 24 Comparison of ER to Golgi transport by VSVG assay in control and GRASP double knockdown

BSC1 cells were transfected with control and GRASP65 & 55 siRNAs for 48 hr and then infected with adenovirus to express a YFP-tagged ts045 VSV-G protein for 1 hr at 37 °C. They were then transferred to 39.5 °C and incubated for 16-18 hr. The cells were fixed after 0 min and 20 min upon the release of the cargo (YFP- tagged VSV-G ts045) from the ER by a temperature shift to 31.5 °C. The boxplots (A,B and C) show the results of three individual experiments of VSVG assay in control cells (Neg9) and GRASP65 and 55 double depleted cells (GRKD). The Y-axis represents the ratio of integrated FI of the Golgi to integrated FI of the total cell, normalised to the zero time point (t0) of the respective depletions. Each point represents the ratio of an individual cell and dot in the centre of the boxplot indicates the mean value. The boxplot D represents the data from all the three experiments.

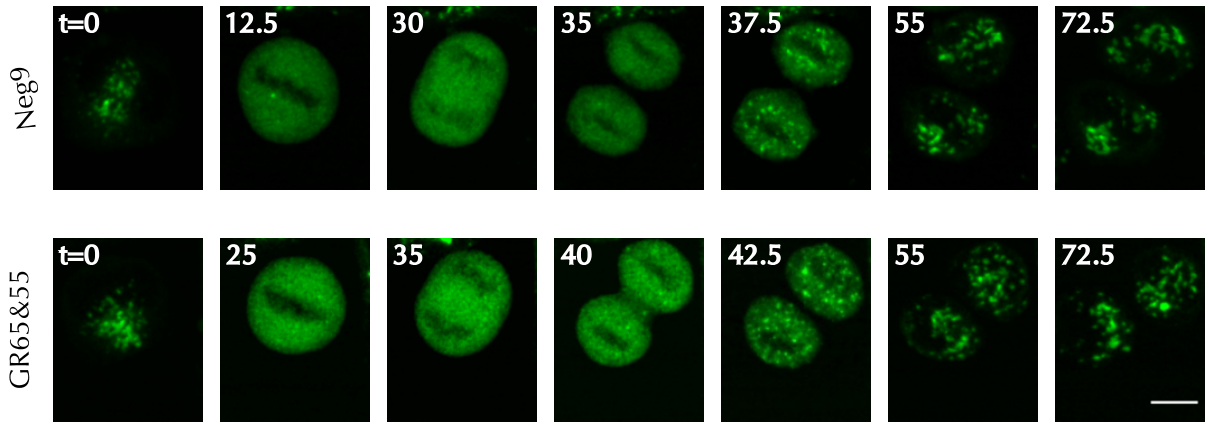

Figure 25 Golgi biogenesis during mitosis in GRASP 65 & 55 depleted cells

HeLa Kyoto cells expressing GalNacT2-GFP and H2B-mCherry were treated with control siRNA Neg9 and GRASP 65 & 55 siRNA. The images show the Golgi marker GalNacT2-GFP. The upper panel shows an example of a cell undergoing mitosis under control conditions (Neg9). The lower panel shows an example of GRASP 65 & 55 double knockdown cell during mitosis. The time indicated is in minutes during the time-lapse after identifying the mitotic cells. Scale bar: 10 μm.

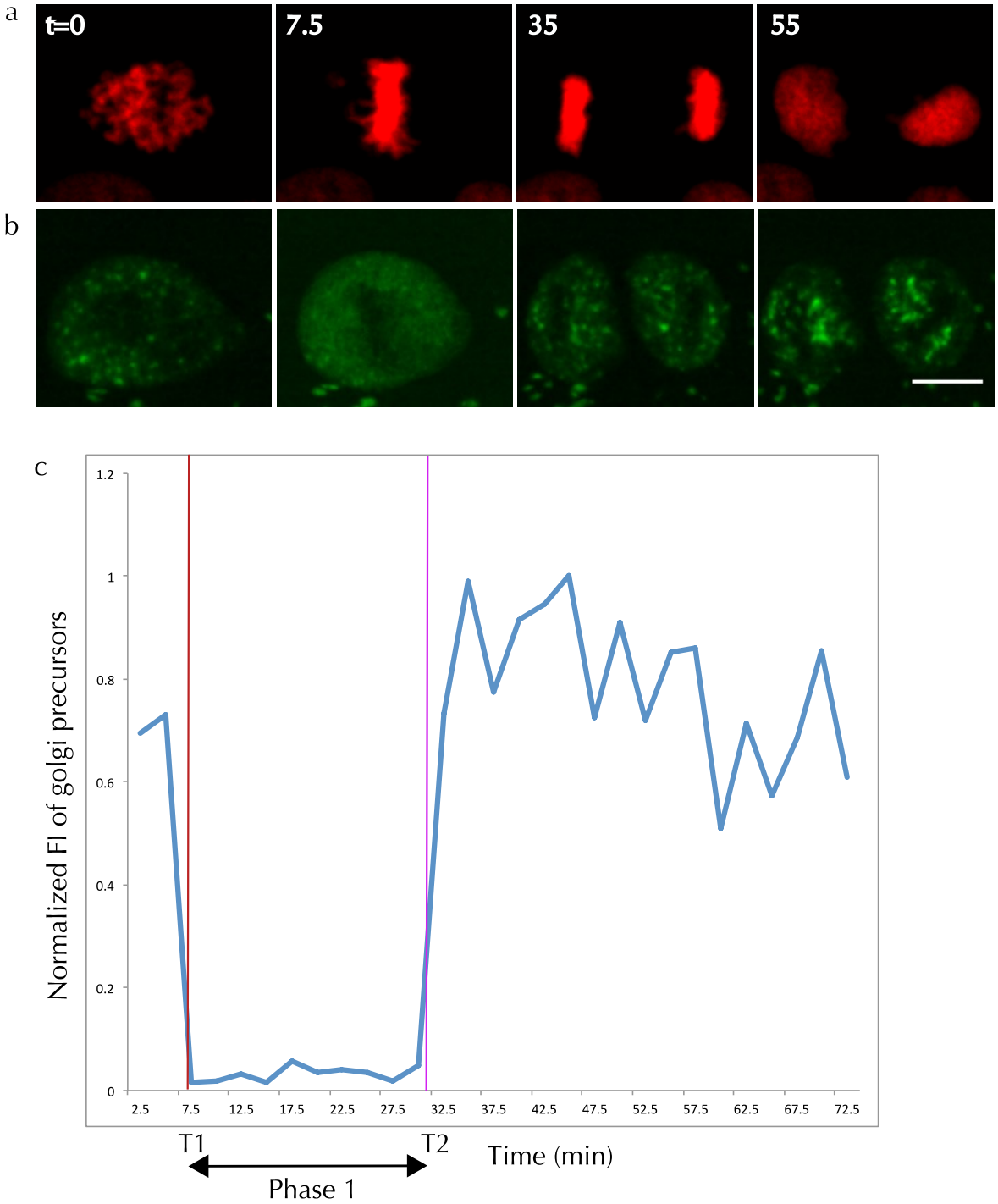

Figure 26 Time-lapse curve showing duration of phase 1 in mitotic cells

HeLa Kyoto cells expressing GalNacT2-GFP and H2B-mCherry were treated with control siRNA. The mitotic cells were identified during the pro-metaphase and were imaged by a confocal microscope for 1hr with a 2.5 min time resolution throughout the mitosis. The upper panel (a) shows the H2B-mCherry (nucleus) and the middle panel (b) shows GalNacT2-GFP (Golgi). The Golgi precursors were segmented from the Golgi channel using Cell profiler from the time-lapse data and the TIFI of the structures was extracted. The normalized TIFI of Golgi precursors were plotted against time (c). Edge detection analysis was used to identify the switching points (T1 and T2) based on the normalised TIFI. Phase 1 was calculated as the difference between T2 and T1. The upper panels (a, b) show the time-lapse images of the cell corresponding to the plot in the lower panel (c). Scale bar: 10 μm and t: time (min).

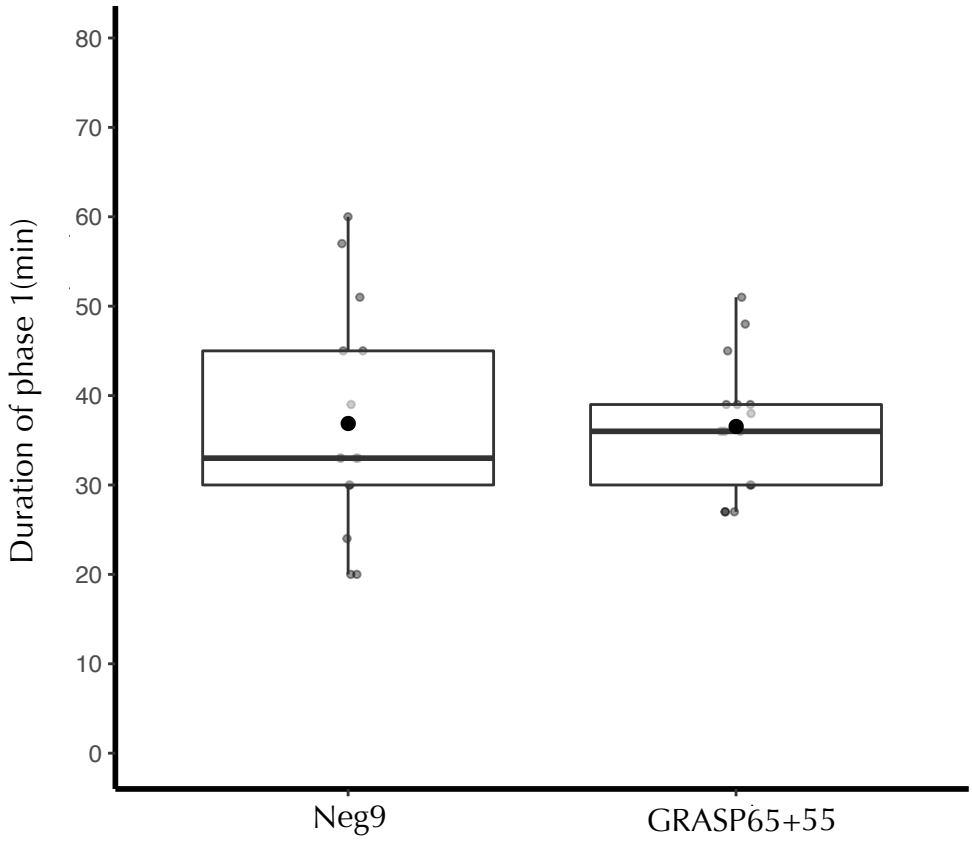

Figure 27 Duration of phase 1 in mitotic cells upon depletion of GRASPs

The duration of phase 1(min) extracted from the time-lapse data from control cells (Neg9) and upon depletion of GRASP65+55 is plotted. Each point in the plot represents a cell (n=15). The mean value of each condition is represented as a black dot and the line represents the median.

4 Discussion

Although, the Golgi complex was first identified more than hundred years ago, the knowledge about the precise function of the molecules that localise to it is still lacking. Despite of a number of Golgi proteins being known, their role in the Golgi biogenesis process is still not very clear due to large amounts of conflicting data. The goal of my PhD work was to get more insights about the key molecular regulators of this event and their role in the process, by taking advantage of the laser nanosurgery approach previously developed in our laboratory.

I used Golgi localisation as a first criterion to identify putative candidate proteins that might be involved in Golgi biogenesis process. First, I screened the Human Protein Atlas (HPA) database (Berglund et al. 2008) and selected a list of 31 proteins exclusively localised to the Golgi and with structural domains that might be important in Golgi biogenesis. Localisation of these proteins after treatment of cells with Brefeldin A allowed me to cluster these proteins into three classes: (i) Golgi matrix-like proteins which accumulate as distinct structures throughout the cytoplasm (ii) Golgi enzyme-like proteins, which relocate to the ER and (iii) TGN/Centrosome-like proteins which remained concentrated in the juxta-nuclear region of the cell similar to the TGN marker TGN46 or localised to dot like structure similar to centrosomal marker CNAP. This revealed the behaviour of several new proteins (CCDC146, TMEM165, TMCO3, DENN4DB and PLEKHA3), some of which (TMEM165 and CCDC146) showed Golgi matrix-like and Centrosome-like localisations respectively and thus might be good candidates to represent new regulators of Golgi function.

In an attempt to characterise the role of these selected proteins for *de novo* Golgi biogenesis, I used a combination of RNAi and laser nanosurgery techniques to achieve acute depletion of these proteins followed by siRNA mediated inhibition of their synthesis during Golgi biogenesis. I validated the acute depletion for 7 proteins and used the combinatory approach to identify their roles in Golgi biogenesis. These proteins also include known Golgins and GRASPs, which have been proposed to play an important role in Golgi maintenance and function.

Acute depletion of none of these individual proteins tested showed a significant effect on the kinetics of Golgi biogenesis process, despite of their efficient depletion. This implies that Golgi biogenesis is highly robust and can occur even under the depletion of individual putative candidate proteins. When double knockdowns of some protein combinations were performed, I identified a significant delay in the earlier stages of the process upon knockdown of certain combinations (GRASP65 & GRASP55, GRASP65 & Giantin). This suggests a possible redundancy among proteins involved in this process. The main events occur during the earlier stages are tethering and stabilization of post-ER material.

When I looked at the ultra structure of the Golgi upon acute depletion of individual proteins, I could not identify morphological changes in the Golgi structure with any of the single knockdowns tested. This also ascertains the robustness of the Golgi biogenesis process and being able to compensate for the loss of certain proteins. When I looked at the double knockdown of GRASP65 and GRASP55, cisternae in stacks appeared to be much thicker and not very flat compared to other protein depletions or control experiments. This also suggests that there is a redundancy among Golgi proteins and hence an effect on the ultra structure was identified only upon double depletion.

There exist at least two possibilities to explain the delay in initial stages of Golgi biogenesis. The first one is a possible delay in the ER to Golgi transport and the second is a key role of these proteins in initial stages of the process. To investigate which of these two possibilities may be true, I performed a VSVG transport assay and the results of this experiment showed that, under the conditions used here in this work, there is no significant delay in ER to Golgi traffic upon double depletion of GRASP65 and 55. This implies that these two proteins play a crucial role in the initial stages of the Golgi biogenesis process or the VSVG assay was not sensitive enough in my experiments to detect the delay in the ER to Golgi transport. As the double depletion of GRASPs also affected the final Golgi ultra structure and previous literature studies suggested their role in tethering, I consider it more likely that these proteins play an important role in the events occurring in the initial stages of the process. To further clarify this, I looked

at the ultrastructure of the Golgi precursors during the initial stages of the Golgi biogenesis. I identified that the intermediate structures differ in the GRASP65 & 55 double depleted cells compared to control cells. This shows that GRASPs play a complementary role in initial phases of Golgi biogenesis and are important in the formation of compact, convoluted structures which give rise to a proper stacked Golgi.

4.1 Combinatory approach to identify the molecular regulators of Golgi biogenesis

The methods and tools used to study the Golgi biogenesis previously in the literature have a common limitation due to their inability to remove the Golgi completely. Hence the laser nanosurgery technique developed in our lab is very useful tool to understand the key players in this process, as it allows the complete removal of Golgi and its associated proteins (Tängemo et al. 2011). RNAi approaches have been used to study various molecules to understand their role(s) in Golgi biogenesis. In such approach, cells are treated with siRNA to degrade the mRNA, thus resulting in blockage of specific protein synthesis. But degradation of existing proteins in the Golgi usually can take several hours to days depending on the lifetime of specific protein under view. As the depletion in this case is not acute, it might allow enough time for cells to activate alternative mechanisms to compensate for the loss of the specific protein. Hence, the effects observed in such studies might not always reflect direct functional significance of individual proteins, which may explain the numerous conflicting literature data existing e.g. for Golgi Matrix proteins. Hence, to overcome these limitations, I used a combinatory approach of RNAi and laser nanosurgery to study the role of individual Golgi proteins during Golgi biogenesis. It has been shown earlier that there was no sign of any Golgi membranes or remnants in the karyoplast after the laser nanosurgery was performed to deplete the Golgi (Tängemo et al. 2011). Thus acute depletion of specific Golgi localised proteins was shown to be achieved by combining this approach with RNAi, to inhibit the re-synthesis of these proteins (Tängemo et al. 2011).

Although laser nanosurgery approach is quite advantageous, the Golgi biogenesis process occurring in this context might not exactly mimic physiological mitotic Golgi

reassembly. But the molecular players involved in this process should be the same, as it leads to the formation of a fully functional Golgi complex. Hence I used this combinatory approach to identify and characterise the role of different molecular players in the Golgi biogenesis process, rather than characterising the process itself.

Along with the many pros, there are also certain cons for this approach. As only a small percentage of cells show a Golgi displacement from the nucleus, it allows Golgi depletion only in these cells. As only a few cells can be studies at any time, performing experiments with a number of gene combinations is time-consuming. Hence it is a very low throughput, technically challenging method.

4.2 Selection and Classification of candidate proteins

Most of the proteins that were suggested to play different key roles in maintenance of the Golgi so far are localised to the Golgi complex (e.g: GM130, GRASP65 and GRASP55). So it might be crucial for proteins to localise to the Golgi if they are involved in events like tethering, stacking or ribbon formation occurring during Golgi biogenesis. Hence our selection of candidate proteins is based on the hypothesis that proteins localised exclusively to the Golgi are important for biogenesis process. I took advantage of the HPA localisation database to identify exclusively Golgi localised proteins. As I only considered exclusively Golgi localised proteins, I excluded any cargo proteins travelling through the Golgi (also localised in other organelles) and thus may not necessarily play a role in the biogenesis.

In my project I took advantage of the well-established BFA treatment of the cells as a way to distinguish proteins behaving like Golgi matrix, Golgi enzyme or TGN (Seemann et al. 2000). Interestingly, I also identified proteins localised to centrosome-like structures upon BFA treatment. Though the significance of this centrosome-like localisation upon BFA treatment is not very clear, they might be proteins that link the Golgi complex to the centrosome thus maintaining its peri-centrosomal localisation in the cell. It will be very interesting to follow up on these candidate proteins to understand their clear function.

It has been several years since the concept of Golgi matrix was introduced through identification of detergent insoluble proteinaceous structure (Slusarewicz et al. 1994), several components of this matrix have been detected. These are identified as proteins mainly belonging to the Golgin, GRASP and coiled-coil protein families (Lupashin and Sztul 2005; Ramirez and Lowe 2009; Short, Haas, and Barr 2005). But the functional characterisation of most of these identified proteins have not been yet performed. So this assay is very useful to give insights into the function of already known proteins or reveal new protein candidates by distinguishing Golgi proteins based on their behaviour. Hence it has the potential for a comprehensive screen to classify all the Golgi localised proteins according to their behaviour like the Golgi matrix, Golgi enzyme or TGN.

One caveat for this approach might be that the antibodies used, being unspecific. This can be overcome by testing and validating them through methods such as RNAi. I did this siRNA validation for the 7 candidate proteins chosen for the laser nanosurgery experiments and efficient protein depletions were confirmed.

4.3 Effect of protein depletions on Golgi ultrastructure

There was no significant change in the overall ultra structure of Golgi formed after 20-22 hr of Golgi biogenesis (stacking, Golgi ribbon etc.,) upon acute depletion of individual proteins by RNAi and laser nanosurgery. This is also consistent with literature studies where there were only subtle changes upon siRNA knockdown of some of these proteins (Giantin, GRASP55 and GRASP65) whereas overall stacking, cisternal length etc., remained unchanged (Koreishi et al. 2013; Tang, Yuan, and Yanzhuang 2010; Yi Xiang and Wang 2010b). It has been shown that knockdown of GMAP210 results in fragmentation of the Golgi when observed under light microscopy and a complete disassembly of Golgi stack under electron microscopy (Sato et al. 2014). The Golgi ultra structure upon depletion of GMAP210 hasn't been yet studied with my experimental set up but it will be addressed in the near future.

The double depletion of GRASP55 and 65 by RNAi and laser nanosurgery resulted in swollen unflat cisternae in the Golgi stack (Figure 15). This is in agreement with results

obtained by another group, where they observed that the double knockdown of GRASP65 and 55 also resulted in swollen cisternae. The same results were demonstrated and reproduced using a different set of siRNAs for the target genes (Lee et al. 2014). These results imply a crucial role of GRASP65 and 55 in flattening of the cisternae rather than stacking itself. As the individual depletions of GRASPs didn't show this effect, it implies that these proteins play complementary roles in this process. But these results contradict the study where it was shown that siRNA knockdown of GRASP55 and 65 results in complete disruption of the Golgi stack at the ultra structural level (Y. Xiang and Wang 2010). And hence it was proposed that GRASPs are involved in stacking of the Golgi cisternae and their depletion results in complete disassembly of the Golgi stack (Y. Xiang and Wang 2010). This discrepancy among different studies might be explained by the usage of different siRNAs or different sensitivities of cell lines. The combinatory approach used in this project is unique compared to the other above-mentioned studies as it achieves an acute depletion of the protein. And hence, the effects of the depletion can rather be direct allowing the characterisation of the role of the depleted proteins. Further experiments are necessary to study the Golgi ultra structure upon double depletion of GRASP65 & Giantin and any other possible combinations, which show an effect in the Golgi biogenesis process. This can help in identification of specific roles of proteins working in tandem based on their effects on the ultra structure.

4.4 Initial stages of Golgi biogenesis – the rate limiting step

The analysis of kinetics of Golgi biogenesis upon depletion of different individual proteins by RNAi and laser nanosurgery showed a significant acceleration in the initial phase of the process only in case of GMAP210. This suggests that GMAP210 acts as a negative regulator of Golgi biogenesis. GMAP210 was shown to be involved in binding to microtubules or anchoring microtubules to Golgi membranes (Infante et al. 1999; Ríos et al. 2004), so it can be speculated that its presence results in a distribution of post-ER material throughout the cytoplasm through microtubule tracks. Whereas its absence might leave the material at the site of synthesis, leading to faster fusion and

accumulation of the material. In support of this hypothesis depolymerisation of the microtubule network by nocodazole resulted in an acceleration of Golgi biogenesis (Ronchi et al., 2014). This hypothesis needs to be further tested and validated to understand the role of GMAP210 in this process. Although individual depletions of GM130 and GRASP65 showed a slight delay in the phase 1, the effect was not statistically significant when a t-test was performed. This delay in the phase 1 upon depletion of GM130 is consistent with the previously published results (Tängemo et al. 2011).

Among different combinations of double depletions performed, GRASP65 & GRASP55 and GRASP65 & Giantin showed a significant delay in the initial phase of the Golgi biogenesis process. This delay can be explained either by the crucial role of these proteins in the initial phases of Golgi biogenesis or their role in the ER to Golgi transport. The evidence from the VSVG transport assay upon siRNA knockdown of GRASP65 and 55 showed that, there was no evident delay in the ER to Golgi transport. Hence, this implies that GRASP65 and 55 play an important role in initial stages of the process. Also, this delay can be the source for the lack of cisternal flatness in the Golgi ultra structure. Consistent with these findings increased levels of GRASP65 and GRASP55 were observed in the earlier stages of Golgi biogenesis compared to other proteins (Giantin and AKAP9) (Ronchi et al. 2014).

The later stages (phase 2) of Golgi biogenesis were not affected upon depletion of individual proteins. Also there was no significant delay or acceleration of phase 2 upon double depletions of selected proteins. This suggests that the critical rate-limiting step for Golgi biogenesis process is phase 1 rather than phase 2, at least for the proteins tested in this work. But whether this concept of rate-limiting step is true under physiological mitotic Golgi biogenesis is questionable, as the system used in this study is not exactly identical to the events occurring during mitosis. Hence this approach is highly useful to study the molecular regulators of the process rather than the process itself.

4.5 Ultrastructure of Golgi precursors during Golgi biogenesis

To test our hypothesis, whether the delay in initial phases of Golgi biogenesis upon GRASP double knockdown can be the source for the lack of cisternal flatness in the Golgi ultra structure, I looked at the ultra structure of Golgi precursors. The CLEM data from GRASP double depleted cells showed a lack of typical compact and convoluted structures observed in control cells during the transition from phase 1 to 2 or 2 to 3. Though the accumulation of the post-ER material at the ER exit sites occurs in both cases, the formation of these Golgi intermediates (or precursors) is delayed or impaired in GRASP double depleted cells. As there were structures ranging from accumulation of material at ER exit sites to accumulation of vesicular structures during the transition, I could not find a robust way to quantify these data. Overall, there is an apparent difference in the Golgi intermediates upon double depletion of these proteins compared to the control condition, supporting our hypothesis. The inability of these cells to form the proper Golgi precursors can be the reason for cisternal swelling at the end of the Golgi biogenesis process. It also explains the delay in the initial phases of the biogenesis process.

4.6 Golgi biogenesis in mitotic cells

To understand if this delay in the initial phase of the Golgi biogenesis can also be seen in physiologically relevant process such as mitosis, I performed time-lapse analysis of Golgi biogenesis in mitotic cells which were double depleted of GRASP65 & 55. Automated adaptive feedback microscopy, as it has been developed in our laboratory (Conrad et al., 2011), was used to automatically identify mitotic pro-metaphase cells based on their nuclear DNA morphology. There was no significant difference in the kinetics of appearance of Golgi precursors at the anaphase/telophase transition, which I defined as equivalent to the phase 1 in the laser nanosurgery experiments.

Possible reasons for this can be that as mitosis occurs at a very fast pace, it is not easy to detect the subtle differences occurring during this process with the 2.5 min time resolution possible with the microscope system available for these experiments. In addition, as GRASP65 & 55 knockdown is not as acute as in case of laser nanosurgery

experiments there might be still remnant protein molecules that are enough to compensate for the loss of others. Another possibility is that the effect can be accumulative and can only be observed when more rounds of cell division are analysed. Unfortunately, this is technically challenging to do, as the exposure to light for longer periods might stress the cells and hence it might be difficult to follow them for several mitotic rounds. Also, imaging mitotic cells with less time intervals is stressful for the cells and might lead to apoptosis.

As I use an artificial system (depleting Golgi by laser nanosurgery) in my experiments the Golgi biogenesis process occurs with different kinetics compared to Golgi biogenesis after mitosis. This has allowed me to reveal the effects on Golgi biogenesis as described in this work. Whether these effects are also relevant for Golgi biogenesis after mitosis currently remain elusive.

4.7 Redundancy of Golgi proteins in Golgi biogenesis

As mentioned earlier, depletion of most of the individual proteins didn't show any effect on Golgi biogenesis but some double depletion of the same proteins led to a significant delay in the process. This strongly shows functional redundancy among certain candidate proteins, where the effect could only be seen if proteins with concerted functions are simultaneously depleted. This redundancy is also supported from previous literature studies, which showed the knockdown of combination of specific Golgins and GRASPs (Golgin45, GRASP65 and 55) led to complete disassembly of the Golgi stack. But the depletion of GM130, GRASP65 and 55 led only to a partial disassembly of the Golgi stack (Lee et al. 2014). This also implies that so far there has no single protein acting as a master regulator of this process been detected and may not even exist. Golgi biogenesis is a complex mechanism and it can be speculated that it involves partial redundancy among specific Golgi proteins making the process more robust. Further systematic analysis of different combinations is necessary to interpret specific functions of the proteins involved in this process.

4.8 Proposed role of GRASPs

Based on our results and from the CLEM data in control cells and GRASP 65 & 55 double depleted cells, I propose that these two proteins play an important role in the initial stages of Golgi biogenesis. In particular, they are crucial for the formation of Golgi intermediates that are needed for maturation of the precursors into a proper Golgi. The different steps in the process based on the CLEM data in the presence and absence of GRASPs can be depicted as outlined in Figure 28.

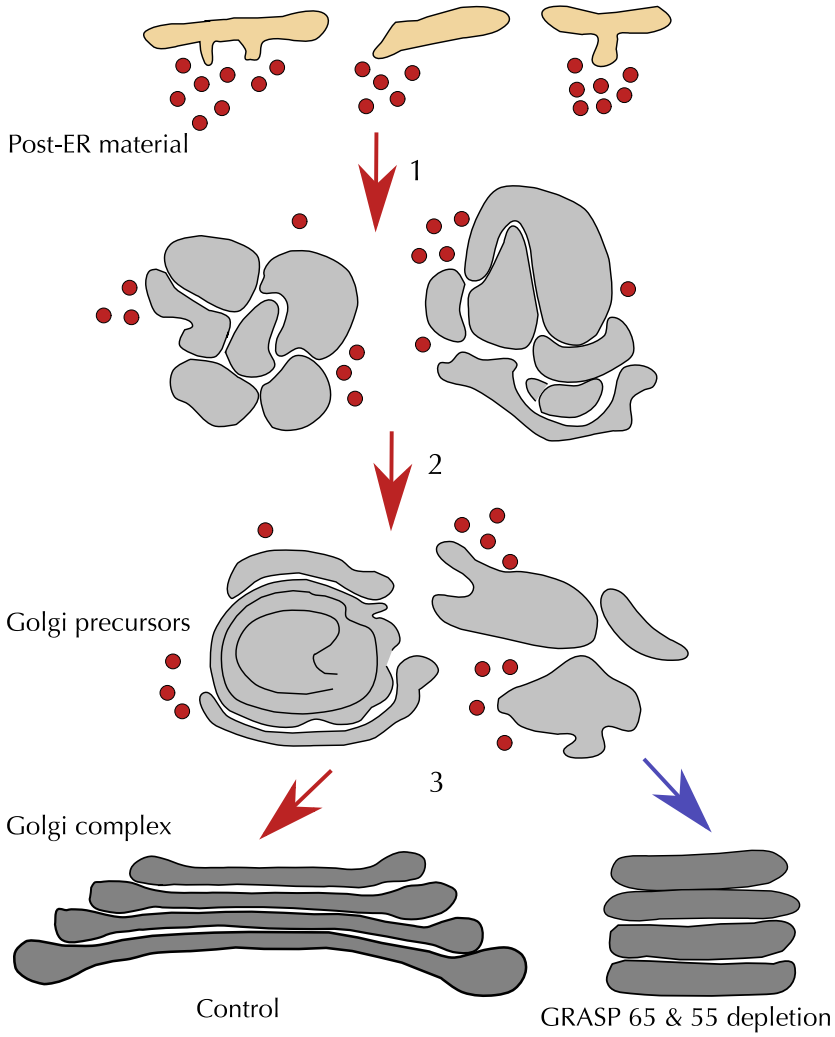

Figure 28 Events occurring at ultra structural level during Golgi biogenesis in control and GRASP double depletion

Events occurring during Golgi biogenesis in control cells include formation and accumulation of post-ER material (step 1), formation of Golgi precursors (step 2) and their maturation giving rise to Golgi complex (Step 3). Upon depletion of GRASPs, the formation of Golgi precursors is delayed or impaired resulting in unflat Golgi stack.

The scheme in Figure 28 shows the formation and accumulation of post-ER material in the initial phase of Golgi biogenesis both in control and GRASP 65 & 55 depleted cells. The accumulation of post-ER material occurs in later phases under both conditions. But the formation of Golgi intermediates does not occur in GRASP 65 & 55 depleted cells. This might imply either a delay in their formation or inability to form resulting in swollen/unflat Golgi stack in GRASP double depleted cells compared to control cells (Figure 15).

5 Outlook

In this study I identified that GRASP 65 & 55 play a role in concert in the initial stages of Golgi biogenesis. And this role is important for formation and maturation of Golgi precursors into a proper Golgi. Further CLEM experiments on intermediate stages of Golgi biogenesis upon depletion of these two proteins might be necessary to fully understand their role. This study also shows that this combinatory approach is a very useful tool to validate the role of other proteins in Golgi biogenesis. But as this method is not high throughput, it is possible to validate only a limited number of candidate proteins.

In this study, I was not able to identify the major players that might be very crucial for the Golgi biogenesis process, although it should be possible using this method. One reason for this might be that the right genes were not tested due to the limitations of their knockdown or the availability of antibodies for those proteins. Hence, to overcome this limitation laser nanosurgery approach can be combined with single cell sequencing methods (Bandyopadhyay et al. 2014; Lovatt et al. 2014) to analyse the transcriptome of the Golgi depleted cells over time in order to identify interesting new candidates involved in Golgi biogenesis revealed by their altered expression in comparison to control cells. The transcriptomics data might reveal new candidate proteins or already known candidates that are very important for the Golgi biogenesis process. The role of such few major players can be validated by their acute depletion through RNAi and laser nanosurgery.

Another promising approach to identify major regulators of Golgi biogenesis is through scaling up the BFA assay to classify identified Golgi localised proteins at a genome scale. This can be expected to reveal more Golgi proteins behaving like Golgi matrix and playing an important role in the Golgi biogenesis process. However, characterisation of the identified proteins in a comprehensive manner by laser nanosurgery approach might be challenging. This limitation could be overcome by using a multi-labelling approach (Schubert et al. 2006), where several tens of proteins can be labelled with antibodies in a single cell. This can be used to label fixed cells for

multiple proteins at different time-points during the Golgi biogenesis. Hence, it would allow ranking of the proteins according to their order of arrival or abundance in different phases of Golgi biogenesis and thus narrow the selection of candidates that could be further validated using laser nanosurgery approach.

6 Materials

6.1 Cell culture

6.1.1 Eukaryotic cell lines

Cell line	Description	Source	Media
BSC-1	African green monkey kidney cells	ATCC (CCL-26)	MEM
BSC-1-GalT-GFP2	BSC-1 cell line stably expressing GalT-GFP2	EMBL, Heidelberg	MEM
HeLa Kyoto	Strongly adherent HeLa isolate	Kyoto University, Japan	DMEM
HeLa-GalNacT2-GFP	HeLa cell line stably expressing GalNacT2-GFP	Brian Storrie, Virginia Polytechnic Institute and State University, Virginia	DMEM

6.1.2 Reagents for Cell culture

All culture media and reagents were purchased from Gibco unless indicated and FCS was purchased from PAA laboratories GmBH.

Media	Cat. No.
MEM (Modified Eagle's Medium)	21090-022
DMEM (Dulbecco's Modified Eagle Medium, 1 g/L D-glucose)	31885-023
OptiMEM	51958
FCS (Fetal Calf Serum)	A15-101
0.05% Trypsin-EDTA	25300-054
Geneticin	10131
CO_2 Independent medium	ME080051L1

6.1.3 Cell culture and imaging media

Media Composition	Cell types
MEM complete 10% (v/v) FCS	BSC-1, BSC-1-GalT-GFP2

1% (v/v) L-glutamine	
DMEM complete 10% (v/v) FCS 1% (v/v) L-glutamine	HeLa Kyoto, HeLa-GalNacT2-GFP
Freezing medium DMEM/MEM 20% (v/v) FCS 10% (v/v) DMSO	BSC-1, BSC-1-GalT-GFP2, HeLa Kyoto, HeLa-GalNacT2-GFP
Imaging medium CO2 Independent Medium 10% (v/v) FCS 1% (v/v) L-glutamin	BSC-1, BSC-1-GalT-GFP2, HeLa Kyoto, HeLa-GalNacT2-GFP
Low FCS MEM Medium MEM 1% (v/v) FCS 1% (v/v) L-glutamine	BSC-1-GalT-GFP2 for laser nanosurgery experiments

6.1.4 Chemicals and drugs

Chemical	**Source**	**Cat.No.**
Brefeldin A	Sigma-Aldrich	B7651
Dimethylsulphoxide (DMSO)	Merck	102952
Hoechst	Sigma-Aldrich	33258
Methanol	Merck	106009
Mowiol	Calbiochem	475904
Oligofectamine	Invitrogen	12252-011
Paraformaldehyde	Polysciences Inc.,	00380-250
Saponin	Sigma-Aldrich	47036
Acetone	Merck	1.00014
Ethanol	Merck	100983
Adenoviral vector VSVG-t045-YFP (JJ_2015: Dilution 1:200)	Vector biolabs	-

6.1.5 Buffers and solutions

Buffer/Solution	**Source and Composition**
Phosphate Buffer Saline (PBS)	EMBL Media kitchen

	137 mM NaCl 2.7 mM KCl 1.4 mM KH2PO4 4.8 mM NA2HPO4/Na2CO3 Adjusted to pH 7.4, autoclaved
3% Paraformaldehyde (PFA)	Electron Microscopy Science 16% (#15710)
Saponin solution	Sigma-Aldrich 0.1% Saponin 10% FCS PBS

6.1.6 Special equipment and material/Others

Equipment/Material	**Source**
Centrifuge 5804R	Eppendorf
Microcentrifuge 5417R	Eppendorf
10cm Cell culture dishes	Nunc™
0.5 ml, 1.5 ml, 2 ml tubes	Eppendorf
15 ml and 50 ml Falcon tubes	BD Biosciences
Glass bottom dishes	MatTek COrporation
Cryotubes 1.5 ml	Nunc™
4 well LabTeks	Nunc™
Incubator	Binder
Water bath	GFLR
Table centrifuge	Sarstedt
Cell freezing container	Nalgene
Cell counting chamber	Superior Marienfeld

6.2 Microcontact printing

6.2.1 Reagents

Reagent	Source	Cat. No.
Fibronectin (from Bovine plasma)	Sigma-Aldrich	F1141-1MG
Glisseal N (Silicon-free grease)	Borer Chemie	-
Sylgard 184 kit (Silicone elastomer)	Dow Corning	1064291
Compressed Nitrogen gas	MESSER	50719294
mPEG-SPA-2000/5000	Shearwater	-

6.2.2 Other equipment and material

Material/Equipment	Source
Glass coverslips (~15 mM)	Menzel Glaser
Petri dishes (~35 mM)	Falcon
Plasma Prep2	Structure Probe
Vacuum Desiccator	Sybron Corporation

6.3 Oligonucleotides

All siRNAs were ordered from Life technologies unless mentioned.

Gene Symbol	siRNA ID	Sense siRNA Seq. 5'->3'	Antisense siRNA Seq. 5'->3'
GORASP2	s24914	CUAUUACACCUCUUAAAGAtt	UCUUUAAGAGGUGUAAUAGgt
GORASP1	s34818	CGCUCAUCGAGUCUCAUGAtt	UCAUGAGACUCGAUGAGCGta
GORASP1	s34819	GAAUUUCUCUCUUGGACAAtt	UUGUCCAAGAGAGAAAUUCcc
Giantin	s5951	GAAGCUUGAGGAACACGAAtt	UUCGUGUUCCUCAAGCUUCct
TMEM165	s31677	GCUCUCAACUAACUACAAUtt	AUUGUAGUUAGUUGAGAGCga
Neg9	s444246	UACGACCGGUCUAUCGUAGtt	CUACGAUAGACCGGUCGUAtt
TMF1	s14227	GGAGAUACCCAAACUUAGAtt	UCUAAGUUUGGGUAUCUCCtt
GOLGA2	145093	GGCUGGCAUGCAGCUUAACtt	GUUAAGCUGCAUGCCAGCCtt
GMAP210 (Dharmacon)	ON-TARGETplus	GGAGAUAGCAUCAUCAGUA CAAGAACAGUUGAAUGUAG GGACAUUACUAAAGAGUUA	UACUGAUGAUGCUAUCUCC CUACAUUCAACUGUUCUUG UAACUCUUUAGUAAUGUCC

	SMART pool	GGGCAAGACUGGAGAGUUA	UAACUCUCCAGUCUUGCCC

Custom designed siRNAs are listed in the table below.

Gene Symbol	**Sense siRNA Seq. 5'->3'**	**Antisense siRNA Seq. 5'->3'**
GORASP1	CCUGGACGUGUCAGGAAUUtt	AAUUCCUGACACGUCCAGGaa
GORASP1	CCAGGCAGAGUGACUACAUtt	AUGUAGUCACUCUGCCUGGaa
GORASP2	CUGUCGAGAAGUGAUUAUUtt	AAUAAUCACUUCUCGACAGtt

6.4 Immunofluorescence

6.4.1 Primary Antibodies

Protein	**Host**	**Source**	**Fixation**	**Dilution**
GM130	mouse	BD Biosciences	PFA	1:400
Giantin	rabbit	Abcam	PFA	1:600
CNAP	goat	Elmar Schiebel Group Heidelberg University	Methanol	
TGN46	sheep	Biozol	PFA	1:300
GRASP65	sheep	Martin Lowe, University of Manchester	PFA	

All the below mentioned antibodies were produced in rabbit, obtained from Emma Lundberg (Human Protein Atlas, SciLifeLab, Stockholm, Sweden) and were used with PFA fixation.

Protein	**Dilution**
STX5	1:45
GPRC5A	1:69
RP11-49K24	1:6
ACBD3	1:54
WDR45L	1:40
LRBA	1:100
RASSF6	1:9

COPG1	1:50
TMCO3	1:98
BET1L	1:200
DENND4B	1:104
GOLGA5	1:69
GOLIM4	1:10
AKAP9	1:222
TMF1	1:72
GOLM1	1:32
B4GALT1	1:10
GOLGB1	1:90
MANEA	1:30
GALNT2	1:19
PDE4DIP	1:10
SYNGR2	1:87
CCDC146	1:200
GCC1	1:100
CCDC25	1:20
BICD2	1:10
GAK	1:50
DYRK4	1:106
PLEKHA3	1:169
GORASP2	1:43
RASGEF1A	1:159
TMEM165	1:88
USO1	1:31
SNAPIN	1:65
TMED10	1:56
COG8	1:55

6.4.2 Secondary Antibodies

All the below mentioned secondary antibodies conjugated with AlexaFluor are obtained from Molecular probes.

Protein/Label	**Host**	**Dilution**
AlexaFluor 488-mouse	goat	1:200
AlexaFluor 568-mouse	donkey	1:200

AlexaFluor 647-mouse	donkey	1:200
AlexaFluor 647-sheep	donkey	1:200
AlexaFluor 568-rabbit	donkey	1:200
AlexaFluor 647-rabbit	donkey	1:200
AlexaFluor 568-sheep	donkey	1:50
AlexaFluor 568-rabbit	goat	1:200
AlexaFluor 488-mouse	chicken	1:200

6.5 Electron Microscopy

6.5.1 Chemicals

Chemical	**Source**
Cacodylic acid (Sodium cacodylate trihydrate)	Sigma-Aldrich
Malachite green oxalate salt	Sigma-Aldrich
25% Glutaraldehyde in H_2O	EMS
Osmium (OsO_4, 4% in H_2O)	Serva
Sodium citrate dehydrate	Merck
Epon	Serva
Tannic acid	EMS
Uranyl acetate (UA, 2% in 70% Methanol)	Serva
Lead nitrate	Sigma
$K_3Fe(CN)_6$	Merck
Methanol	Merck
Ethanol	Merck
Propylene oxide	Merck
Potassium chloride	Merck
Magnesium chloride	Merck
Calcium chloride	Merck
Sucrose	USB corporation
Epon resin chemicals	Serva

6.5.2 Fixative and solutions

All the compositions mentioned in this section are calculated to prepare 10 ml solutions.

Solution	Composition
Fixative 1	1 ml of 25% Glutaraldehyde 0.5 ml of 1 M KCl 0.26 ml of 0.1 M $MgCl_2$ 0.26 ml of 0.1 M $CaCl_2$ 7.98 ml of 50 mM Cacodylate buffer + 2% Sucrose
Fixative 2	1 ml of 25% Glutaraldehyde 0.5 ml of 1% Malachite green 5 ml of 0.2 M Sodium cacodylate buffer 3.5 ml of molecular grade distilled water
Post fixation solution	5 ml of 0.2 M Sodium cacodylate buffer 2.5 ml of 4% OsO4 2 ml of 4% $K_3Fe(CN)_6$ 0.5 ml of molecular grade distilled water
Tannic acid solution	0.1 g of Tannic acid 10 ml of molecular grade distilled H_2O Mix and filter
Uranyl acetate solution	0.1 g of Uranyl acetate 10 ml of molecular grade distilled H_2O
Lead citrate solution	0.266 g of $Pb(NO_3)_2$ 0.352 g of $Na_3(C_6H_5O_7)2H_2O$ 10 ml of molecular grade distilled H_2O
EPON 812	Mixture A: Glycid ether 100 (62 ml) + DDSA (100 ml) Mixture B: Glycid ether 100 (100 ml) + MNA (89 ml) EPON resin: Mixture A 3.23 g + Mixture B 8.48 g + 150 µl of DMP-30
Osmium solution	2% OsO_4 in 50 mM Cacodylate buffer

6.5.3 Other materials

Material	Source
Copper-palladium slot grids	Plano
Capsules	EMS
Oven (Incu-line)	VWR
Ultramicrotome	Leica Microsystems
Diamond knife	Diatome
Forceps (INOX)	Dumont
Biowave Pro	TED Pella

6.6 Microscopic setups

6.6.1 Wide field and electron microscopes

Microscope	Source
Zeiss Axiovert 200	Carl Zeiss
ScanR (Automated screening)	Olympus
Olympus CutR (with laser nanosurgery setup)	Olympus Rapp Optoelectronics
Biotwin CM120	FEI

6.6.2 Confocal Microscopes

Microscope	Source
Laser scanning microscope (LSM 780)	Carl Zeiss
2-Photon LSM 780 NLO	Carl Zeiss
Spinning disk Ultraview ERS	PerkinElmer
Spinning disk Ultraview VoX	PerkinElmer
Laser scanning microscope SP5 MSA	Leica

6.7 Software tools for data analysis and web tools

6.7.1 Software tools

Software	Source
Image J 1.51a	Wayne Rasband, National Institutes of Health (NIH), USA
RStudio 2.1	Free software foundation Inc., Boston, USA
MatLab R2012a	MathWorks Inc.
Cell Profiler 2.1.1	Broad Institute, Cambridge, USA
ScanR	Olympus, Hamburg, Germany

6.7.2 Web tools

Source	Usage
Bluegecko (EMBL internal) http://bluegecko.embl.de/cgi-bin/	siRNA search and screen data
Life Technologies RNAi Designer	siRNA design

https://rnaidesigner.thermofisher.com/rnaiexpress/	
ENSEMBLE BLAST/BLAT http://www.ensembl.org/Multi/Tools/Blast	Oligonucleotide mapping

7 Methods

7.1 Soft Lithography/Microcontact printing

To perform microcontact printing on coverslips, the first step is to produce PDMS stamps containing the desired three-dimensional pattern. These stamps were then used to print the fibronectin on the coverslips.

7.1.1 Production of PDMS stamps

The layout design for the stamp was done using CleWin software (WieWeb) and it was first translated into a 5 inch chromium photolithography mask by Delta Mask V.O.F (Enschede). This mask contains the repeated pattern for multiple stamps and was used to produce stamps with a silicone elastomer by a positive tone resist process. Poly DiMethyl Siloxane (PDMS) stamps were fabricated using a Sylgard 184 kit. The kit contains a silicone elastomer base and a curing agent, which were mixed thoroughly in a 10:1 ratio. This mixture was then placed in a vacuum desiccator to remove the air bubbles, which can otherwise interfere with the pattern. Once the bubbles are completely removed, the mixture was poured onto the mask and it is placed in the vacuum desiccator for another round of bubble removal. It was then polymerized overnight in an oven at 55°C. The polymerized elastomer was peeled off carefully by slowly lifting it up taking care not to damage the mask. Individual stamps containing 6 μm lines were cut out and stored in the fridge at +4°C. These stamps were used to print fibronectin on the coverslips and were washed and re-used for several rounds of microcontact printing.

7.1.2 Printing of fibronectin lines on coverslips and seeding cells

For printing the fibronectin lines on 15 mm glass coverslips, the coverslips were first washed with acetone, ethanol and deionised water to remove any dirt from the surface. The coverslips were then dried using compressed nitrogen gas. The PDMS stamps were pre-incubated with 100 μl of fibronectin solution (50 μg/ml in PBS) for 30 min. To perform Laser nanosurgery experiments, a 10 cm hole was drilled in the centre of

35 mm petri dish and a 15 mm glass coverslip patterned with fibronectin lines was attached. The coverslips were treated with oxygen plasma for 2 min at a power of 2.5 for an efficient attachment and printing by the PDMS stamps. The stamps were washed with deionised water to remove the excess fibronectin and dried using the compressed nitrogen gas. These fibronectin-coated stamps were gently placed on the coverslips, with the side of the pattern contacting the surface of the coverslip. The stamps were left to transfer the fibronectin onto the coverslips for 10 min. After incubation, the stamps were carefully removed and washed with ethanol and water. They were dried and stored at +4°C for later use. The coverslips were now incubated with 100 µl of Poly L-Lysine-g-Poly Ethylene Glycol (PLL-g-PEG) (1 mg/ml) diluted 1:100 in PBS for 30-45 min. The coverslips were washed twice in PBS by dipping it in and out in a 50 ml falcon tube as quickly as possible, while keeping in mind the patterned side. This allows the water film to reach the bottom of the coverslip, leaving the rest of the coverslip dry. The remaining small droplet of water can be removed carefully by using a soft tissue without touching the region with the pattern. These coverslips were placed individually in 3 cm petri dishes with the fibronectin pattern facing upwards and stored at +4°C for a couple of weeks. To glue these coverslips to a 35 mm dishes, 10 mm holes were drilled in the centre. The coverslips were glued to the bottom these dishes with the help of Glisseal (grease) and nail polish (to ensure the stability). These dishes are allowed to dry for a few minutes and then used to seed cells.

7.2 Cell biology

7.2.1 Cell culture

All the material used for the cell culture must be sterile to prevent any contamination of the cells. BSC1-GalT-GFP2 cells were cultured in MEM medium supplemented with 10% FCS, 1% L-Glutamine and 400 µg/ml of fresh Geneticin at 37°C in 5% CO_2. Geneticin is added in order to maintain the selection pressure for the GalT-GFP2 positive clones. The cells were continuously passaged once they reach 80% confluence, until 25 passages. To do this, the cells were washed once with 2.5 ml of trypsin-EDTA

solution and incubated with 2 ml of the same in the incubator for a few minutes till the cells detach. Once the cells detach, 8 ml of the supplemented medium was added to saturate the trypsin. The cells were then pipetted in and out of the petri dish a few times, to de-clump them. These cells were seeded into a new 10 cm petri dish according to desired confluence and need for the experiments (1:2, 1:5, 1:10).

HeLa-GalNac-GFP cells were cultured in low glucose (1 g/l) DMEM supplemented with 10% FCS, 1% L-Glutamine and 400 μg/ml of fresh Geneticin at 37°C in 5% CO_2. The cells were passaged continuously for 20 passages in a similar way as in the case of BSC1-GalT-GFP2 cells.

7.2.2 Plating cells

The cells were counted and plated on coverslips or glass bottomed dishes depending on the duration of the experiment and the size of the dish. The following tables show number of BSC1-GalT-GFP2 cells plated for different durations of knockdown in a MatTek dish with a total volume of 2.5 ml as well as the number of cells seeded in a 4 well Labtech with a total volume of 900 μl. To perform Laser nanosurgery experiments the following day, BSC1-GalT-GFP2 cells were counted and 10×10^4 cells were seeded on a 35 mm dish prepared by gluing a 15 mm patterned coverslip (see 7.1.2).

Dish size	**Number of cells**	**Knockdown duration**
35 mm	1.5×10^4	96 h
35 mm	3×10^4	72 h
35 mm	6×10^4	48 h

Labtech	**Number of cells**	**Knockdown duration**
4 well	0.7×10^4	96 h
4 well	1.2×10^4	72 h
4 well	2.2×10^4	48 h

7.2.3 Freezing and thawing cells

The cells were frozen and stored in liquid nitrogen to maintain stocks for later use. In order to freeze the cells, the freezing media was prepared and stored at +4°C. The cells

were detached from 10 cm confluent petri dishes using trypsin-EDTA and were re-suspended (see 7.2.1) into 15 ml falcon tubes. The cells were centrifuged at 1000 rpm for 5 min in a centrifuge (5804R) to obtain a cell pellet. After carefully removing the supernatant, the cell pellet was re-suspended in 0.5 ml of cold FCS and 0.5 ml of cold freezing media. This mixture was carefully transferred into pre-chilled cryotubes. The cryotubes were transferred into a cell freezing container which promotes slow freezing of the cells. The container was immediately stored at -80°C for 1-2 days before transferring into the liquid nitrogen container (-160°C) for long-term storage.

To thaw a frozen vial of cells, the cryotubes were placed in a 37°C water bath with the help of a float, taking care not to immerse or contact the lid with the water. After quickly thawing the cells, they were transferred into a 15 ml falcon tube containing 9 ml of pre-warmed medium supplemented with FCS and L-Glutamine (see 7.2.1). These tubes containing cells were further centrifuged at 1000 rpm for 5 min and the supernatant containing DMSO was carefully removed leaving the cell pellet in the tube. The cells were further suspended in 10 ml of complete medium and transferred and distributed into a 10 cm petri dish. These cells were passaged at least three times before using them to perform any experiments.

7.2.4 Transfection of eukaryotic cells

To inhibit the re-synthesis of selective proteins and thus to obtain a gene knockdown, the cells were transfected with small interfering RNAs (siRNAs). To perform the transfections, the required numbers of cells were seeded onto a 35 mm MatTek dish or a 35 mm dish with a fibronectin-patterned coverslip (see 7.1.2) the day before (see 7.2.2). The transfection protocol involves the preparation of two separate solution mixtures and incubating them for 5 min. The contents of the mixture 1 were transferred into the tube containing mixture 2 and the resulting solution was incubated for 20 min. Mean while the MEM/DMEM complete medium of the cells was washed and replaced with the MEM/DMEM growth medium (without FCS) and placed back in the incubator at 37°C and 5% CO_2. After the incubation, the MEM/DMEM growth medium (without

FCS) was replaced with 200 µl of the same medium and the transfection mixture was carefully added dropwise.

The following table shows the compositions of mixture 1 and 2 used for transfection.

Dish size and volume	**Mixture 1**	**Mixture 2**	**Incubation time**
35 mm (2.5 ml)	OptiMEM 26 µl Oligofectamine 1.5 µl Incubate for 5 min	OptiMEM 70 µl siRNA 3.33 µl Incubate for 5 min	Mix.1+Mix.2 for 20 min
4 well Labtech	OptiMEM 13 µl Oligofectamine 0.75 µl Incubate for 5 min	OptiMEM 35 µl siRNA 1.5 µl Incubate for 5 min	Mix.1+Mix.2 for 20 min

7.2.5 Brefeldin A (BFA) Treatment

The BSC1-GalT-GFP2 cells were seeded on autoclaved coverslips (~11 mm) placed in a 10 cm dish the day before in a 1:2 ratio from a confluent dish. BFA (1:1000) was diluted into MEM complete medium in a 15 ml falcon tube the following day. The MEM complete medium was removed and replaced with the medium containing BFA. The cells were placed back into the incubator for 30 min. After the incubation, the medium was removed and the cells were washed with PBS and fixed with 3% PFA (see 7.2.6). The individual coverslips were then stained for different proteins, markers and mounted onto the glass slides with Mowiol for imaging.

7.2.6 Immunofluorescence

The cells seeded on petri dishes or coverslips were fixed with 3% PFA for 20 min. To permeabilize the cells, saponin solution (0.1% Saponin and 10% FCS in PBS) was used. One or more primary antibodies were diluted in saponin solution and incubated for 1 hr in a humid chamber. The cells were washed thrice with PBS with a 3 min time interval. The cells were subsequently stained with one or more secondary antibodies (tagged a fluorescent molecule e.g. AlexaFluor), which were also diluted in saponin solution and this was incubated for 1 hr. This was followed by another round of

washing with PBS three times with a 3 min time interval. The cells were subsequently treated with Hoechst (dilution 1:5000) for 5 min to stain the nuclei. The coverslips were further rinsed twice with PBS and mounted onto glass slides with Mowiol and allowed to dry overnight on the bench or for 30 min in the incubator (37°C). In case of petri dishes, the cells were washed and imaged directly in PBS without the need for mounting. The samples can be stored at +4°C for a couple of days for imaging.

7.3 Laser nanosurgery and Microscopy

For performing laser nanosurgery to deplete the Golgi, the laser must be optimized, calibrated and the cells showing a displaced Golgi from the nucleus must be identified.

7.3.1 Calibration of laser nanosurgery system

To perform a successful laser nanosurgery, the x,y plane of the laser must be calibrated or aligned to the x,y plane of the field of view. This must be done using the same objective, which will be later used for laser nano surgery experiments. To perform this, a 35 mm glass bottomed petri dish was used and an area without cells was selected. For the calibration, the Rapp UGA software was switched to calibration mode, which generates small circles along the four corners of the screen sequentially. Using the keys of the keyboard the laser scanner must be moved to the centre of these displayed circles. After the calibration of these borders of the field of view, the software generates 16 points evenly distributed in the field of view. The laser scanner must be moved to these points, which allows the software to determine the deviations between the aimed position and the actual position of the laser spot. Once the calibration is successfully done, it can be saved and re-used for several days. To quickly check if the laser is still properly calibrated, the glass can be etched and compared with the drawn pattern (see 7.3.3).

7.3.2 Laser nanosurgery to deplete the Golgi apparatus from the cell

Once the laser calibration is checked, the cells showing a displaced Golgi from the nucleus must be identified from the dish. The laser nanosurgery was performed with a

60X water immersion objective (1.2 NA) at 1% of the total laser power. An image of the cell was taken with both the GFP channel and the transmission to visualize the Golgi and the nucleus. A line was drawn perpendicular to the axis of the cell between the nucleus and the Golgi using Rapp UGA software. The laser nanosurgery was performed in multiple cycles by moving the z-focus position from the top of the cell to the bottom in 3-4 s, having the laser on 1% power. This allows the disruption of actin cytoskeleton and as a result in the separation of the cell into two parts by thinning and closing the membrane. These cycles were repeated by giving a 1 min interval for the cell to recover. This was done till the Golgi is depleted from the cell.

7.3.3 Laser inscription for tracing back the cells

After performing a successful laser nanosurgery and depleting the Golgi from the cell, one can loose track of the cell if the dish is accidentally touched or moved. It will be very difficult to trace back the cell by looking and going through the entire dish. It is also difficult to trace back the cell after performing Immunofluorescence or other treatments. So the region of these cells of interest must be marked few minutes after the laser nanosurgery. This was done by inscribing a rectangle in the field of view of the cell of interest, inside the coverslip. This was done with a 3% laser power, while making sure to focus the laser inside the glass coverslip (by verifying that the cells are out of focus while performing the etching). This is particularly important because focusing the laser on outer surface of the coverslip can damage or even kill the cells of interest. The inscribed pattern was used to find back the cells of interest.

7.3.4 Time lapse imaging of the karyoplast

The karyoplasts were allowed to recover for 2 hr after the laser nanosurgery and then followed by time-lapse imaging. The time-lapse imaging was performed with the help of Cell^R or Xcellence rt software using a 20X (UPlanSAPo, NA 0.75) objective on either the Olympus CutR or ScanR equipped with a 37°C environmental box. During the acquisition, the chamber was setup to be humid and at 37°C. As the karyoplasts moved a lot along the fibronectin lines during the acquisition, a low magnification objective (20X) was used instead of a higher magnification. The karyoplasts were imaged every

12 min for 20-22 hr time period in transmission and GFP channels. This time resolution and magnification were enough to follow the karyoplasts and to quantify the newly formed fluorescent structures during the Golgi biogenesis process. At the end of the timelapse, the cells are either fixed with 3% PFA for staining with antibodies for different proteins or fixed for performing CLEM.

7.3.5 Wide field imaging of fixed cells

After performing the immuno-staining to label different proteins in the cell, they were imaged using a Zeiss axiovert 200 widefield microscope or ScanR. The images were acquired using either 40X/NA 1.3 oil immersion objective or 63X/NA 1.4 oil immersion objective. The images of the VSVG assay were acquired using ScanR using a 20X air objective.

7.3.6 Confocal imaging of fixed cells

The confocal imaging of fluorescently labelled Golgi, mitotic cells and BFA treated cells were performed using the following microscopes. Zeiss LSM780 or LSM780 NLO, Perkin Elmer Ultraview ERS or VOX and Leica SP5 MA. Z-stacks were acquired to cover the entire cell while imaging.

7.3.7 Automated imaging of Mitotic cells

I used adaptive feedback microscopy (Tischer et al. 2014) to identify cells in the early stages of mitosis (pro-metaphase) similar to previous publication method (Conrad et al. 2011). Online image analysis used to classify cells was based on supervised machine learning trained by example. The imaging was done using a confocal microscope SP5A with the HCS software extension (or matrix screener). We set up a low magnification pre-scan (512×512 and zoom: 1X) and these images were analysed online using the Cell cognition software package (Held et al. 2010). This cell cognition software package includes a classifier that needs to be trained beforehand with a training set of images, in order to identify the cells of interest.

To do so, images were acquired for 24 hr with HeLa-GalNacT2-GFP H2B-mCherry expressing stable cell line with the low magnification pre-scan. These set of images were used to train the classifier in Cell cognition software for pro-metaphase during mitosis.

This was done by picking positive and negative examples of cells and annotating them to two different classes. Cells showing a condensing DNA to enter metaphase were picked and annotated as pro-metaphase and all other cells showing interphase morphology, dead cells etc., were annotated as others. After successful annotation and training of the software with good number of examples, the training set was saved. The communication between Leica matrix screener software and Cell cognition was established using a python script similar to previous publication (Hilsenstein 2014). Once a mitotic cells are detected, a high magnification (512×512 and zoom: 4X) time-lapse imaging was started and the mitotic cell was imaged every 2.5 min for 2 channels (Golgi and nucleus) with 20 z-slices at a distance of 1 μm for 30 time points. Upon completion of the high magnification imaging, the software was set-up to switch back to the low magnification mode to find cells of interest. This process was looped and images were acquired for 24 hr. The analysis of this time-lapse data is described in section (see 7.5.4).

7.3.8 Correlative light and electron microscopy (CLEM)

CLEM was used to examine the same sample with fluorescence microscopy and to get the details of the ultra structure (of the regions of interest) using electron microscopy. Images were acquired using a light microscope prior to chemical fixation for EM. The sample was then fixed using chemical fixation protocol for EM. The cell of interest was traced back on the light microscope and the surface is etched or removed along a desired pattern to generate grooves on the glass coverslip. The sample was further processed and embedded into epon resin which generates ridges, helping to easily locate the region of interest. (Tängemo et al. 2011)

7.3.8.1 Cell preparation

Cells were seeded the day before the experiment on 35 mm dishes glued with glass coverslip at the bottom (see 7.1.2) in a low FCS medium. The cells were transfected with siRNA (to inhibit the re-synthesis of the selected proteins) 5 hr before the laser nanosurgery. After 4 hr medium was replaced by CO_2 independent medium with 10% FCS, which allows cells to migrate resulting in a displacement of the Golgi from the

nucleus. The laser nanosurgery was performed on cells and they were imaged till a desired time point was reached. At the end of the time-lapse, the cells were imaged in the GFP channel with a 60X water immersion objective. The cells were then fixed following either of the EM fixation protocol mentioned below.

7.3.8.2 EM fixation protocol

All the below steps were performed in a Biowave Pro without the lid of the petri dish containing cells.

1. The cells were fixed with Fixative 1 in the Biowave Pro for 14 min under vacuum and a power of 0 watts and 100 watts alternating between two minute cycles.
2. They were rinsed twice with 50 mM Cacodylate buffer and put back in the Biowave Pro for 80 s at a power of 250 watts under vacuum.
3. The etching of the coverslip surface was either performed at this step or at a later step mentioned below. The cells were traced back on the light microscope and the surface of the coverslip was etched to form grooves.
4. The mixture A of epon resin was prepared by adding all the chemicals and placing it on a magnetic stirrer. Once these contents were mixed well, mixture B was also added and left stirring. The speed of the magnetic stirrer was kept low to avoid formation of any air bubbles.
5. The cells were further treated with osmium solution and placed back in the Biowave Pro for 14 min under vacuum and a power of 0 watts and 150 watts alternating between two minute cycles.
6. The cells were rinsed twice with water and put back in the Biowave Pro for 80 s at a power of 250 watts under vacuum.
7. The etching of the coverslip could also be performed at this step. The cells were treated with UA solution for 7 min under vacuum and a power of 0 watts and 150 watts alternating between one minute cycles.
8. Subsequently, the cells were washed twice with water and put back in the Biowave Pro for 80 s at a power of 250 watts under vacuum.

9. The cells were dehydrated using different concentrations of ethanol (25%, 50%, 75%, 90%, 100% and 100%) slowly and sequentially under vacuum for 40 s in each concentration at a power of 250 watts.
10. The coverslips were carefully detached from the 35 mm dish or a 35 mm MatTek while immersing them into the 100% ethanol (not to dry out the sample). The coverslips were quickly rinsed in propylene oxide and twice in ethanol and placed immediately on the pre-prepared epon resin (filled in a capsule) for flat embedding. For this step, the coverslip is placed in such a way that the cells were in contact with the epon resin.
11. Making sure the coverslip is in complete contact with the resin, the capsule is quickly turned upside down to finally have the coverslip at the bottom with the resin on top. Care should be taken not to move the coverslip or allow the resin to spill out of the capsule, which might effect the embedding. This allows the air bubbles to float up to the top of the capsule without interfering with the embedding of the sample.
12. The sample was left to polymerize at 60°C for 24 hr. Upon polymerization, the coverslip was removed from the resin block by using alternate freeze thaw cycles in liquid nitrogen and hot water. This results in irregular expansion of the glass coverslip, allowing it to break and detach from the resin block.

7.3.8.3 EM Fixation protocol with Malachite green

1. The cells were fixed with Fixative 2 in the Biowave Pro for 14 min under vacuum and a power of 0 watts and 100 watts alternating between two minute cycles.
2. They were rinsed twice with 0.1 M Cacodylate buffer and put back in the Biowave Pro for 80 s at a power of 250 watts under vacuum.
3. The etching of the coverslip surface was either performed at this step or at a later step mentioned below. The cells were traced back on the light microscope and the surface of the coverslip was etched to form grooves.
4. The mixture A of epon resin was prepared by adding all the chemicals and placing it on a magnetic stirrer. Once these contents were mixed well, mixture B

was also added and left stirring. The speed of the magnetic stirrer was kept low to avoid formation of any air bubbles.

5. The cells were further treated with Post fixation solution and placed back in the Biowave Pro for 14 min under vacuum and a power of 0 watts and 100 watts alternating between two minute cycles.
6. The cells were rinsed twice with Cacodylate buffer and put back in the Biowave Pro for 80 s at a power of 250 watts under vacuum.
7. The cells were treated with Tannic acid solution for 7 min under vacuum and a power of 0 watts and 150 watts alternating between one minute cycles.
8. The cells were again washed twice with Cacodylate buffer and put back in the Biowave Pro for 40 s at 250 watts power.
9. The Cacodylate buffer was replaced with water and placed back in the Biowave Pro for 80 s and a power of 250 watts.
10. The etching of the coverslip could also be performed at this step. The remaining steps of the protocol is same as described above from steps 7 to 12.

7.3.8.4 Etching of the glass coverslip

To locate the cells of interest after the flat embedding of cells upon EM fixation, the coverslip surface was etched by laser. This was done either before treating the cells with osmium or before the Uranyl acetate as mentioned in the protocol earlier. Two rectangular line patterns were etched on both sides of the cell of interest with a 5% of the total laser power. This higher energy (~600 nJ) per pulse result in the formation of plasma accompanied by cavitation, which is the formation of transient hypersonic bubbles. These bubbles can potentially harm cells in the close proximity (~20 μm). So the etching was performed at least 100 μm away from the cells of interest. This ensures that the etching of the glass surface will not effect the cells of interest. In case of multiple cells, additional lines or patterns were etched to distinguish one cell from the other. The etching was done with a 63X/1.2 NA Water objective.

To perform the etching, the cells of interest were located using the 20X or 10X objective lens and the positions were marked using the CellR software. The objective lens was

changed to 63X/1.2 NA water and a desired line pattern was drawn at least 100 μm away from the cell of interest on one side. The glass was etched with the laser to form grooves on the surface. The same was repeated on the other side of the cell. Once the etching was done, the objective lens was changed back to 20X and images were taken of the entire field of view with the line patterns and the cells. This was used as a map to locate the cell of interest upon flat embedding and sectioning the sample.

7.3.8.5 Trimming and Sectioning of the resin block

The trimming and sectioning of the resin block was kindly performed by Paolo Ronchi (EMBL Heidelberg). The ridges on the polymerized resin blocks help in easily identifying the position of the cells using a dissecting microscope. Upon identification of these positions, the resin block was trimmed with a razor blade into a trapezoid shape, removing the resin around it and just keeping the area of interest with the markings. Serial ultrathin sections (thickness 70 nm) were prepared using a Leica UC7 ultra microtome, which were transferred to copper palladium slot grids (2×1 mm) freshly coated with Formvar. The cells fixed without malachite green protocol (see 7.3.8.2) were contrasted with UA (2% in methanol) and lead citrate. Finally the cells were identified based on the cell map from the light microscope and imaged using the Transmission Electron Microscope (TEM).

Note: It was often not possible to trim more than five cells on a single coverslip mark as the razor blade or a saw used to trim the block is not precise enough to separate many different positions on the resin block.

7.3.9 Quantification of the time-lapse/Golgi biogenesis

To analyse and quantify the time-lapse imaging (after laser nanosurgery and during mitosis), Image J and Cell profiler were used. And to extract the time taken for different phases during the Golgi biogenesis, a Matlab script was used. The cells were segmented and images were processed using Image J (see 7.5.2), a cell profiler pipeline (see 7.5.3) was used to identify and segment the GalT-GFP2 structures and to quantify the fluorescence intensities. MatLab (see 7.5.4) was used to plot the data from the Cell profiler and to extract the time taken for different phases of Golgi biogenesis.

7.4 VSVG assay

VSVG protein from ts045 mutant strain of Vesicular Stomatitis Virus (VSV) has been widely used to study membrane transport. This is a temperature sensitive mutant which is misfolded, retained in the ER at 40°C and upon temperature shift to 32°C, the protein moves out of ER (Beckers, Keller, and Balch 1987; Bergmann 1989; Kreis and Lodish 1986).

In this assay we used YFP tagged VSVG protein from ts045 mutant strain to visualise its localization and study protein transport from the ER to Golgi. This was done in control cells and cells treated with GRASP65 and 55 siRNA to quantify and measure the transport efficiency from ER to Golgi in both cases.

7.4.1 Protocol for VSVG assay

1. BSC1 cells (8×10^4) were seeded in 5 cm petri dishes with coverslips inside.
2. After 24 hr cells were transfected with control and GRASP65+55 siRNAs in individual dishes.
3. A moist chamber was prepared and a Parafilm was placed inside, to add droplets of virus for infection.
4. Cells were infected with the VSVG-YFP from Vector bio labs by placing 50µl drops of diluted virus on a Parafilm and placing individual coverslips on each drop. Cells were incubated with virus for 1 hr at 37°C.
5. A 12 well plate with cell culture medium was prepared to put each coverslip into individual wells after infection. Coverslips were transferred to the 12 well plate.
6. Cells were washed with 2 ml of medium to remove any residual virus and 12 well plate was placed at 37°C for 20 min.
7. Plates were transferred to 40°C and leave it for 16-18 h.
8. After the incubation, 2 µl of Cyclohexamide (dilution 1:1000) and 50 µl of HEPES buffer (25mM) was added to the individual wells and incubated at 32°C according to respective release times (20 min) to stop new protein synthesis and release the existing protein from the ER. The cells with zero time point were immediately fixed without the addition of Cyclohexamide.

9. Cells were fixed with 3% PFA (20 min) and permeabilise with Saponin (0.1%) and FCS (10%). Immuno-staining was performed with anti mouse GM130 primary antibody for 45 min followed by washing with PBS and staining with Secondary antibody (tagged with Alexa Flour 568).
10. Nucleus was stained with Hoechst (dilution 1:5000) for 5 min. Coverslips were mounted with Mowiol and dried at room temperature overnight. The samples were then imaged using ScanR microscope.

7.5 Computational Biology

7.5.1 Image Analysis

7.5.2 Image J

Image J was used to visualize all the images acquired for different experiments.

7.5.2.1 Analysis of Golgi biogenesis

To analyse the increase in the fluorescence intensity of the GalT-GFP2 structures, the GFP channel of the time-lapse was loaded into Image J. A mask was drawn around the cell of interest for each frame of the time-lapse and the images were named as mask and saved as an image sequence. A mask was drawn for the background (without any cells) by z-projecting all the frames of the time-lapse, named as BG and saved as an image sequence. The time-lapse of the GalT-GFP2 channel was also saved as an image sequence containing GFP in the name. These images were further analysed by Cell Profiler.

The z-stacks from obtained from confocal imaging were sum projected for the GFP channel for Golgi. Then masks for background and cell were created in the same way as mentioned above. Also the time-lapse was saved as an image sequence as mentioned earlier. These images were further analysed by Cell profiler with an additional module to convert the 32-bit images to 8-bit.

7.5.2.2 Analysis upon Brefeldin A treatment

For the Co-localization analysis with Golgi matrix, Golgi enzyme or TGN/Centrosome upon BFA treatment the confocal images were loaded into the software and z-stacks were projected with maximum intensity.

7.5.2.3 Quantification of luminal width of Golgi cisternae

To quantify the changes in the morphology of Golgi cisternae upon double depletion of GRASP55 and GRASP65, we measure the maximum luminal width of the Golgi cisternae. The scale bar of EM images was used to find the unit length in the image and the line tool in Image J was used to obtain the maximum luminal width by measuring number of units (Lee et al. 2014). The maximum luminal width was converted to nanometres based on unit length in the image.

7.5.3 Cell Profiler

7.5.3.1 Analysis of Golgi biogenesis

The image sequences saved in the input folder from Image J (see 7.5.2.1) were analysed by a Cell Profiler pipeline developed by Christian Tischer (EMBL Heidelberg). The Cell Profiler pipeline contains different modules, which perform different tasks. The following is a brief workflow of the Golgi biogenesis pipeline.

A *LoadImages* module loads all the images from the selected input folder. The module *EnhanceOrSuppressFeatures* was used to enhance the fluorescent signal of the particles using a tophat filter by subtracting the local background. The module *IdentifyPrimaryObjects* was used to identify the background from the images with background mask. The fluorescent signal and the background were measured using *MeasureImageIntensity* module. The background subtraction was done using the *ImageMath* module. *IdentifyPrimaryObjects* module identifies the objects within the cell outline using the mask created by the user. The *Crop* module crops the region with the cell outline. The primary objects or dots were identified from the cropped cell using *IdentifyPrimaryObjects*. The threshold parameters in this module were adjusted and verified according to the intensity of the structures. The dots or objects size was measured using *MeasureObjectSizeShape* module and the objects were filtered based on

their size as small dots and big dots using two *FilterObjects* modules. The identified objects were converted into image using *ConvertObjectsToImage* module and the intensity values in the image were rescaled to stretch the intensity to its full range using *RescaleIntensity*. The outlines of the big and small dots were overlaid onto the image using *OverlayOutlines* module. These images were saved in a tile format with the rescaled gfp image, the gfp overlay image with identified objects/dots, mask outlines for cell and background and the image with all identified dots using *Tile* and *SaveImages* modules. The object intensities, size and shape were measured and they were assigned back to the objects using *MeasureObjectIntensity*, *MeasureObjectSizeShape* and *RelateObjects* modules respectively. Finally the measured parameters were exported and saved as a .csv file as individual files for cell, image, smalldots and big dots. This data was further normalized and plotted using MatLab. The following is the general cell profiler pipeline used to analyse the structures formed during the Golgi biogenesis.

LoadImages
EnhanceOrSuppressFeatures
IdentifyPrimaryObjects
MeasureImageIntensity
ImageMath
IdentifyPrimaryObjects
Crop
IdentifyPrimaryObjects
MeasureObjectSizeShape
FilterObjects
FilterObjects
ConvertObjectsToImage
RescaleIntensity
OverlayOutlines
Tile
SaveImages
MeasureObjectIntensity
MeasureObjectIntensity
MeasureObjectSizeShape
RelateObjects
RelateObjects
RelateObjects
ExportToSpreadsheet
ExportToSpreadsheet

A cell profiler pipeline with same modules was used to segment structures in mitotic cells.

7.5.3.2 Analysis of ER to Golgi transport by VSVG assay

The images obtained from the VSVG assay were analysed by a Cell Profiler pipeline developed by Christian Tischer (EMBL Heidelberg). The following is a brief workflow of the Golgi biogenesis pipeline. The images include a DAPI channel stained for nucleus, GFP channel with YFP-tagged VSVG and a Cy3 channel containing Golgi stained for GM130.

A *LoadImages* module loads all the images from the selected input folder by specifying names of different channels. The intensity values in the image were rescaled to stretch the intensity to its full range using *RescaleIntensity* by specifying intensity range of the image. *IdentifyPrimaryObjects* module identifies and segments the nuclei from the DAPI channel. *IdentifySecondaryObjects* module expands the specified distance from the nucleus to mark approximate cell boundaries. *IdentifyPrimaryObjects* module identifies and segments the Golgi from the Cy3 channel. The background subtraction was done using the *ImageMath* module. The *Crop* module crops the image to remove the incomplete cells on the edges of the image. *MaskImage* module is used to mask identified cells. The fluorescent signal and the background of cells were measured using *MeasureImageIntensity* module. *Smooth* module is used to smooth the image using a Gaussian filter to properly segment the cells. *IdentifySecondaryObjects* module uses a watershed method to find the exact outlines of the cell. *MeasureObjectSizeShape* module is used to measure the size and shape of the segmented cells. *DisplayDataOnImage* displays the segmented cell on the background corrected image with the measured area. *FilterObjects* module is used to exclude improperly segmented or too big cells from the analysis also based on size of the nucleus. *MeasureObjectSizeshape* is applied to measure the Golgi size and shape. expands the specified distance from the nucleus to mark approximate cell boundaries. Upon applying proper threshold to remove the saturated cells (*ApplyThreshold*) and filtering improperly segmented Golgi (*FilterObjects*)

the intensities are measured. The Golgi mask from Cy3 channel is applied on the GFP channel to identify the Golgi (*MaskImage*) and the intensities are re-scaled back.

The outlines of the cell, nucleus and Golgi were overlaid onto the image using *OverlayOutlines* module. These images were saved with the rescaled GFP image, the nucleus and Golgi overlay with identified objects/dots, mask outlines for cell using *SaveImages* modules. The objects were assigned to cells using *RelateObjects* module. Briefly, cells are segmented using GFP channel, the Golgi is segmented using Cy3 channel and the Golgi mask is created. This mask was applied and the fluorescence intensity is measured on GFP channel for individual cells. Finally the measured parameters were exported and saved as a .csv file with individual cell measurements and image measurements. This data was further normalized and plotted using R.

The following is the general cell profiler pipeline used to measure the amount of VSVG in the Golgi.

LoadImages
RescaleIntensity
RescaleIntensity
IdentifyPrimaryObjects
IdentifySecondaryObjects
IdentifyPrimaryObjects
MeasureImageQuality
ImageMath
Crop
MaskImage
MeasureImageIntensity
Smooth
IdentifySecondaryObjects
MeasureObjectSizeShape
DisplayDataOnImage
FilterObjects
MeasureObjectSizeShape
DisplayDataOnImage
FilterObjects
ApplyThreshold
MeasureObjectIntensity
FilterObjects
MeasureObjectIntensity
DisplayDataOnImage
FilterObjects
MaskImage
MeasureObjectIntensity

RescaleIntensity
RescaleIntensity
RescaleIntensity
GrayToColor
OverlayOutlines
SaveImages
RelateObjects
ExportToSpreadsheet
CreateBatchFiles

7.5.4 MatLab

The duration of phase 1 and phase 2 were extracted through a MatLab script developed by Aliaksandr Halavati (EMBL Heidelberg). The following is a brief outline of MatLab script used for the analysis of multiple .csv files containing data from Golgi biogenesis of single cells with different protein depletions. The first part of the script *choose files to iterate* clears all the existing data in the MatLab and then it goes to the specified path to load the files. In *Make a new file to record summary*, it makes a new excel file to save the extracted values called *Analysis summary*. In the next step *perform calculations* it calculates the t1, t2, t1s and t2s which are the durations of phase1, phase2 from raw values and smoothed values respectively.

These values are calculated using a function called "Total Variation Regularized Numerical Differentiation" (TVDiff). This function deals with the noisy data. It regularizes the differentiation process to avoid the noise amplification of finite-difference methods. So total variation regularization is used and it allows for discontinuous solutions. The resulting algorithm accurately differentiates noisy functions, including the ones that have a discontinuous derivative (reference paper rick chartrand). The parameters regularization factor and number of iterations must be adjusted based on the data. In this section, the data is imported (*data import*) from the table and the intensity of the post-ER structures or Golgi precursors is obtained by multiplying the number by the mean integrated intensity of the segmented structures. In the next section, *calculations* are performed to obtain the regularized differentiation values. These values are further integrated (*integration)* and the switching points of different phases were obtained from *Getting switch time points.* These switching points

and the derivatives with raw and smoothed values are plotted in a single plot by the commands in *plotting.*

In the script for multiple analysis, the above mentioned function is looped to perform the same calculations for all the files in the folder. At the end the values of the t1, t2, t1s and t2s are saved in the excel file created as the *Analysis summary*.

Multiple file analysis

```
clear
%% choose files to iterate
dir_pth='Z:\vegesna\Bsc1_GalT_cut_cells\12. GR65(01+02)_new'; %path to the input directory
d = dir(fullfile(dir_pth,'*.csv'));
nfiles=length(d);


%% Make a new file to record summary
outTblPth=fullfile(dir_pth,'AnalysisSummary.xls');
header={'DataName', 't1raw', 't2raw', 't1smooth', 't2smooth'};
if (exist(outTblPth,'file')==2)
   delete (outTblPth);
end
xlswrite(outTblPth,header,'Analysis Summary','A1')


%% perform calculations
for k = 1:nfiles
   close all
  filenm=d(k).name;
   [t1, t2, t1s, t2s]=Niki_analysis_individualfiles_func(dir_pth,filenm);
   writeOutput={filenm t1 t2 t1s t2s};
   xlswrite(outTblPth,writeOutput,'Analysis Summary',strcat('A',num2str(k+1)))
   %save plot
   [a, nm2, b]=fileparts(filenm);
   set(gcf, 'PaperUnits', 'points');
   set(gcf, 'PaperSize', [1000 1000]);
   set(gcf, 'PaperPositionMode', 'manual');
   set(gcf, 'PaperPosition', [0 0 1000 1000]);
   set(gcf, 'renderer', 'painters');
   print(gcf,'-dpdf',fullfile(dir_pth,strcat(nm2,'.pdf')));
end
fprintf('DONE!!!\n\n\n')
```

Function used

```
function [tPhase1,tPhase2,tPhase1Sm,tPhase2Sm]=Niki_analysis_individualfiles_func(dpath, dfnm)
    %% Default Parameters
    %Parameters of TVDiff method (robust derivative calculation)
    regAlpha=0.02; %regularisation factor
    nIter=100; %number of iterations for total variance regularisation
    ep=1e-9;    %division by 0 parameter
    navg=15; %how many points to take for the moving average
    %Parameters of AnalyseEdges function (finding switching timepoints)
    scales=[1 2 4];
    thresholds=0.2*ones(1,length(scales));
    tranrad=4;
    if (nargin==2)
      dt_pth=dpath;
       dt_fnm=dfnm;
    else
       % path to the folder and file name. Use only if not provided by
       % function arfuments
       dt_pth='Y:\vegesna\cp_analyse\To plot'; %'Z:/halavaty'%path to the data
       dt_fnm='cell.csv';                  %data file name
    end
    %% add required folders to matlab Path
    %addpath(dt_pth)
    addpath('./TVDiff')
    addpath('./edge_detector_1d')

    %% Data import
     expd=readtable(fullfile(dt_pth,dt_fnm),'Delimiter',',','ReadVariableNames',true);
    tVals=(expd{:,1}-1)*12;
    intensVals=expd{:,5}.*expd{:,8};
    intensVals=intensVals/max(intensVals);
    intensVals(isnan(intensVals)) = 0 ;
    [nVals, xx]=size(intensVals);
    intensValsSmooth=conv(intensVals,repmat(1/navg,navg,1),'valid');
    tValsSmooth=tVals(((navg+1)/2):(nVals-(navg-1)/2));

    %% Calculations
    tsteps=diff(tVals);
    tsteps=vertcat(tsteps(1), tsteps);
    tstepsSmooth=tsteps(((navg+1)/2):(nVals-(navg-1)/2));
    tvDerVals = TVRegDiff( intensVals, nIter, regAlpha, [], 'small', ep, [], 0, 1 );
    tvDerVals=tvDerVals(2:end);
    tvDerVals=tvDerVals/nVals;
    tvDerVals=tvDerVals./tsteps;
    tvDerValsSmooth = TVRegDiff( intensValsSmooth, nIter, regAlpha, [], 'small', ep, [], 0, 1 );
    tvDerValsSmooth=tvDerValsSmooth(2:end);
    tvDerValsSmooth=tvDerValsSmooth/(nVals-navg+1);
    tvDerValsSmooth=tvDerValsSmooth./tstepsSmooth;
```

```
   %% Integration
   restorVals=cumsum(tvDerVals.*tsteps)+intensVals(1);
   restorValsSmooth=cumsum(tvDerValsSmooth.*tstepsSmooth)+intensValsSmooth(1);

%% Getting switch time points
   function [tSwitch1,grRate1,tSwitch2,grRate2]= getSwitchPoints(dVals,tVals)
      %initial values are 0 to find those that were not defined
      tSwitch1=0;
      grRate1=0;
      tSwitch2=0;
      grRate2=0;
       [dDifs, minmax, stats] = AnalyzeEdges_AH(dVals, scales, thresholds,tsteps(1), tVals(1),
tVals(end), tranrad);
      tSwitch=tVals(minmax>0);
      nSwitch=length(tSwitch);
      if(nSwitch>0)
         if (nSwitch==1)
            if (stats(1,1)<stats(2,1))
               tSwitch1=tSwitch(1);
               grRate1=stats(1,1);
            else
               tSwitch2=tSwitch(1);
               grRate2=stats(1,1);
             end;
         else % nSwitch>1
            if (stats(1,1)<stats(2,1))
               tSwitch1=tSwitch(1);
               grRate1=stats(1,1);
               tSwitch2=tSwitch(2);
               grRate2=stats(2,1);
            else
               tSwitch2=tSwitch(1);
               grRate2=stats(1,1);
            end;
         end;
      end;
   end
 [tPhase1,grRate1,tPhase2,grRate2]= getSwitchPoints(tvDerVals,tVals);
   [tPhase1Sm,grRate1Sm,tPhase2Sm,grRate2Sm]= getSwitchPoints(tvDerValsSmooth,tValsSmooth)

%% Plotting
   function []=putSwitchLabels(tPh1, tPh2)
      yl=ylim;
      hold on
      if(tPh1>0)
         line([tPh1 tPh1],yl,'Color','r');
      end;
      if(tPh2>0)
```

```
        line([tPh2 tPh2],yl,'Color','m');
      end;
      hold off
    end
    fg=figure( 'Position', [ 100, 100, 800, 800 ] );
    subplot(3,2,1)
    plot(tVals,intensVals,'LineWidth',2);
    putSwitchLabels(tPhase1, tPhase2)
    subplot(3,2,3)
    plot(tVals,tvDerVals,'LineWidth',2);
    putSwitchLabels(tPhase1, tPhase2)
     subplot(3,2,5)
    plot(tVals,intensVals,'LineWidth',2);
    putSwitchLabels(tPhase1, tPhase2)
    hold on
    plot(tVals,restorVals,'-b','LineWidth',3);
    hold off
    subplot(3,2,2)
   plot(tValsSmooth,intensValsSmooth,'LineWidth',2);
    putSwitchLabels(tPhase1Sm, tPhase2Sm)
    subplot(3,2,4)
    plot(tValsSmooth,tvDerValsSmooth,'LineWidth',2);
    putSwitchLabels(tPhase1Sm, tPhase2Sm)
    subplot(3,2,6)
    plot(tValsSmooth,intensValsSmooth,'LineWidth',2);
    putSwitchLabels(tPhase1Sm, tPhase2Sm)
    hold on
    plot(tValsSmooth,restorValsSmooth,'-b','LineWidth',3);
    hold off

    %% Text output
    fprintf('\n*****************************************************\n');
    fprintf('Results of automated phase identification:\n')
    if (tPhase1>0)
      fprintf('Phase 1 was identified\n');
      fprintf('End of the first phase %g\n',tPhase1);
      fprintf('Growth rate of the first phase %g\n',grRate1);
    else
      fprintf('Phase 1 was not identified\n');
    end;
    if (tPhase2>0)
     fprintf('Phase 2 was identified\n');
     fprintf('End of the second phase %g\n',tPhase2);
     fprintf('Growth rate of the second phase %g\n',grRate2);
    else
       fprintf('Phase 2 was not identified\n');
    end;
end % end of main function
```

A similar script was used to extract the phase 1 of mitosis. As the data obtained in this case had sharp increase and decrease in intensities, the script doesn't use the *TVDiff* to calculate the derivative. Instead the switching points were identified directly from the raw data. The following was the script used to extract the duration of phase 1 in mitotic cells.

Matlab script for analysing data of mitotic cells:

```
clear
%% choose files to iterate
dir_pth='Y:\vegesna\cp_analyse\all_mitosis\diff.columns_2'; %path to the input directory
d = dir(fullfile(dir_pth,'*.csv'));
nfiles=length(d);


%% Make a new file to record summary
outTblPth=fullfile(dir_pth,'AnalysisSummary.xls');
header={'DataName', 't1raw', 't2raw', 't1smooth', 't2smooth'};
if (exist(outTblPth,'file')==2)
   delete (outTblPth);
end
xlswrite(outTblPth,header,'Analysis Summary','A1')


%% perform calculations
for k = 1:nfiles
   close all
   filenm=d(k).name;
[t1, t2]=Niki_mitotic_analysis_individualfiles_func(dir_pth,filenm);
   writeOutput={filenm t1 t2};
   xlswrite(outTblPth,writeOutput,'Analysis Summary',strcat('A',num2str(k+1)))
   %save plot
   [a, nm2, b]=fileparts(filenm);
   set(gcf, 'PaperUnits', 'points');
   set(gcf, 'PaperSize', [1000 1000]);
   set(gcf, 'PaperPositionMode', 'manual');
   set(gcf, 'PaperPosition', [0 0 500 1000]);
   set(gcf, 'renderer', 'painters');
   print(gcf,'-dpdf',fullfile(dir_pth,strcat(nm2,'.pdf')));
end
fprintf('DONE!!!\n\n\n')
```

7.5.5 R Studio

7.5.5.1 Plotting the Golgi biogenesis results

A self written script in R Studio was used to plot the values of T1 and T2-T1 extracted from the plot using MatLab script.

To briefly explain the script, specific packages required for the plot ggplot2, scales, plyr, reshape2 and zoo were loaded in the first part. Then the data was loaded from the text file and the name of the knockdown was extracted from the table and used as a label for x-axis. The ggplot2 was used to plot the boxplot by specifying maximum y-value, y-scale, axis label text orientation and font. The mean value for each condition was plotted as a dot in centre of the box plot. Finally the plot was saved as a PDF file of a specified height and width.

The following was the script used to plot the duration of Phase 1 (T1).

```
# Boxplot script by N V Gayathri Vegesna
# txt file with two columns knockdown condition and duration of phases
# quartz() # to test the plot while its open
library(ggplot2)
library(scales)
library(plyr)
library(reshape2)
library(zoo)
data = read.table(file.choose(), header=T, sep="\t") # save excel file as tab delimited text and open it
#Turn your 'knockdown' column into a character vector
data$Knockdown <- as.character(data$Knockdown)
#Then turn it back into an ordered factor
data$Knockdown <- factor(data$Knockdown, levels=unique(data$Knockdown))
pos = position_jitter(w = .1, h = .0)
q<- ggplot(data, aes(x = Knockdown,
                     y = Duration.of.Phase1..min.,
                     group=Knockdown,
                     # color="black",
                     ymax= max(Duration.of.Phase1..min.))) +
  geom_point(position = pos, alpha=0.4, size=2) + # geom_boxplot()
  coord_cartesian(ylim=c(-20, 1000)) +
scale_y_continuous(breaks=c(0,100,200,300,400,500,600,700,800,900,1000))+
  geom_boxplot(outlier.shape = NA, alpha=0.5)+stat_summary(fun.y=mean, geom="point",
colour="black",size=2.5)+
  theme(axis.title.x = element_blank()) +   # Remove x-axis label
  ylab("Duration of Phase 1 (min)") + theme(panel.background = element_rect(fill = "white")) +
  theme(axis.line = element_line(size = 0.5, colour = "black")) + theme(axis.text.x =
element_text(angle=70, vjust=0.5, size=8, colour="black"))
```

```
# theme(legend.position = "bottom") +                    # Set y-axis label
pdf(file="q.pdf", width = 6, height = 5)
print(q)
dev.off()
```

The following similar script was used for plotting the duration of Phase 2 (T2-T1).

```
# Boxplot script by N V Gayathri Vegesna
# input txt file with two columns knockdown condition and duration of phases
# quartz() # to test the plot while its open
library(ggplot2)
library(scales)
library(plyr)
library(reshape2)
library(zoo)
data = read.table(file.choose(), header=T, sep="\t") # save excel file as tab delimited text and open it
#Turn your 'knockdown' column into a character vector
data$Knockdown <- as.character(data$Knockdown)
#Then turn it back into an ordered factor
data$Knockdown <- factor(data$Knockdown, levels=unique(data$Knockdown))
pos = position_jitter(w = .1, h = .0)
r<- ggplot(data, aes(x = Knockdown,
                     y = Duration.of.Phase2..min.,
                     group=Knockdown,
                     # color="black",
                     ymax= max(Duration.of.Phase2..min.))) +
  geom_point(position = pos, alpha=0.4, size=2) + # geom_boxplot()
  coord_cartesian(ylim=c(-20, 1000)) +
scale_y_continuous(breaks=c(0,100,200,300,400,500,600,700,800,900,1000))+
  geom_boxplot(outlier.shape = NA, alpha=0.5)+stat_summary(fun.y=mean, geom="point",
colour="black",size=2.5)+
  theme(axis.title.x = element_blank()) +   # Remove x-axis label
  ylab("Duration of Phase 2 (min)") + theme(panel.background = element_rect(fill = "white")) +
  theme(axis.line = element_line(size = 0.5, colour = "black")) + theme(axis.text.x =
element_text(angle=70, vjust=0.5, size=8, colour="black"))
pdf(file="r.pdf", width = 6, height = 5)
print(r)
dev.off()
```

7.5.5.2 Plotting Golgi biogenesis data from mitotic cells

The following similar script was used to plot duration of phase 1 in mitotic cells.

```
# Boxplot script by N V Gayathri Vegesna
# input txt file with two columns knockdown condition and duration of phases
# quartz() # to test the plot while its open
library(ggplot2)
library(scales)
```

```
library(plyr)
library(reshape2)
library(zoo)
data = read.table(file.choose(), header=T, sep="\t") # save excel file as tab delimited text and open it
#Turn your 'knockdown' column into a character vector
data$Knockdown <- as.character(data$Knockdown)
#Then turn it back into an ordered factor
data$Knockdown <- factor(data$Knockdown, levels=unique(data$Knockdown))
pos = position_jitter(w = .1, h = .0)
r<- ggplot(data, aes(x = Knockdown,
                     y = Duration.of.Phase1..min.,
                     group=Knockdown,
                     # color="black",
                     ymax= max(Duration.of.Phase1..min.))) +
  geom_point(position = pos, alpha=0.4, size=2) + # geom_boxplot()
  coord_cartesian(ylim=c(0,80)) + scale_y_continuous(breaks=c(0,10,20,30,40,50,60,70,80))+
  geom_boxplot(outlier.shape = NA, alpha=0.5)+stat_summary(fun.y=mean, geom="point",
colour="black",size=2)+
  theme(axis.title.x = element_blank()) +   # Remove x-axis label
  ylab("Duration of Phase 1 (min)") + theme(panel.background = element_rect(fill = "white")) +
  theme(axis.line = element_line(size = 0.5, colour = "black")) + theme(axis.text.x =
element_text(angle=70, vjust=0.5, size=8, colour="black"))
p1=q+theme(axis.line.x = element_line(color="black", size = 1),axis.line.y = element_line(color="black",
size = 1))
pdf(file="p1.pdf", width = 5, height = 5)
print(p1)
dev.off()
```

7.5.5.3 Plotting the data from VSVG assay

A similar R script using ggplot2 mentioned above was used to plot the individual cell data from VSVG assay. The script was used to sort the cells based on experiment and time point. Then the ratio of the Golgi integrated FI to integrated FI of total cell was calculated for each cell. The values are normalised for zero time point in each condition by subtracting the mean of zero time point. The resulting data were plotted as a box plot, with the mean represented a dot. The individual experiments were plotted by specifying the input file name of the specific experiment. The data from all the experiments was pooled together and plotted by specifying input file names of all files as comma separated names.

The following is the R script used for analysis

```
rm(list=ls())
```

```
library(ggplot2)
library(scales)
library(plyr)
library(reshape2)
library(zoo)

dataPath<-'/Users/gayathrivegesna/Documents/All_data_analysis/24. VSVG_assay/Tables for analysis'
inputFileNames<-c('Cells_Exp_1.2.txt','Cells_Exp_1.3.txt','Cells_Exp_4.txt')
minimal_golgi_ratio<-0.0

#allConditions<-c('Neg9_t0','GRKD_t0','Neg9_t20','GRKD_t20')

timeConditions<-c('t0','t20')
treatmentConditions<-c('Neg9','GRKD')

data_all<-data.frame()
for (fileName in inputFileNames){
  data_replicate = read.table(file.path(dataPath,fileName), header=T, sep="\t",as.is=TRUE) # save excel file as tab delimited text and open it
  conditions<-do.call(rbind,strsplit(data_replicate$Metadata_siRNA,'_'))
  data_replicate$Treatment<-factor(conditions[,1],levels=treatmentConditions)
  data_replicate$Time<-factor(conditions[,2],levels=timeConditions)

  data_replicate$Ratio_Golgi<-
data_replicate$Intensity_IntegratedIntensity_TOTALbgcorrGolgiMask/data_replicate$Intensity_IntegratedIntensity_TOTALbgcorr
  data_replicate<-data_replicate[data_replicate$Ratio_Golgi>minimal_golgi_ratio,]#0

  data_replicate_t0<-data_replicate[data_replicate$Time=='t0',]
  t0_coefficients<-aggregate(Ratio_Golgi~Treatment,data=data_replicate_t0,FUN='median')
  names(t0_coefficients)[2]<-'t0_value'
  data_replicate<-merge(x=data_replicate,y=t0_coefficients)

  data_replicate$Ratio_Golgi_t0subtr<-data_replicate$Ratio_Golgi-data_replicate$t0_value

  data_all<-rbind(data_all,data_replicate)
}

pos = position_jitter(w = .5, h = .0)
q<- ggplot(data_all, aes(x = Metadata_siRNA,
                         y = Ratio_Golgi_t0subtr,
                         #group=Treatment,
                         # color="black",
                         ymax= max(Ratio_Golgi_t0subtr))) +
  geom_point(aes(colour=factor(Metadata_Experiment)),position = pos, alpha=0.4, size=0.3) +
#coord_cartesian(ylim=c(0, max(data_all_non0$NormalisedValue))) +
  #scale_y_continuous(trans = 'log10')+# geom_boxplot()
scale_y_continuous(breaks=c(0,100,200,300,400,500,600,700,800))+
```

```
 geom_boxplot(outlier.shape = NA, alpha=0.5)+stat_summary(fun.y=mean, geom="point", colour="black",size=2)+
 theme(axis.title.x = element_blank()) +  # Remove x-axis label
 ylab("FI") + theme(panel.background = element_rect(fill = "white")) +
 theme(axis.line = element_line(size = 0.5, colour = "black")) + theme(axis.text.x = element_text(angle=70, vjust=0.5, size=8, colour="black"))
# theme(legend.position = "bottom") +                 # Set y-axis label
p1=q+theme(axis.line.x = element_line(color="black", size = 1),axis.line.y = element_line(color="black", size = 1))
p1
pdf(file="p1.pdf", width = 7, height = 5)
print(p1)
dev.off()
```

8 References

Alvarez, C., R. Garcia-Mata, H. P. Hauri, and E. Sztul. 2001. "The p115-Interactive Proteins GM130 and Giantin Participate in Endoplasmic Reticulum-Golgi Traffic." *Journal of Biological Chemistry* 276(4):2693–2700.

Antonny, B., D. Madden, S. Hamamoto, L. Orci, and R. Schekman. 2001. "Dynamics of the COPII Coat with GTP and Stable Analogues." *Nature cell biology* 3(6):531–37.

Asante, David et al. 2013. "A Role for the Golgi Matrix Protein Giantin in Ciliogenesis through Control of the Localization of Dynein-2." *Journal of cell science* 126(Pt 22):5189–97.

Axelsson, Magnus A. B. and Graham Warren. 2004. "Rapid, Endoplasmic Reticulum-Independent Diffusion of the Mitotic Golgi Haze." *Molecular biology of the cell* 15(4):1843–52.

Ballensiefen, W. et al. 1998. "Recycling of the Yeast v-SNARE Sec22p Involves COPI-Proteins and the ER Transmembrane Proteins Ufe1p and Sec20p." *Journal of cell science* (11):1507–20.

Bandyopadhyay, Urmi, Wayne A. Fenton, Arthur L. Horwich, and Maria Nagy. 2014. "Production of RNA for Transcriptomic Analysis from Mouse Spinal Cord Motor Neuron Cell Bodies by Laser Capture Microdissection." *Journal of Visualized Experiments* (83):e51168–e51168.

Bannykh, S. I. and W. E. Balch. 1997. "Membrane Dynamics at the Endoplasmic Reticulum-Golgi Interface." *The Journal of cell biology* 138(1):1–4.

Barr, F. a, M. Puype, J. Vandekerckhove, and G. Warren. 1997. "GRASP65, a Protein Involved in the Stacking of Golgi Cisternae." *Cell* 91:253–62.

Barr, Francis A. 2004. "Golgi Inheritance: Shaken but Not Stirred." *The Journal of cell biology* 164(7):955–58.

Barr, Francis A. and Benjamin Short. 2003. "Golgins in the Structure and Dynamics of the Golgi Apparatus." *Current Opinion in Cell Biology* 15(4):405–13.

Baschieri, Francesco, Edith Uetz-von Allmen, Daniel F. Legler, and Hesso Farhan. 2015. "Loss of GM130 in Breast Cancer Cells and Its Effects on Cell Migration, Invasion

and Polarity." *Cell Cycle* 14(8):1139–47.

Beckers, C. J., D. S. Keller, and W. E. Balch. 1987. "Semi-Intact Cells Permeable to Macromolecules: Use in Reconstitution of Protein Transport from the Endoplasmic Reticulum to the Golgi Complex." *Cell* 50(4):523–34.

Ben-Tekaya, Houchaima, Kota Miura, Rainer Pepperkok, and Hans-Peter Hauri. 2005. "Live Imaging of Bidirectional Traffic from the ERGIC." *Journal of cell science* 118(Pt 2):357–67.

Berglund, Lisa et al. 2008. "A Genecentric Human Protein Atlas for Expression Profiles Based on Antibodies." *Molecular & cellular proteomics : MCP* 7(10):2019–27.

Bergmann, J. E. 1989. "Using Temperature-Sensitive Mutants of VSV to Study Membrane Protein Biogenesis." *Methods in cell biology* 32:85–110.

Bisel, Blaine et al. 2008. "ERK Regulates Golgi and Centrosome Orientation towards the Leading Edge through GRASP65." *The Journal of cell biology* 182(5):837–43.

Bonfanti, Lidia et al. 1998. "Procollagen Traverses the Golgi Stack without Leaving the Lumen of Cisternae: Evidence for Cisternal Maturation." *Cell* 95(7):993–1003.

Canny, J. 1986. "Edge Detector 1D." Retrieved (http://www.cs.unc.edu/~nanowork/cismm/download/edgedetector/#references).

Chang, Seung-Hee et al. 2012. "GOLGA2/GM130, Cis-Golgi Matrix Protein, Is a Novel Target of Anticancer Gene Therapy." *Molecular therapy : the journal of the American Society of Gene Therapy* 20(11):2052–63.

Chartrand, Rick. 2011. "Numerical Differentiation of Noisy, Nonsmooth Data." *ISRN Applied Mathematics* 2011:1–11.

Chen, Ji-Long et al. 2005. "Coatomer-Bound Cdc42 Regulates Dynein Recruitment to COPI Vesicles." *The Journal of Cell Biology* 169(3):383–89.

Cluett, E. B. and W. J. Brown. 1992. "Adhesion of Golgi Cisternae by Proteinaceous Interactions: Intercisternal Bridges as Putative Adhesive Structures." *Journal of cell science* 773–84.

Colanzi, Antonino and Daniela Corda. 2007. "Mitosis Controls the Golgi and the Golgi Controls Mitosis." *Current opinion in cell biology* 19(4):386–93.

Cole, N. B., N. Sciaky, A. Marotta, J. Song, and J. Lippincott-Schwartz. 1996. "Golgi

Dispersal during Microtubule Disruption: Regeneration of Golgi Stacks at Peripheral Endoplasmic Reticulum Exit Sites." *Molecular biology of the cell* 7(4):631–50.

Conrad, Christian et al. 2011. "Micropilot: Automation of Fluorescence Microscopy–based Imaging for Systems Biology." *Nature Methods* 8(3):246–49.

D'Angelo, Giovanni et al. 2009. "GRASP65 and GRASP55 Sequentially Promote the Transport of C-Terminal Valine-Bearing Cargos to and through the Golgi Complex." *The Journal of biological chemistry* 284(50):34849–60.

Demaegd, Didier et al. 2013. "Newly Characterized Golgi-Localized Family of Proteins Is Involved in Calcium and pH Homeostasis in Yeast and Human Cells." *Proceedings of the National Academy of Sciences of the United States of America* 110(17):6859–64.

Diao, A., L. Frost, Y. Morohashi, and M. Lowe. 2008. "Coordination of Golgin Tethering and SNARE Assembly: GM130 BINDS SYNTAXIN 5 IN A p115-REGULATED MANNER." *Journal of Biological Chemistry* 283(11):6957–67.

Drin, Guillaume, Vincent Morello, Jean-François Casella, Pierre Gounon, and Bruno Antonny. 2008. "Asymmetric Tethering of Flat and Curved Lipid Membranes by a Golgin." *Science* 320(May):670–73.

Dunphy, William G. and James E. Rothman. 1985. "Compartmental Organization of the Goigi Stack." 42(August):13–21.

Elkis, Yoav et al. 2015. "TMF/ARA160 Governs the Dynamic Spatial Orientation of the Golgi Apparatus during Sperm Development." *PloS one* 10(12):e0145277.

Farquhar, M. G. and G. E. Palade. 1981. "The Golgi Apparatus (Complex)-(1954-1981)-from Artifact to Center Stage." *The Journal of cell biology* 91(3 Pt 2):77s–103s.

Feng, Yanbin et al. 2013. "Structural Insight into Golgi Membrane Stacking by GRASP65 and GRASP55 Proteins." *The Journal of biological chemistry* 288(39):28418–27.

Follit, John a et al. 2008. "The Golgin GMAP210/TRIP11 Anchors IFT20 to the Golgi Complex." *PLoS genetics* 4(12):e1000315.

Foulquier, François et al. 2012. "TMEM165 Deficiency Causes a Congenital Disorder of Glycosylation." *American journal of human genetics* 91(1):15–26.

Franke, W. W. et al. 1972. "Inter- and Intracisternal Elements of the Golgi Apparatus." *Zeitschrift für Zellforschung und Mikroskopische Anatomie* 132(3):365–80.

Fridmann-Sirkis, Yael, Symeon Siniossoglou, and Hugh R. B. Pelham. 2004. "TMF Is a Golgin That Binds Rab6 and Influences Golgi Morphology." *BMC cell biology* 5:18.

Friggi-Grelin, F., C. Rabouille, and P. Therond. 2006. "The Cis-Golgi Drosophila GMAP Has a Role in Anterograde Transport and Golgi Organization in Vivo, Similar to Its Mammalian Ortholog in Tissue Culture Cells." *Eur J Cell Biol* 85(11):1155–66.

Glick, Benjamin S. and Alberto Luini. 2011. "Models for Golgi Traffic: A Critical Assessment." *Cold Spring Harbor Perspectives in Biology* 3(11):1–16.

Hara-Kuge, S. et al. 1994. "En Bloc Incorporation of Coatomer Subunits during the Assembly of COP-Coated Vesicles." *The Journal of cell biology* 124(6):883–92.

Hauri, H., C. Appenzeller, F. Kuhn, and O. Nufer. 2000. "Lectins and Traffic in the Secretory Pathway." *FEBS letters* 476(1–2):32–37.

Held, Michael et al. 2010. "CellCognition: Time-Resolved Phenotype Annotation in High-Throughput Live Cell Imaging." *Nature methods* 7(9):747–54.

Hilsenstein, Volker. 2014. "Cellprofiler Modules for Interfacing with Leica Matrix Screener Module of LASAF."

Hu, Fen et al. 2015. "Structural Basis for the Interaction between the Golgi Reassembly-Stacking Protein GRASP65 and the Golgi Matrix Protein GM130." *Journal of Biological Chemistry* 290(44):jbc.M115.657940.

Infante, C., F. Ramos-Morales, C. Fedriani, M. Bornens, and R. M. Rios. 1999. "GMAP-210, A Cis-Golgi Network-Associated Protein, Is a Minus End Microtubule-Binding Protein." *The Journal of cell biology* 145(1):83–98.

Jesch, S. A., T. S. Lewis, N. G. Ahn, and A. D. Linstedt. 2001. "Mitotic Phosphorylation of Golgi Reassembly Stacking Protein 55 by Mitogen-Activated Protein Kinase ERK2." *Molecular biology of the cell* 12(6):1811–17.

Jesch, S. A. and A. D. Linstedt. 1998. "The Golgi and Endoplasmic Reticulum Remain Independent during Mitosis in HeLa Cells." *Molecular biology of the cell* 9(3):623–35.

Jesch, S. A., A. J. Mehta, M. Velliste, R. F. Murphy, and A. D. Linstedt. 2001. "Mitotic Golgi Is in a Dynamic Equilibrium between Clustered and Free Vesicles

Independent of the ER." *Traffic (Copenhagen, Denmark)* 2(12):873–84.

Jokitalo, E., N. Cabrera-Poch, G. Warren, and D. T. Shima. 2001. "Golgi Clusters and Vesicles Mediate Mitotic Inheritance Independently of the Endoplasmic Reticulum." *The Journal of cell biology* 154(2):317–30.

Jollivet, Florence et al. 2007. "Analysis of De Novo Golgi Complex Formation after Enzyme-Based Inactivation." *Molecular Biology of the Cell* 18(11):4637–47.

Kasap, Murat et al. 2004. "Dynamic Nucleation of Golgi Apparatus Assembly from the Endoplasmic Reticulum in Interphase Hela Cells." *Traffic (Copenhagen, Denmark)* 5(8):595–605.

Klausner, R. D., J. G. Donaldson, and J. Lippincott-Schwartz. 1992. "Brefeldin A: Insights into the Control of Membrane Traffic and Organelle Structure." *The Journal of cell biology* 116(5):1071–80.

Kodani, Andrew, Irene Kristensen, Lan Huang, and Christine Sütterlin. 2009. "GM130-Dependent Control of Cdc42 Activity at the Golgi Regulates Centrosome Organization." *Molecular biology of the cell* 20(4):1192–1200.

Kodani, Andrew and Christine Sütterlin. 2008. "The Golgi Protein GM130 Regulates Centrosome Morphology and Function." *Molecular biology of the cell* 19(2):745–53.

Koreishi, Mayuko et al. 2013. "The Golgin Tether Giantin Regulates the Secretory Pathway by Controlling Stack Organization within Golgi Apparatus" edited by C. L. Jackson. *PLoS ONE* 8(3):e59821.

Kreis, T. E. and H. F. Lodish. 1986. "Oligomerization Is Essential for Transport of Vesicular Stomatitis Viral Glycoprotein to the Cell Surface." *Cell* 46(6):929–37.

Lee, Intaek et al. 2014. "Membrane Adhesion Dictates Golgi Stacking and Cisternal Morphology." *Proceedings of the National Academy of Sciences of the United States of America* 111(5):1849–54.

Lerer-Goldshtein, Tal et al. 2010. "TMF/ARA160: A Key Regulator of Sperm Development." *Developmental biology* 348(1):12–21.

Levine, T. P., C. Rabouille, R. H. Kieckbusch, and G. Warren. 1996. "Binding of the Vesicle Docking Protein p115 to Golgi Membranes Is Inhibited under Mitotic Conditions." *The Journal of biological chemistry* 271(29):17304–11.

Lin, C. Y. et al. 2000. "Peripheral Golgi Protein GRASP65 Is a Target of Mitotic Polo-like Kinase (Plk) and Cdc2." *Proceedings of the National Academy of Sciences of the United States of America* 97(23):12589–94.

Linstedt, A. D. et al. 2000. "Binding Relationships of Membrane Tethering Components. THE GIANTIN N TERMINUS AND THE GM130 N TERMINUS COMPETE FOR BINDING TO THE p115 C TERMINUS." *Journal of Biological Chemistry* 275(14):10196–201.

Linstedt, A. D. and H. P. Hauri. 1993. "Giantin, a Novel Conserved Golgi Membrane Protein Containing a Cytoplasmic Domain of at Least 350 kDa." *Molecular biology of the cell* 4(7):679–93.

Lippincott-Schwartz, J. et al. 1991. "Brefeldin A's Effects on Endosomes, Lysosomes, and the TGN Suggest a General Mechanism for Regulating Organelle Structure and Membrane Traffic." *Cell* 67(3):601–16.

Lippincott-Schwartz, Jennifer, Lydia C. Yuan, Juan S. Bonifacino, and Richard D. Klausner. 1989. "Rapid Redistribution of Golgi Proteins into the ER in Cells Treated with Brefeldin A: Evidence for Membrane Cycling from Golgi to ER." *Cell* 56(5):801–13.

Lovatt, Ditte et al. 2014. "Transcriptome in Vivo Analysis (TIVA) of Spatially Defined Single Cells in Live Tissue." *Nature methods* 11(2):190–96.

Lowe, M. et al. 1998. "Cdc2 Kinase Directly Phosphorylates the Cis-Golgi Matrix Protein GM130 and Is Required for Golgi Fragmentation in Mitosis." *Cell* 94(6):783–93.

Lowe, M., N. K. Gonatas, and G. Warren. 2000. "The Mitotic Phosphorylation Cycle of the Cis-Golgi Matrix Protein GM130." *The Journal of cell biology* 149(2):341–56.

Lowe, Martin. 2002. "Golgi Complex: Biogenesis de Novo?" *Current biology : CB* 12(5):R166-7.

Lowe, Martin. 2011. "Structural Organization of the Golgi Apparatus." *Current Opinion in Cell Biology* 23(1):85–93.

Lucocq, J. M. and G. Warren. 1987. "Fragmentation and Partitioning of the Golgi Apparatus during Mitosis in HeLa Cells." *The EMBO journal* 6(11):3239–46.

Lupashin, Vladimir and Elizabeth Sztul. 2005. "Golgi Tethering Factors." *Biochimica et Biophysica Acta (BBA) - Molecular Cell Research* 1744(3):325–39.

Malkus, P., Laurie A. Graham, Tom H. Stevens, and Randy Schekman. 2004. "Role of Vma21p in Assembly and Transport of the Yeast Vacuolar ATPase." *Molecular Biology of the Cell* 15(11):5075–91.

Malkus, Per, Feng Jiang, and Randy Schekman. 2002. "Concentrative Sorting of Secretory Cargo Proteins into COPII-Coated Vesicles." *The Journal of cell biology* 159(6):915–21.

Mancias, Joseph D. and Jonathan Goldberg. 2005. "Exiting the Endoplasmic Reticulum." *Traffic* 6(4):278–85.

Marra, Pierfrancesco et al. 2001. "The GM130 and GRASP65 Golgi Proteins Cycle through and Define a Subdomain of the Intermediate Compartment." 3(December):1101–14.

Martínez-Menárguez, J. A., H. J. Geuze, J. W. Slot, and J. Klumperman. 1999. "Vesicular Tubular Clusters between the ER and Golgi Mediate Concentration of Soluble Secretory Proteins by Exclusion from COPI-Coated Vesicles." *Cell* 98(1):81–90.

Mellman, Ira and Kai Simons. 1992. "The Golgi Complex: In Vitro Veritas?" *Cell* 68(5):829–40.

Mironov, Alexander A. et al. 2003. "ER-to-Golgi Carriers Arise through Direct En Bloc Protrusion and Multistage Maturation of Specialized ER Exit Domains." *Developmental Cell* 5(4):583–94.

Misteli, T. and G. Warren. 1994. "COP-Coated Vesicles Are Involved in the Mitotic Fragmentation of Golgi Stacks in a Cell-Free System." *The Journal of cell biology* 125(2):269–82.

Mori, Katsuhiro and Hiroyuki Kato. 2002. "A Putative Nuclear Receptor Coactivator (TMF/ARA160) Associates with hbrm/hSNF2α and BRG-1/hSNF2β and Localizes in the Golgi Apparatus." *FEBS Letters* 520(1–3):127–32.

Müller, J. M. et al. 1999. "An NSF Function Distinct from ATPase-Dependent SNARE Disassembly Is Essential for Golgi Membrane Fusion." *Nature cell biology* 1(6):335–40.

Munro, S. 2011. "The Golgin Coiled-Coil Proteins of the Golgi Apparatus." *Cold Spring Harbor Perspectives in Biology* 3(6):a005256–a005256.

Nakamura, N. et al. 1995. "Characterization of a Cis-Golgi Matrix Protein, GM130." *The Journal of cell biology* 131(6 Pt 2):1715–26.

Nakamura, Nobuhiro. 2010. "Emerging New Roles of GM130, a Cis -Golgi Matrix Protein, in Higher Order Cell Functions." *Journal of Pharmacological Sciences* (112):255–64.

Nozawa, Kazuhisa, Marvin J. Fritzler, Carlos A. von Mühlen, and Edward K. L. Chan. 2004. "Giantin Is the Major Golgi Autoantigen in Human Anti-Golgi Complex Sera." *Arthritis research & therapy* 6(2):R95-102.

Palade, G. 1975. "Intracellular Aspects of the Process of Protein Synthesis." *Science (New York, N.Y.)* 189(4200):347–58.

Pernet-Gallay, Karin et al. 2002. "The Overexpression of GMAP-210 Blocks Anterograde and Retrograde Transport Between the ER and the Golgi Apparatus." *Traffic* 3(11):822–32.

Pfeffer, S. R. 2010. "How the Golgi Works: A Cisternal Progenitor Model." *Proceedings of the National Academy of Sciences* 107(46):19614–18.

Potelle, Sven, André Klein, and François Foulquier. 2015. "Golgi Post-Translational Modifications and Associated Diseases." *Journal of Inherited Metabolic Disease* 38(4):741–51.

Presley, J. F. et al. 1997. "ER-to-Golgi Transport Visualized in Living Cells." *Nature* 389(6646):81–85.

Preuss, Daphne, Jon Mulholland, Alex Franzusoff, Nava Segev, and David Botsteint. 1992. "Characterization of the Saccharomyces Golgi Complex through the Cell Cycle by Immunoelectron Microscopy." *Molecular Biology of the Cell* 3(7):789–803.

Puri, S. and Adam D. Linstedt. 2003. "Capacity of the Golgi Apparatus for Biogenesis from the Endoplasmic Reticulum." *Molecular Biology of the Cell* 14(12):5011–18.

Puthenveedu, Manojkumar A., Collin Bachert, Sapna Puri, Frederick Lanni, and Adam D. Linstedt. 2006. "GM130 and GRASP65-Dependent Lateral Cisternal Fusion Allows Uniform Golgi-Enzyme Distribution." *Nature cell biology* 8(3):238–48.

Ramirez, Irene Barinaga-Rementeria and Martin Lowe. 2009. "Golgins and GRASPs: Holding the Golgi Together." *Seminars in cell & developmental biology* 20(7):770–79.

Reinhardt, Timothy a, John D. Lippolis, and Randy E. Sacco. 2014. "The Ca(2+)/H(+) Antiporter TMEM165 Expression, Localization in the Developing, Lactating and Involuting Mammary Gland Parallels the Secretory Pathway Ca(2+) ATPase (SPCA1)." *Biochemical and biophysical research communications* 445(2):417–21.

Ríos, Rosa M., Arancha Sanchís, Anne Marie Tassin, Concepción Fedriani, and Michel Bornens. 2004. "GMAP-210 Recruits γ-Tubulin Complexes to Cis-Golgi Membranes and Is Required for Golgi Ribbon Formation." *Cell* 118(3):323–35.

Ronchi, Paolo, Christian Tischer, Devrim Acehan, and Rainer Pepperkok. 2014. "Positive Feedback between Golgi Membranes, Microtubules and ER-Exit Sites Directs Golgi de Novo Biogenesis." *Journal of cell science* 4620–33.

Rothman, J. E. and G. Warren. 1994. "Implications of the SNARE Hypothesis for Intracellular Membrane Topology and Dynamics." *Current biology : CB* 4(3):220–33.

Sahashi, K. et al. 2004. "Progressive Myopathy with Circulating Autoantibody against Giantin in the Golgi Apparatus." *Neurology* 62(10):1891–93.

Saito, Y., K. Kimura, T. Oka, and A. Nakano. 1998. "Activities of Mutant Sar1 Proteins in Guanine Nucleotide Binding, GTP Hydrolysis, and Cell-Free Transport from the Endoplasmic Reticulum to the Golgi Apparatus." *Journal of biochemistry* 124(4):816–23.

Sato, K., P. Roboti, A. A. Mironov, and M. Lowe. 2014. "Coupling of Vesicle Tethering and Rab Binding Is Required for in Vivo Functionality of the Golgin GMAP-210." *Molecular Biology of the Cell* 26(3):537–53.

Scales, S. J., R. Pepperkok, and T. E. Kreis. 1997. "Visualization of ER-to-Golgi Transport in Living Cells Reveals a Sequential Mode of Action for COPII and COPI." *Cell* 90(6):1137–48.

Schubert, Walter et al. 2006. "Analyzing Proteome Topology and Function by Automated Multidimensional Fluorescence Microscopy." *Nature biotechnology* 24(10):1270–78.

Schweizer, A. et al. 1990. "Identification of an Intermediate Compartment Involved in

Protein Transport from Endoplasmic Reticulum to Golgi Apparatus." *European journal of cell biology* 53(2):185–96.

Seelig, H. P., P. Schranz, H. Schröter, C. Wiemann, and M. Renz. 1994. "Macrogolgin--a New 376 kD Golgi Complex Outer Membrane Protein as Target of Antibodies in Patients with Rheumatic Diseases and HIV Infections." *Journal of autoimmunity* 7(1):67–91.

Seemann, J., E. Jokitalo, M. Pypaert, and G. Warren. 2000. "Matrix Proteins Can Generate the Higher Order Architecture of the Golgi Apparatus." *Nature* 407(6807):1022–26.

Seemann, Joachim, Marc Pypaert, Tomohiko Taguchi, Jorg Malsam, and Graham Warren. 2002. "Partitioning of the Matrix Fraction of the Golgi Apparatus during Mitosis in Animal Cells." *Science (New York, N.Y.)* 295(5556):848–51.

Shamseldin, Hanan E., Alexis H. Bennett, Majid Alfadhel, Vandana Gupta, and Fowzan S. Alkuraya. 2016. "GOLGA2, Encoding a Master Regulator of Golgi Apparatus, Is Mutated in a Patient with a Neuromuscular Disorder." *Human Genetics* 135(2):245–51.

Shima, D. T., N. Cabrera-Poch, R. Pepperkok, and G. Warren. 1998. "An Ordered Inheritance Strategy for the Golgi Apparatus: Visualization of Mitotic Disassembly Reveals a Role for the Mitotic Spindle." *The Journal of cell biology* 141(4):955–66.

Shima, D. T., K. Haldar, R. Pepperkok, R. Watson, and G. Warren. 1997. "Partitioning of the Golgi Apparatus during Mitosis in Living HeLa Cells." *The Journal of cell biology* 137(6):1211–28.

Shima, D. T., S. J. Scales, T. E. Kreis, and R. Pepperkok. 1999. "Segregation of COPI-Rich and Anterograde-Cargo-Rich Domains in Endoplasmic-Reticulum-to-Golgi Transport Complexes." *Current biology : CB* 9(15):821–24.

Short, Benjamin, Alexander Haas, and Francis A. Barr. 2005. "Golgins and GTPases, Giving Identity and Structure to the Golgi Apparatus." *Biochimica et Biophysica Acta (BBA) - Molecular Cell Research* 1744(3):383–95.

Shorter, J. et al. 1999. "GRASP55, a Second Mammalian GRASP Protein Involved in the Stacking of Golgi Cisternae in a Cell-Free System." *The EMBO journal* 18(18):4949–

60.

Sinka, Rita, Alison K. Gillingham, Vangelis Kondylis, and Sean Munro. 2008. "Golgi Coiled-Coil Proteins Contain Multiple Binding Sites for Rab Family G Proteins." *The Journal of cell biology* 183(4):607–15.

Slusarewicz, P., T. Nilsson, N. Hui, R. Watson, and G. Warren. 1994. "Isolation of a Matrix That Binds Medial Golgi Enzymes." *The Journal of Cell Biology* 124(4):405–13.

Sönnichsen, B. et al. 1998. "A Role for Giantin in Docking COPI Vesicles to Golgi Membranes." *The Journal of cell biology* 140(5):1013–21.

Stephens, D. J. and R. Pepperkok. 2001. "Illuminating the Secretory Pathway: When Do We Need Vesicles?" *Journal of cell science* 114(Pt 6):1053–59.

Sütterlin, Christine, Roman Polishchuk, Matt Pecot, and Vivek Malhotra. 2005. "The Golgi-Associated Protein GRASP65 Regulates Spindle Dynamics and Is Essential for Cell Division." *Molecular biology of the cell* 16(July):1–13.

Tang, Danming, Kari Mar, Graham Warren, and Yanzhuang Wang. 2008. "Molecular Mechanism of Mitotic Golgi Disassembly and Reassembly Revealed by a Defined Reconstitution Assay." *The Journal of biological chemistry* 283(10):6085–94.

Tang, Danming, Hebao Yuan, and Wang Yanzhuang. 2010. "The Role of GRASP65 in Golgi Cisternal Stacking and Cell Cycle Progression." 11(6):827–42.

Tängemo, Carolina et al. 2011. "A Novel Laser Nanosurgery Approach Supports de Novo Golgi Biogenesis in Mammalian Cells." *Journal of cell science* 124(Pt 6):978–87.

Terasaki, M. 2000. "Dynamics of the Endoplasmic Reticulum and Golgi Apparatus during Early Sea Urchin Development." *Molecular biology of the cell* 11(3):897–914.

Thyberg, J. and S. Moskalewski. 1992. "Reorganization of the Golgi Complex in Association with Mitosis: Redistribution of Mannosidase II to the Endoplasmic Reticulum and Effects of Brefeldin A." *Journal of submicroscopic cytology and pathology* 24(4):495–508.

Tischer, Christian, Volker Hilsenstein, Kirsten Hanson, and Rainer Pepperkok. 2014. "Adaptive Fluorescence Microscopy by Online Feedback Image Analysis." *Methods in cell biology* 123:489–503.

Turner, F. R. and W. G. Whaley. 1965. "INTERCISTERNAL ELEMENTS OF THE

GOLGI APPARATUS." *Science (New York, N.Y.)* 147(3663):1303–4.

Veenendaal, Tineke et al. 2014. "GRASP65 Controls the Cis Golgi Integrity in Vivo." *Biology open* 1–13.

Wang, Yanzhuang, Ayano Satoh, and Graham Warren. 2005. "Mapping the Functional Domains of the Golgi Stacking Factor GRASP65." *The Journal of biological chemistry* 280(6):4921–28.

Wang, Yanzhuang and Joachim Seemann. 2011. "Golgi Biogenesis." *Cold Spring Harbor perspectives in biology* 3(10):a005330.

Wang, Yanzhuang, Joachim Seemann, Marc Pypaert, James Shorter, and Graham Warren. 2003a. "A Direct Role for GRASP65 as a Mitotically Regulated Golgi Stacking Factor." *The EMBO journal* 22(13):3279–90.

Wang, Yanzhuang, Joachim Seemann, Marc Pypaert, James Shorter, and Graham Warren. 2003b. "A Direct Role for GRASP65 as a Mitotically Regulated Golgi Stacking Factor." *The EMBO journal* 22(13):3279–90.

Waters, M.Gerard and Suzanne R. Pfeffer. 1999. "Membrane Tethering in Intracellular Transport." *Curr Opin Cell Biol* 11:453–59.

Weber, T. et al. 1998. "SNAREpins: Minimal Machinery for Membrane Fusion." *Cell* 92(6):759–72.

Wei, Jen-Hsuan et al. 2015. "GM130 Regulates Golgi-Derived Spindle Assembly by Activating TPX2 and Capturing Microtubules." *Cell* 162(2):287–99.

Wei, Jen-Hsuan and Joachim Seemann. 2009. "The Mitotic Spindle Mediates Inheritance of the Golgi Ribbon Structure." *The Journal of cell biology* 184(3):391–97.

Wei, Jen-Hsuan and Joachim Seemann. 2010. "Unraveling the Golgi Ribbon." *Traffic (Copenhagen, Denmark)* 11(11):1391–1400.

Xiang, Y. and Y. Wang. 2010. "GRASP55 and GRASP65 Play Complementary and Essential Roles in Golgi Cisternal Stacking." *The Journal of Cell Biology* 188(2):237–51.

Xiang, Yi et al. 2013. "Regulation of Protein Glycosylation and Sorting by the Golgi Matrix Proteins GRASP55/65." *Nature Communications* 4:1659.

Xiang, Yi, Joachim Seemann, Blaine Bisel, Sukanya Punthambaker, and Yanzhuang

Wang. 2007. "Active ADP-Ribosylation Factor-1 (ARF1) Is Required for Mitotic Golgi Fragmentation." *The Journal of biological chemistry* 282(30):21829–37.

Xiang, Yi and Yanzhuang Wang. 2010a. "GRASP55 and GRASP65 Play Complementary and Essential Roles in Golgi Cisternal Stacking." *The Journal of cell biology* 188(2):237–51.

Xiang, Yi and Yanzhuang Wang. 2010b. "GRASP55 and GRASP65 Play Complementary and Essential Roles in Golgi Cisternal Stacking." *The Journal of cell biology* 188(2):237–51.

Xiang, Yi and Yanzhuang Wang. 2011. "New Components of the Golgi Matrix." *Cell and Tissue Research* 344:365–79.

Yadav, Smita, Sapna Puri, and Adam D. Linstedt. 2009. "A Primary Role for Golgi Positioning in Directed Secretion, Cell Polarity, and Wound Healing." *Molecular biology of the cell* 20(6):1728–36.

Yamane, Junko et al. 2007. "Functional Involvement of TMF/ARA160 in Rab6-Dependent Retrograde Membrane Traffic." *Experimental cell research* 313(16):3472–85.

Yorimitsu, Tomohiro, Ken Sato, and Masaki Takeuchi. 2014. "Molecular Mechanisms of Sar/Arf GTPases in Vesicular Trafficking in Yeast and Plants." *Frontiers in plant science* 5:411.

Yoshihisa, T., C. Barlowe, and R. Schekman. 1993. "Requirement for a GTPase-Activating Protein in Vesicle Budding from the Endoplasmic Reticulum." *Science (New York, N.Y.)* 259(5100):1466–68.

Yu, Xinchao, Marianna Breitman, and Jonathan Goldberg. 2012. "A Structure-Based Mechanism for Arf1-Dependent Recruitment of Coatomer to Membranes." *Cell* 148(3):530–42.

Zaal, K. J. et al. 1999. "Golgi Membranes Are Absorbed into and Reemerge from the ER during Mitosis." *Cell* 99(6):589–601.

Zeevaert, R. et al. 2013. "Bone Dysplasia as a Key Feature in Three Patients with a Novel Congenital Disorder of Glycosylation (CDG) Type II Due to a Deep Intronic Splice Mutation in TMEM165." *JIMD Reports*.